

Dissertation zur Erlangung des Doktorgrades
der Fakultät für Chemie und Pharmazie
der Ludwig-Maximilians-Universität München

**Actin-dependent mechanosensing in endothelial cells:
Regulatory aspects and targeting potential**

Florian Anton Gegenfurtner
aus München, Deutschland

2018

Erklärung

Diese Dissertation wurde im Sinne von §7 der Promotionsordnung vom 28. November 2011 von Herrn Prof. Dr. Stefan Zahler betreut.

Eidesstattliche Versicherung

Diese Dissertation wurde eigenständig und ohne unerlaubte Hilfe erarbeitet.

München, den 08.05.2018

Florian Anton Gegenfurtner

Dissertation eingereicht am:	08.05.2018
1. Gutachter:	Prof. Dr. Stefan Zahler
2. Gutachterin:	Prof. Dr. Angelika M. Vollmar
Mündliche Prüfung am:	12.06.2018

Meinen Eltern

Contents

Contents

Table of Contents

1	Abstract	1
2	Introduction	3
2.1	Angiogenesis in health and disease	3
2.1.1	Basic aspects of angiogenesis	3
2.1.2	Pathophysiological role of angiogenesis	3
2.2	Mechanosensitive gene regulation: feel the force	4
2.2.1	General mechanisms and physiological relevance of mechanosensing	4
2.2.2	The MRTF-SRF axis: a direct sensor of actin polymerization.....	5
2.2.3	The Hippo-YAP/TAZ pathway: a major mechanosensitive hub	6
2.2.4	MRTF and YAP in angiogenesis: happy together?	7
2.3	Nuclear actin and its novel role as a transcriptional regulator	7
2.3.1	Actin in the nucleus: an emerging field of research	7
2.3.2	Monomeric nuclear actin acts as a transcriptional all-rounder.....	8
2.4	Tools to study mechanosensitive signaling in endothelial cells	9
2.4.1	Natural actin binding compounds: the pharmacological toolbox in actin research	9
2.4.2	Micropatterning allows to study the cytoskeleton in a defined microenvironment....	10
2.5	Aim of the study	11
3	Results I: Regulation of MRTF-A and YAP in angiogenesis	13
3.1	Mechanical aspects of MRTF-A and YAP activity in HUVEC	13
3.1.1	Design of micropatterns to study mechanosensitive signaling cues	13
3.1.2	Cell-cell contacts regulate subcellular localization of MRTF-A and YAP	14
3.1.3	MRTF-A and YAP activity correlates with the provided adhesive surface area.....	16
3.1.4	Influence of cell shape on nuclear levels of MRTF-A and YAP.....	17
3.2	MRTF-A and YAP underlie different regulatory kinetics in HUVEC	18
3.2.1	MRTF-A translocates during cell migration on dumbbell-shaped micropatterns	18
3.2.2	Translocation kinetics of MRTF-A and YAP in response to fluid shear stress.....	19
3.3	Regulation of MRTF-A and YAP in angiogenic model systems	21
3.3.1	Spatiotemporal differences in MRTF-A and YAP activity during tube formation	21
3.3.2	Retinal whole-mount stainings: expression patterns of MRTF-A and YAP <i>in vivo</i>	22
4	Results II: Targeting of endothelial mechanosensing with actin binding compounds ..	24
4.1	Actin binding compounds regulate endothelial gene transcription	24
4.1.1	Transcriptional profiling of actin binding compounds	24

Contents

4.1.2	Influence on chromatin organization and epigenetic modification.....	27
4.1.3	Influence on polymerase function and rRNA synthesis	28
4.2	Effects of actin binding compounds on nuclear actin	29
4.2.1	Visualization of nuclear actin with different actin probes	29
4.2.2	Miuraenamides A and Latrunculin B bidirectionally shift nuclear actin levels	31
4.2.3	Influence of actin binding compounds on intranuclear polymerization state	32
4.3	Effects of actin binding compounds on mechanosensitive pathways.....	35
4.3.1	Influence of Miuraenamides A on MRTF-A and YAP subcellular localization	35
4.3.2	Promotor activation and MRTF-A / YAP target gene expression.....	36
4.3.3	Role of AMOTp130 in linking F-actin levels to YAP activity.....	37
5	Discussion.....	41
5.1	MRTF and YAP: the unequal twins	41
5.1.1	MRTF and YAP share microenvironmental triggers.....	41
5.1.2	A question of time: how kinetics make the difference	42
5.1.3	Master regulator or one out of many? The relationship between actin and YAP	44
5.2	Actin polymerizers and mechanosensing: surprising selectivity.....	45
5.2.1	Miuraenamides A reveals the difference between MRTF and YAP.....	45
5.2.2	Actin binding compounds as cell biological tools: chances and pitfalls.....	46
5.3	Actin binding compounds predominantly act in the cytoplasm	47
5.3.1	Nuclear actin and transcription: a matter of concentration?.....	47
5.3.2	Transcriptional effects of actin binding compounds: The cytoplasm sets the tone	47
5.4	Outlook and future perspectives.....	48
5.4.1	Transcriptional targets beyond MRTF	48
5.4.2	Temporal control of microadhesive surfaces	49
5.4.3	Let there be light: a route for selective targeting of nuclear actin	49
5.5	Summary and Conclusion.....	50
6	Material and Methods.....	52
6.1	Materials.....	52
6.1.1	Compounds.....	52
6.1.2	Chemicals and reagents	52
6.1.2.1	Antibodies.....	54
6.1.2.2	Buffers and solutions.....	54
6.1.3	Technical equipment.....	56
6.1.4	Consumables	56
6.2	Methods.....	57

Contents

6.2.1	Cell culture.....	57
6.2.1.1	Cell lines and culture media.....	57
6.2.1.2	Cell counting and passaging.....	57
6.2.2	Microcontact printing	57
6.2.3	Confocal Imaging	58
6.2.3.1	Immunofluorescence stainings.....	58
6.2.3.2	Visualization of nuclear actin.....	59
6.2.3.3	Nuclear run on assays.....	59
6.2.3.4	Single cell F- / G-actin ratios	59
6.2.3.5	DNase I chromatin digestion	59
6.2.4	Angiogenesis assays	60
6.2.4.1	Tube formation assay	60
6.2.4.2	Retinal whole-mount stainings.....	60
6.2.5	Plasmids and transfections.....	60
6.2.6	Live cell imaging.....	61
6.2.6.1	Cell migration.....	61
6.2.6.2	Perfusion Assay.....	61
6.2.7	Reporter gene assay.....	62
6.2.8	Duolink proximity ligation assay.....	62
6.2.9	Western blot.....	62
6.2.9.1	Sample preparation.....	62
6.2.9.2	SDS-PAGE.....	62
6.2.9.3	Protein transfer and detection	63
6.2.10	Immunoprecipitation (Co-IP).....	63
6.2.11	Quantitative real-time PCR and primers	63
6.2.11.1	Sample preparation	64
6.2.11.2	Primers.....	64
6.2.12	Transcriptomic analysis	64
6.2.12.1	Sample generation.....	64
6.2.12.2	Data processing and analysis.....	65
6.2.13	FCS.....	65
6.2.14	RICS	66
6.2.15	Statistical analysis	68
7	References	70
8	Appendix	78
8.1	Supplementary Figures	78

Contents

8.2	List of Figures and Tables	81
8.2.1	Figures	81
8.2.2	Tables	82
8.3	Abbreviations.....	82
8.4	List of Publications	84
8.5	Scientific presentations.....	85
8.5.1	Oral presentations	85
8.5.2	Poster presentations	85
8.6	Associated master and bachelor theses	85
8.7	Acknowledgements.....	86

Abstract

1 Abstract

Angiogenesis is a complex developmental process that requires a coordinated migration and morphological adaptation of endothelial cells. During blood vessel sprouting, endothelial cells need to orchestrate biochemical signals alongside with mechanical guidance cues originating from the cellular microenvironment. Due to the pathophysiological relevance of angiogenesis, the relevant biochemical signaling pathways and associated growth factors have been well characterized over the past decades. However, the regulatory aspects underlying mechanosensing in angiogenesis are poorly understood to date. Recent work promoted the two actin-dependent transcription factors MRTF and YAP as potential key players in regulating vessel growth in response to cytoskeletal remodeling.

In the first part of this thesis, a micropatterning approach was used to dissect the regulatory triggers of MRTF and YAP in endothelial cells. By mimicking microenvironmental aspects of angiogenesis within a spatiotemporally controllable experimental setting, changes in the provided adhesive area and the loss of cell-cell contacts were identified as key regulatory parameters regarding MRTF and YAP transcriptional activity in HUVEC. In contrast, endothelial cell shape only marginally affected nuclear levels of both transcription factors at steady state conditions. By analyzing the nuclear redistribution of MRTF and YAP under laminar shear stress conditions and during cell migration across dumbbell-shaped microstructures, it was furthermore demonstrated that MRTF and YAP exhibit differential activation kinetics. The resulting regulatory concept was successfully recapitulated in angiogenic model systems *in vitro* and *in vivo*.

In the second part of the project, the influence of natural actin binding compounds on gene transcription, in particular regarding MRTF and YAP activity, was investigated. It was shown that the actin stabilizer Miuraenamides A and the destabilizing compound Latrunculin B adversatively shift the concentration of nuclear actin. However, intranuclear aspects of transcriptional regulation remained largely unaffected by either compound, thus pointing to the direction that actin binding compounds predominantly regulate transcription via the cytoplasm. The polymerizing compound Miuraenamides A was subsequently identified as an inducer of MRTF nuclear translocation and SRF target gene expression. In contrast, the transcription factor YAP could not be activated by compound-induced actin polymerization. Mechanistically, this was owed to the failing abrogation of AMOTp130-mediated YAP inhibition through Miuraenamides A.

In sum, the present work provides a characterization of the regulatory aspects and functional implications underlying MRTF and YAP activity in endothelial cells. It further promotes natural actin binding compounds as a valuable tool to bidirectionally shift nuclear actin levels and to selectively target actin-dependent signaling pathways.

Introduction

2 Introduction

2.1 Angiogenesis in health and disease

2.1.1 Basic aspects of angiogenesis

Being required for the transport of nutrients, oxygen and biochemical messenger substances such as hormones, blood vessels are a fundamental part of the human body and most other animal organisms. The blood stream further provides a gateway for immune cells and contributes to the maintenance of body temperature and pH homeostasis ¹. In the developing embryo a *de novo* circulatory system is formed by endothelial precursor cells, so-called angioblasts, in a process termed vasculogenesis. In contrast, angiogenesis describes the sprouting of blood vessels from a pre-existing vascular network, which is physiologically relevant in adult tissue during hypoxic adaptation, wound healing and throughout the ovarian cycle ². The angiogenic process is characterized by a spatiotemporally coordinated migration and morphological adaptation of endothelial cells (ECs), which form the inner layer of blood vessels. In response to extracellular growth factors such as VEGFs (vascular endothelial growth factors), ECs start to locally degrade the surrounding basement membrane by secretion of matrix metalloproteases. To ensure a coordinated sprout formation ECs subsequently differentiate into guiding, filopodia-rich tip cells and lumen forming stalk cells. This process is tightly regulated by a negative feedback mechanism involving VEGF signaling and the closely associated DLL4-Notch pathway ³.

2.1.2 Pathophysiological role of angiogenesis

Abnormal angiogenesis is a promoting and sometimes causative factor in various diseases. Insufficient or inadequate blood vessel formation provokes ischemia in neurodegenerative diseases, diabetes and myocardial infarction. On the other hand, excessive angiogenesis and neovascularization contributes to inflammatory and retinal diseases, such as age-related macular degeneration ². Moreover, the increased energy demand of malignant tissues triggers tumor-associated vascular growth, making angiogenesis a hallmark of cancer development and progression ⁴.

The pathophysiological relevance of angiogenesis gave rise to several targeting approaches and the development of both pro- and anti-angiogenic pharmaceuticals ⁵. Although promising candidates, such as the VEGF decoy receptor Aflibercept, have been successfully brought into clinical application, compensatory mechanisms and a potentially pro-metastatic long-term response were severely limiting the initial expectations in recent years ⁶. Thus, the evaluation

2 Introduction

of novel targeting approaches beyond the inhibition of angiogenic growth factor signaling is of significant interest.

2.2 Mechanosensitive gene regulation: feel the force

2.2.1 General mechanisms and physiological relevance of mechanosensing

In order to successfully establish, and to guide vascular sprouts, endothelial tip and stalk cells need to integrate biochemical signals alongside with mechanical cues originating from a constantly changing microenvironment. The translation of mechanical information into an adapted gene expression profile, a process termed mechanosensing, is of fundamental importance not only in angiogenesis but also during other developmental events such as early embryogenesis and nervous system development⁷.

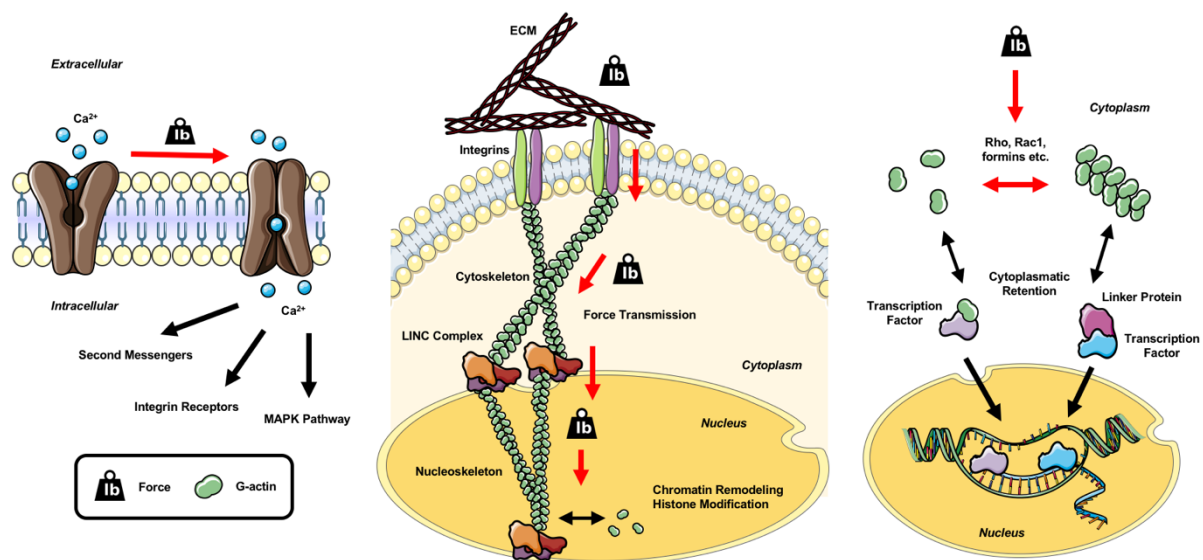


Figure 2-1 | Principle mechanisms of mechanosensitive signal transduction

To enable a precisely regulated transcription of mechanosensitive genes, mechanical information is transmitted to the nuclear compartment via a variety of different mechanisms. First, extracellular physical force can alter the conformation of nuclear pores or membrane proteins, such as mechanosensitive ion channels and phospholipases, which subsequently activate classical downstream effectors like MAPK signaling^{8,9}. Second, the nuclear envelope is coupled to the cytoskeleton via so-called LINC (linker of the nucleoskeleton and the cytoskeleton) complexes^{10,11}. The resulting structural network acts as a direct force transmission route, which ultimately regulates chromatin organization in response to mechanical stress and nuclear deformation¹². A third option is provided by the family of actin-dependent, mechanosensitive transcription factors¹³. In principle, the subcellular localization

2 Introduction

of these proteins is coupled to the polymerization state of actin. Thus, they are either sensitive to the amount of (globular) G-actin or that of (filamentous) F-actin. Two prominent examples of actin-dependent, mechanosensitive transcription factors are introduced in the following sections.

2.2.2 The MRTF-SRF axis: a direct sensor of actin polymerization

Serum response factor (SRF) was first identified in 1986 by the group of Richard Treisman, who described it as a protein mediating the transcriptional response to serum factors¹⁴. In the following years, it was found that actin dynamics are one of the key regulators of SRF activity¹⁵. The missing link between actin polymerization and SRF activity was finally established by the identification of myocardin-related transcription factors (MRTFs, also named MKL1 or MAL) in 2003¹⁶. Mechanistically, the two MRTF isoforms MRTF-A and MRTF-B bind to G-actin via N-terminal RPEL motifs and are thereby sequestered in the cytoplasm.

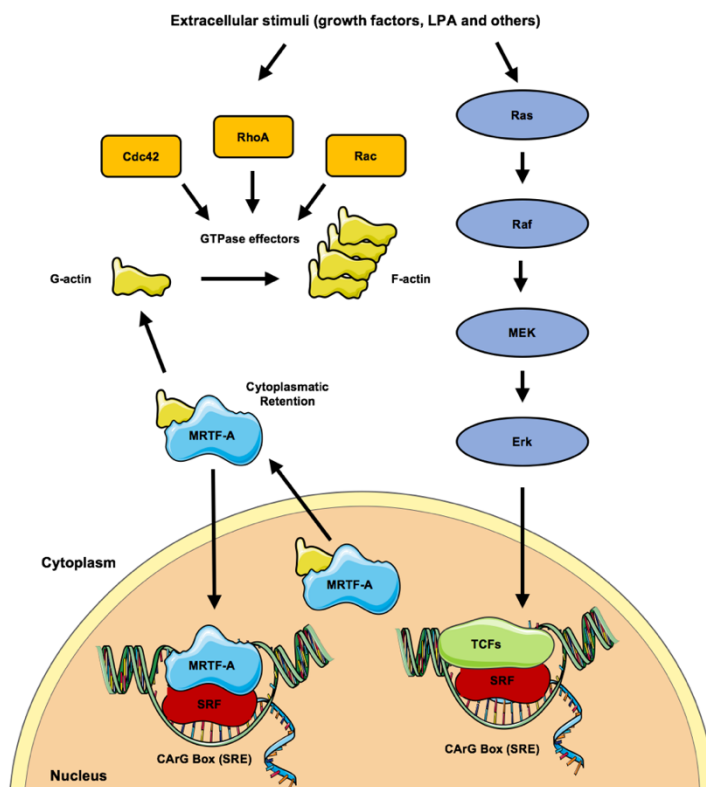


Figure 2-2 | The serum response factor pathway

Upon actin polymerization the binding to G-actin is released and MRTF translocates to the nucleus (Fig. 2-2). Being a transcriptional co-activator, MRTF enhances the activity of SRF at the serum response element (SRE) promoter. In 2007, the Vartiainen lab proved that subcellular localization and activity of MRTF is regulated by both cytoplasmatic and nuclear actin¹⁷. Furthermore, it was found that binding of nuclear G-actin triggers MRTF nuclear export. In turn, nuclear actin polymerization, and therefore depletion of nuclear G-actin, stimulates MRTF-SRF activity¹⁸.

As depicted in Fig. 2-2, MRTFs are not the only coactivators of SRF, since ternary complex factors (TCFs) compete with MRTFs for the binding of SRF at CArG domains. However, TCFs are activated downstream of the small GTPase Ras and therefore not considered as mechanosensitive transcription factors.

2 Introduction

A systematic target gene analysis in 2006 has identified the SRF pathway as a fundamental regulator of cytoskeletal and adhesive genes^{19,20}. Therefore, SRF signaling plays an important role in cellular processes associated to growth, migration and development²¹⁻²⁴. The pathophysiological aspects of inadequate SRF activity, in particular concerning angiogenesis, are described in section 2.2.4.

2.2.3 The Hippo-YAP/TAZ pathway: a major mechanosensitive hub

The Hippo pathway was initially discovered in genetic mosaic screens for tumor suppressor genes in *Drosophila*²⁵⁻²⁷. In the following years, it became clear that the Hippo pathway is a highly conserved kinase cascade regulated similarly in insects and mammals. As schematically shown in Fig. 2-3, the mammalian Hippo kinase ortholog MST1/2 acts as an upstream regulator of the serine/threonine kinases Lats1 and 2. In turn, Lats1/2 phosphorylate the two closely related transcription factors YAP (yes-associated protein) and TAZ

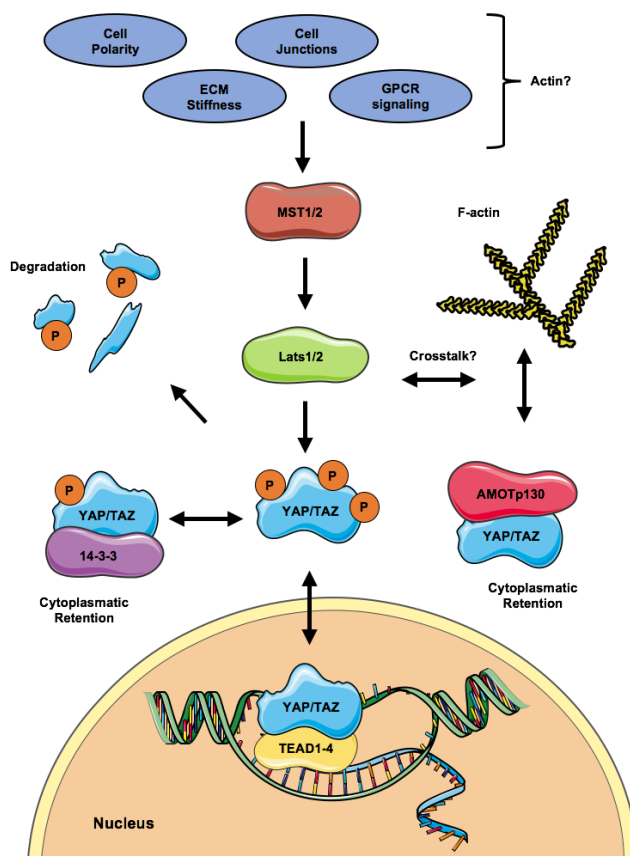


Figure 2-3 | Upstream regulators of mammalian YAP/TAZ

(transcriptional coactivator with PDZ-binding motif), thereby inhibiting their nuclear translocation and the subsequent expression of target genes. Mechanistically, the cytoplasmic sequestration of phosphorylated YAP/TAZ is mediated by an interaction with 14-3-3 proteins.

YAP and TAZ turned out to be fundamental regulators of organ size, cell differentiation, proliferation and apoptosis^{28,29}. However, although the core kinase cascade of Hippo-YAP/TAZ is well described, the relevant extracellular regulators are poorly characterized. The actin cytoskeleton has recently moved into the focus of interest, since it could provide a common downstream element

integrating both G-protein coupled receptors³⁰ and cell polarity based signaling³¹. In addition, a regulatory mechanism independent from canonical Hippo signaling is being discussed as well. In any case, actin appears to be one, if not the key upstream regulator of Hippo-YAP/TAZ, thus rendering this signaling cascade a major mechanosensitive pathway.

2 Introduction

2.2.4 MRTF and YAP in angiogenesis: happy together?

As mentioned before, angiogenesis is a complex developmental process that involves the coordinated migration and proliferation of endothelial cells. Since cell division and movement fundamentally rely on actin dynamics, it is reasonable to assume that mechanosensitive transcription factors influence angiogenesis.

Several studies in the lab of Cláudio A. Franco have demonstrated that MRTF-SRF is required for sprouting angiogenesis³², vascular branching³³ and tip cell invasion³⁴. In turn, an endothelial ablation of MRTF-SRF in adult mice provokes intracerebral hemorrhagic stroke³⁵. In a similar experimental setting, vascular disease phenotypes were observed in murine retinae³⁶. Similar to MRTF-SRF, the Hippo-YAP/TAZ cascade is also functionally required for angiogenesis. For instance, Wang et al. have recently demonstrated that YAP and TAZ act upstream of VEGF-VEGFR2 signaling³⁷. Moreover, YAP contributes to vessel maintenance³⁸ and regulates the cell contact-mediated expression of angiopoetin-2³⁹.

Accumulating evidence suggests that the actin-dependent, mechanosensitive transcription factors MRTF and YAP are required for angiogenesis. However, most of these studies focus on knock-out settings and their functional consequences. In turn, little is known about the regulatory aspects underlying MRTF and YAP activity in endothelial cells. Moreover, the common influence of actin polymerization on MRTF and YAP raises the question whether these two pathways act in concert or serve distinct functions in the regulation of angiogenesis⁴⁰. Both of these aspects need to be answered in order to evaluate the potential of MRTF and YAP as possible target structures for pro- or antiangiogenic therapy strategies.

2.3 Nuclear actin and its novel role as a transcriptional regulator

2.3.1 Actin in the nucleus: an emerging field of research

From a historical perspective, actin was long thought to be exclusively present in the cytoplasmic compartment. As it is one of the most abundant proteins in the cell, the potential identification of actin in nuclear extracts or intranuclear protein complexes was prone to cytoplasmic contamination. Moreover, the physiological significance of *in vitro* findings was frequently questioned⁴¹. Due to progress in the visualization of nuclear actin^{42,43}, the research field has picked up speed in recent years. Today, it is known that cytoplasmic β -actin monomers enter the nucleus in an active transport process mediated by importin-9⁴⁴. Owing to the lack of a nuclear localization sequence (NLS), actin is only imported when bound to NLS-containing cofactors. Conversely, excess actin is exported from the nuclear compartment in a profilin-bound state via exportin-6⁴⁵.

2 Introduction

Under specific conditions, such as growth factor stimulation⁴⁶, or in response to DNA damage^{47,48}, nuclear actin can polymerize into filamentous structures. Moreover, intranuclear actin polymerization has been shown to stabilize the nucleus against gravity in *Xenopus* oocytes⁴⁹. However, classical cytoplasmatic roles of actin, such as cell migration or vesicular transport, cannot be applied to the nucleus. Therefore, the nuclear role of polymerized actin and F-actin binding proteins, such as myosin I, remains largely elusive to date⁵⁰.

Other than its polymerized counterpart, monomeric nuclear actin is fundamentally required for gene expression⁵¹. The contribution of actin monomers to transcriptional regulation will be introduced in the following section.

2.3.2 Monomeric nuclear actin acts as a transcriptional all-rounder

As described in section 2.2, cytoplasmatic actin can serve as a force-sensitive element that translates extracellular mechanical information into biochemical signals, and ultimately into an adapted gene expression profile. However, the influence of actin on gene transcription is not restricted to the cytoplasm. Connected to its long-debated presence in mammalian cell nuclei (section 2.3.1), nuclear actin has begun to emerge as a versatile regulator of gene expression. The involvement of nuclear actin in transcriptional regulation was first suggested in the early 1980s⁵². In 1984, Scheel et al. microinjected actin binding proteins into the nuclei of living *Pleurodeles* oocytes and demonstrated an inhibition of transcription⁵³. In the years to follow, it became clear that actin monomers are subunits of ATP-dependent chromatin remodeling complexes, such as INO80, BAF and SWR1^{54,55}. Although the precise role of actin in these complexes is still unclear, it has been shown that actin forms a functional module with the two actin-related proteins Arp4 and Arp8⁵⁶. Being closely associated with chromatin remodeling, also epigenetic histone modification is influenced by nuclear actin. Initially, actin was identified as a subunit in the NuA4 histone acetyltransferase complex in yeast⁵⁷. More recently, studies reported a role of nuclear actin in regulating class I histone deacetylases⁵⁸.

Next to its influence on chromatin-associated processes, a second feature of monomeric nuclear actin is delineated by its association with RNA polymerases. In 2004, two independent groups reported that nuclear actin binds RNA polymerases I, II and III⁵⁹⁻⁶¹. Apart from its functional requirement for initiation and elongation⁶², actin is also bound to a subset of pre-mRNA binding proteins⁶³, thereby covering the entire transcriptional process from gene activation to nuclear export of the mature mRNA.

2 Introduction

2.4 Tools to study mechanosensitive signaling in endothelial cells

2.4.1 Natural actin binding compounds: the pharmacological toolbox in actin research

Actin binding compounds are a frequently used tool in cell biology. Compounds with cytotoxic activity against the cytoskeleton have been isolated from different organisms ranging from fungi, algae, bacteria and marine sponges to terrestrial plants. Thus, the vast majority of this substance class is composed of natural products⁶⁴.

Actin targeting compounds are classified into filament-destabilizing (depolymerizing) and filament-stabilizing (polymerizing) compounds. The latter class almost exclusively comprises cyclic peptides and depsipeptides. A well-known example of this group is phalloidin, a cyclic peptide synthesized by the 'Death Cap' mushroom *Amanita phalloides*⁶⁵. To stabilize actin filaments in live cells, the membrane permeable compound Jasplakinolide was preferably used. In 2006, Miuraenamides, a cyclic depsipeptide isolated from the halophilic myxobacterium *Paraliomyxa miuraensis*, was discovered as a novel, more potent alternative to the structurally related Jasplakinolide^{66,67}.

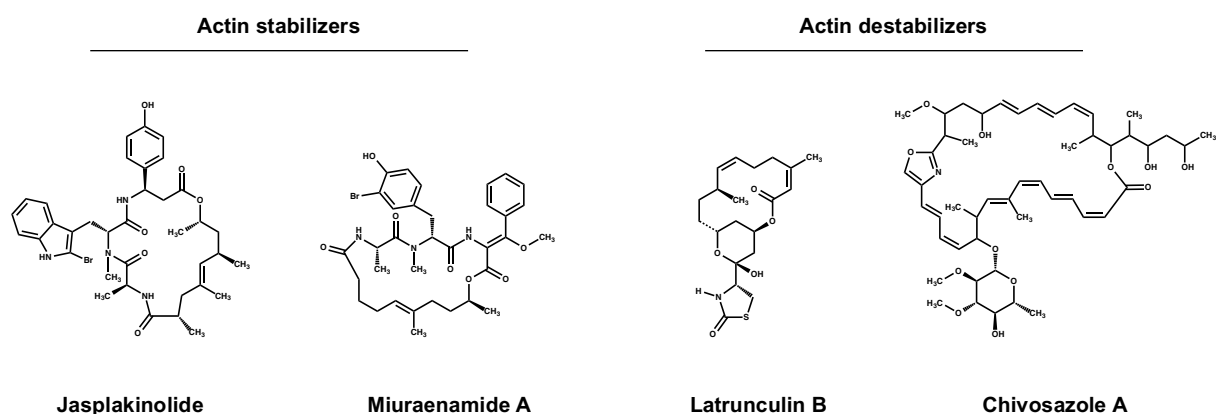


Figure 2-4 | Chemical structures of different natural actin binding compounds

Other than actin stabilizing compounds, depolymerizing substances are a heterogeneous class which follows different modes of filament destabilization. The most widely used depolymerizing compound is Latrunculin B, a thiazolidine ring containing substance isolated from the Red Sea sponge *Negombata magnifica*⁶⁸. Mechanistically, Latrunculin B binds to the ATP-binding cleft of actin, thereby stabilizing the monomeric state⁶⁴. Other examples of actin depolymerizing compounds include the barbed end targeting substance Swinholide A⁶⁹ and the macrolides Chivosazole A and F⁷⁰.

Actin binding compounds are well-characterized in terms of their basic functional effects on cell migration, proliferation or apoptosis. However, their influence on mechanosensitive gene expression remains largely elusive to date. In particular, it has not been described whether

2 Introduction

these compounds are able to regulate mechanosensitive transcription factors or actin-dependent transcriptional processes in the nucleus.

2.4.2 Micropatterning allows to study the cytoskeleton in a defined microenvironment

The cellular microenvironment is a highly structured biological system providing numerous chemical and mechanical signaling cues. Parameters such as extracellular matrix (ECM) architecture, composition and stiffness are sensed by the cell during integrin- or cadherin-based cell adhesion⁷¹. As a consequence, the actin cytoskeleton is remodeled to adapt to the surrounding ECM. Due to their uniform and static properties, standard cell culture surfaces can hardly reflect a given *in vivo* microenvironment⁷².

Micropatterning techniques have emerged as a novel possibility to study distinct aspects of cellular behavior in a tailored microenvironment. Although first micropatterning techniques were described decades ago, they only recently became available for broad application⁷². Besides laser- and photo-patterning based methods, microcontact printing provides an easy-to-access and thus widely used alternative (Fig. 2.5 and section 6.2.2).

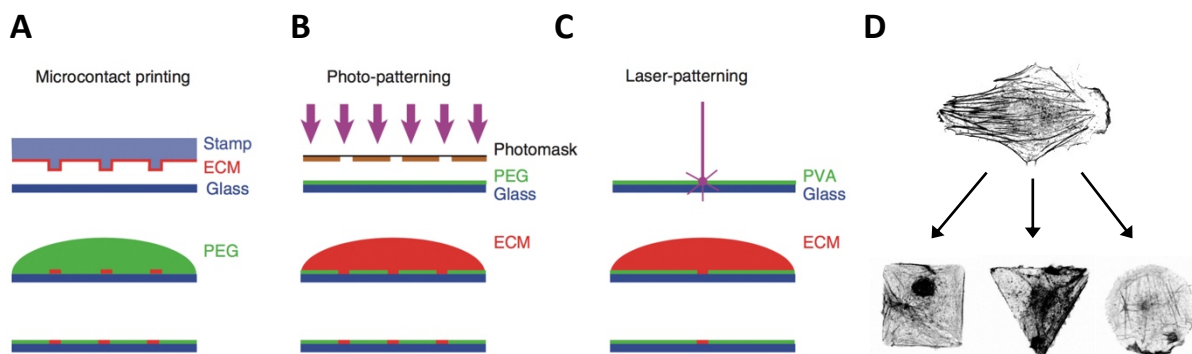


Figure 2-5 | Overview of different micropatterning techniques. (A) Microcontact printing: micro-features are transferred with ECM-coated polydimethylsiloxane (PDMS) stamps onto the uncoated surface of a cell culture dish. Intermediate spaces are blocked with a hydrophilic polymer. **(B)** Photo-patterning: the micropattern is introduced by selective detachment of the hydrophilic polymer under light exposure in combination with a photomask. **(C)** Laser-patterning: Instead of a photomask (B), pulsed laser is used for polymer detachment. **(D)** Single Endothelial cells in unconfined culture (top) or on microstructured surfaces (bottom).

Micropatterning approaches have been employed to study various aspects of endothelial cell morphology and functional behavior in the context of angiogenesis^{73,74}. For example, Vartanian et al. mimicked cell elongation in response to fluid shear stress by culturing ECs on stretched, rectangular patterns⁷⁵. In our lab, microcontact printing was used to simulate endothelial cell migration in low-adhesive, fibrillary matrices such as Collagen I⁷⁶. Due to their ability to spatiotemporally control microenvironmental parameters, microstructured surfaces provide an interesting experimental tool to study the regulation of mechanosensitive signaling pathways, such as MRTF-SRF or Hippo-YAP/TAZ.

2 Introduction

2.5 Aim of the study

Angiogenesis is crucially involved in the development and progression of cancer, the leading cause of death worldwide. The biochemical key players involved in blood vessel sprouting are well-characterized. However, the regulatory aspects and the targeting potential associated to mechanosensitive signaling pathways are poorly understood to date.

The aim of this study was to investigate the physiological regulation of the mechanosensitive transcription factors MRTF-A and YAP in endothelial cells. In addition, the influence of natural actin binding compounds on actin-dependent gene transcription and nuclear actin was investigated.

To provide a clear structure, the results section is subdivided into two parts.

Part I

The aim of the first project was to characterize the physiological regulation of MRTF and YAP in the context of angiogenesis. The precise goals can be described as follows:

- Design and validate a set of micropatterns to study the mechanosensitive regulation of MRTF-A and YAP in primary endothelial cells
- Elucidate the regulatory triggers and kinetics underlying MRTF-A and YAP activity in endothelial cells
- Verify the acquired data in angiogenic model systems

Part II

The aim of the second project was to evaluate the potential of actin binding compounds to target mechanosensitive gene regulation in endothelial cells. Therefore, the actin binding compounds Miuraenamide A and Latrunculin B were characterized according to their influence on the following aspects:

- Cytoplasmatic regulation of MRTF-A and YAP activity
- Actin-dependent transcriptional regulation in the nucleus
- Structural properties and concentration of intranuclear actin

Results

3 Results I: Regulation of MRTF-A and YAP in angiogenesis

3.1 Mechanical aspects of MRTF-A and YAP activity in HUVEC

3.1.1 Design of micropatterns to study mechanosensitive signaling cues

The sprouting of blood vessels is a mechanically complex process characterized by the simultaneous change of several cellular and microenvironmental parameters. In order to spatiotemporally dissect this process into controllable substeps, we designed the set of micropatterns depicted in Fig. 3-1A. A 2500 μm^2 sized microadhesive square, which roughly reflects the area that is normally occupied by unconfined endothelial cells in culture, was chosen as a common element present in every set of patterns.

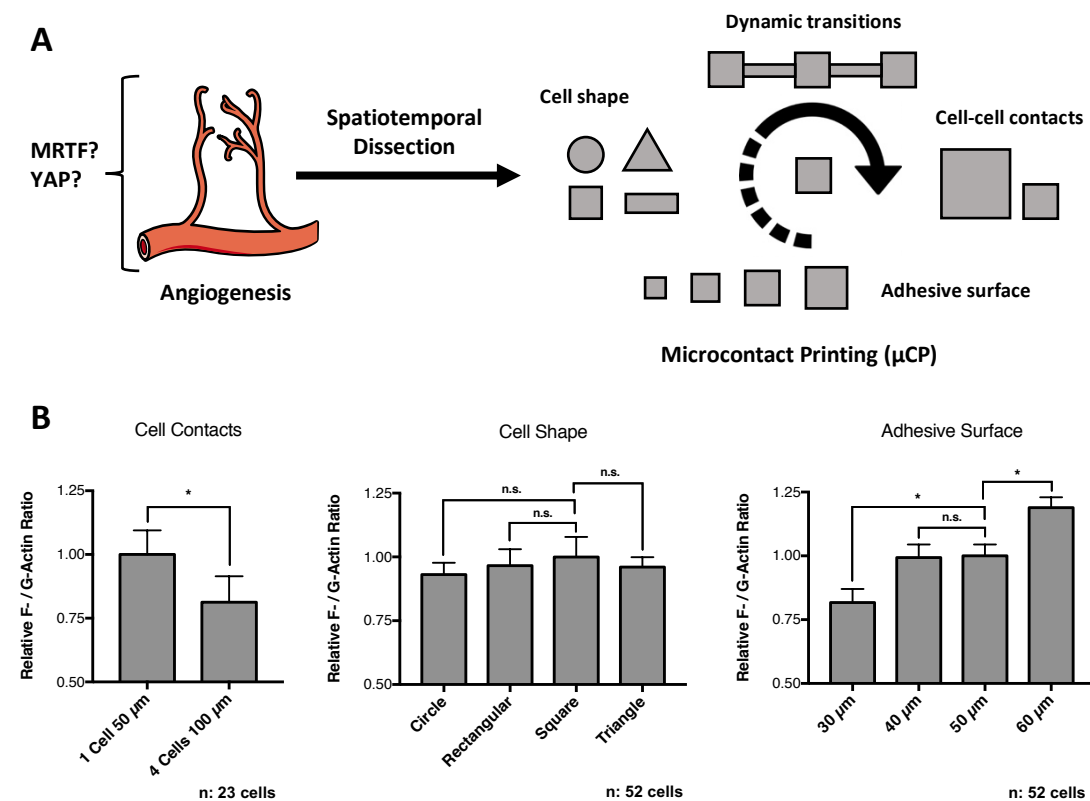


Figure 3-1 | Microcontact printing as a tool to study mechanosensitive signaling cues in endothelial cells.

(A) Based on a 50 x 50 μm square domain as a common starting point (center), four different sets of micropatterns were generated to study the regulatory triggers of MRTF-A and YAP in endothelial cells. (B) Different pattern geometries are associated with changes in cellular F- / G-actin ratio. Endothelial cells were cultured on the micropatterns depicted in (A) and after 20 h co-stained for F-actin (phalloidin) and G-actin (DNase I). F- / G-actin ratios were calculated in terms of total intensity relation between the phalloidin and DNase I signal and are expressed as normalized fractions of the 2500 μm^2 square present in each set. Statistical significance was determined by Sidak corrected one-way ANOVA test, $p < 0.05$.

3 Results I: Regulation of MRTF-A and YAP in angiogenesis

Starting from this reference square, nuclear levels of MRTF-A and YAP could subsequently be studied in response to defined alterations of cell morphology and extracellular parameters such as the provided adhesive surface area.

To ensure that the resulting patterns cover a size range that is capable of imposing distinct mechanical challenges on our cells, we analyzed the impact of pattern geometry on cellular F-actin / G-actin ratio via co-staining of both fractions with phalloidin and DNaseI^{77,78}. We found that, normalized to the reference square, F- / G-actin ratios varied between 80 - 120% within the designed set of micropatterns (Fig. 3-1B).

3.1.2 Cell-cell contacts regulate subcellular localization of MRTF-A and YAP

In order to analyze the impact of cell-cell contacts on endothelial MRTF-A and YAP activity, we cultured single endothelial cells on a 2500 μm^2 sized square and compared the nuclear levels of both transcriptions factors in immunostained cells to the respective activity on a four times larger square harboring four cells (Fig. 3-2A). A quantitative analysis of ≥ 30 cells for each of the two patterns revealed that both MRTF-A and YAP exhibit significantly reduced nuclear levels upon the formation of cell-cell contacts (Fig. 3-2B).

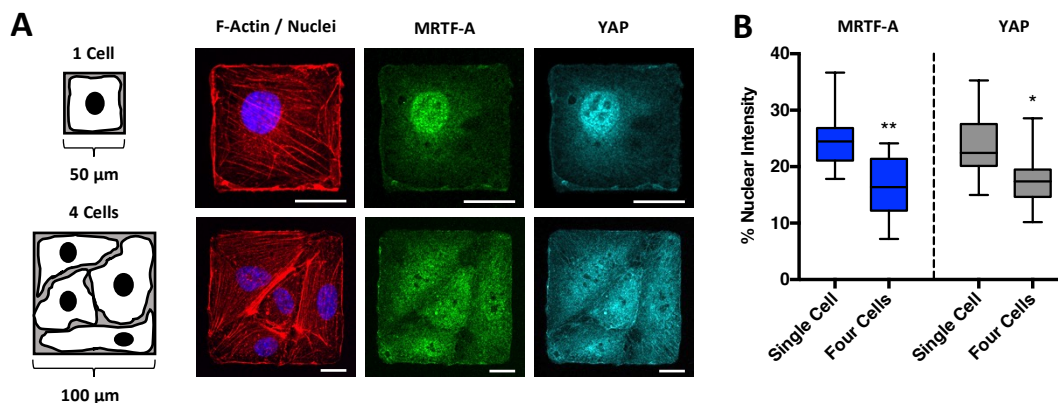


Figure 3-2 | Role of endothelial cell-cell contacts in regulating MRTF-A and YAP subcellular localization. (A) HUVEC were seeded onto the micropatterns depicted on the left and after 20 h co-stained for F-actin, MRTF-A and YAP. Bars = 35 μm . (B) Nuclear levels of MRTF-A and YAP in terms of nuclear intensity divided by total cellular intensity were quantified in ≥ 30 cells for each of the two patterns in three independent experiments. Data is presented as box and whiskers (min to max) plot, significance determined by student t-test, $p < 0.05$.

To further assess the importance of cell-cell contacts in regulating MRTF-A and YAP activity, we analyzed the contribution of VE-cadherin, a key component of endothelial adherens junctions, to this process. For the experiment shown in Fig. 3-3A, HUVEC were grown to confluency and subsequently treated with EGTA to disrupt existing Ca^{2+} dependent cell-cell junctions. Before re-addition of Ca^{2+} , the cells were incubated with an antibody targeted against the extracellular domain of VE-cadherin (anti VE-Cad^{ECD}), thereby inhibiting a reestablishment

3 Results I: Regulation of MRTF-A and YAP in angiogenesis

of disrupted adherens junctions. As it is shown by the quantification depicted in Fig. 3-3B, preincubation with anti VE-Cad^{ECD} clearly enhanced nuclear translocation of MRTF-A and YAP after re-addition of Ca²⁺ compared to untreated control cells. However, we observed different kinetics in the response of both transcription factors to restored Ca²⁺ levels in untreated control cells (Fig. 3-3B). This was particularly evident after 60 min, when MRTF-A was localized predominantly cytoplasmatic in the majority of control cells, while YAP was still localized in the nuclear compartment.

In summary, these results suggest that endothelial cell-cell contacts in general, and VE-cadherin containing junctions in particular, play a major role in regulating MRTF-A and YAP subcellular localization in endothelial cells.

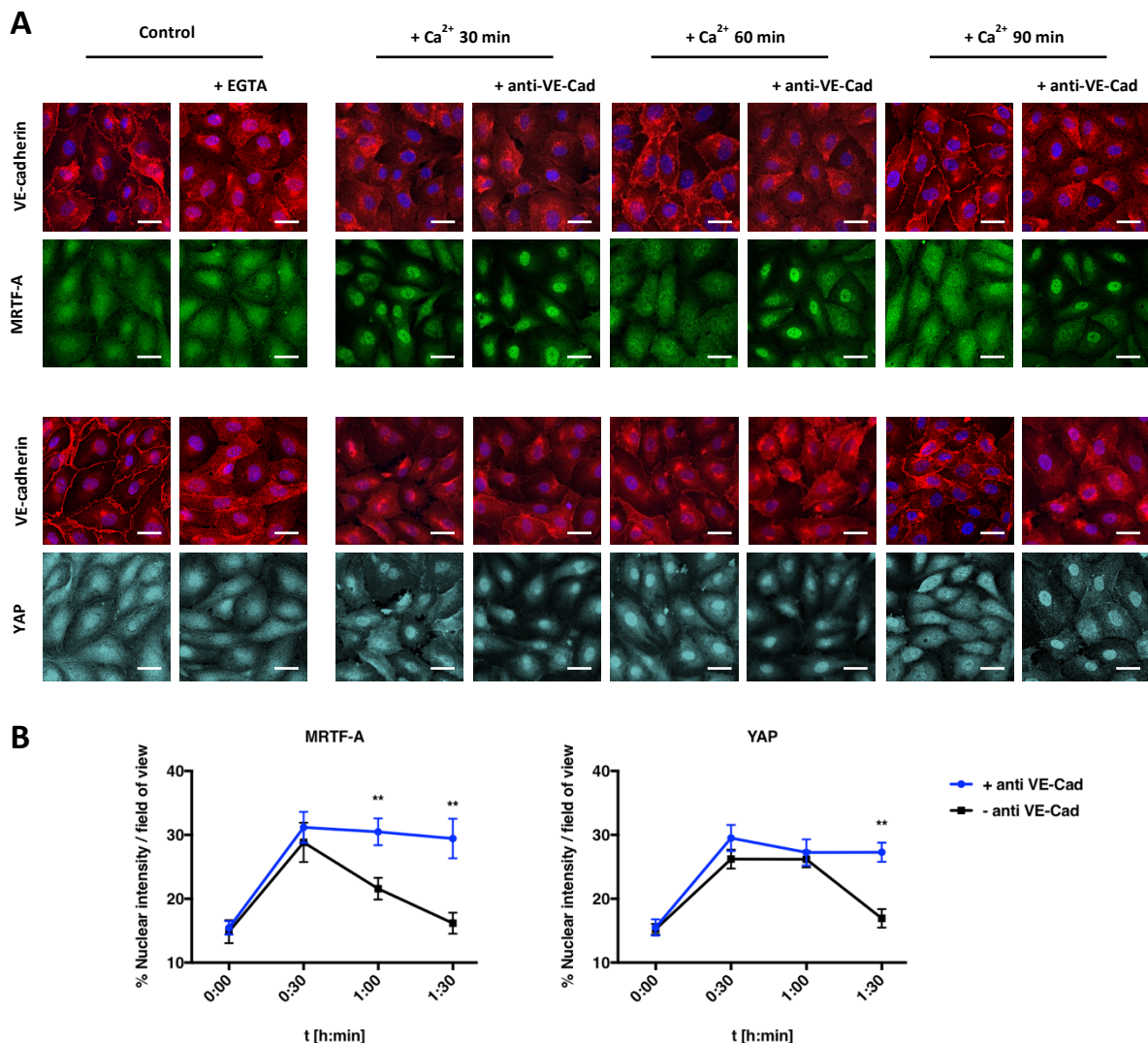


Figure 3-3 | VE-cadherins mediate the inhibitory effect of cell-cell contact formation on MRTF-A and YAP. (A) Confluent HUVEC were pre-treated with EGTA to disrupt VE-cadherin containing cell junctions (left panel). After EGTA removal and re-addition of Ca²⁺, cells were incubated with (+ anti VE-Cad) or without an antibody blocking the extracellular domain of VE-cadherin. Cells are stained for MRTF-A (top) or YAP (bottom). Bars = 35 μ m. (B) Nuclear levels of MRTF-A and YAP were quantified as % nuclear intensity per field of view in ≥ 5 pictures per setting and analyzed in ≥ 50 cells after 30, 60 and 90 min.

3 Results I: Regulation of MRTF-A and YAP in angiogenesis

3.1.3 MRTF-A and YAP activity correlates with the provided adhesive surface area

Having studied the impact of cell-cell contacts on MRTF-A and YAP subcellular localization (3.1.2), we went on to analyze how an alteration of the provided adhesive surface area might affect the regulation of both transcription factors. For this purpose, a set of four different microadhesive squares covering a size range from 900 to 3600 μm^2 was used. The activity of MRTF-A and YAP in terms of their relative nuclear intensities was analyzed in a minimum of 30 cells for each of the squares described in Fig. 3-4A. Regarding the subcellular localization of MRTF-A, we found a significant correlation between the provided adhesive surface area and relative nuclear signal intensities of this protein (Fig. 3-4B). The same tendency was observed for YAP, though slightly less pronounced.

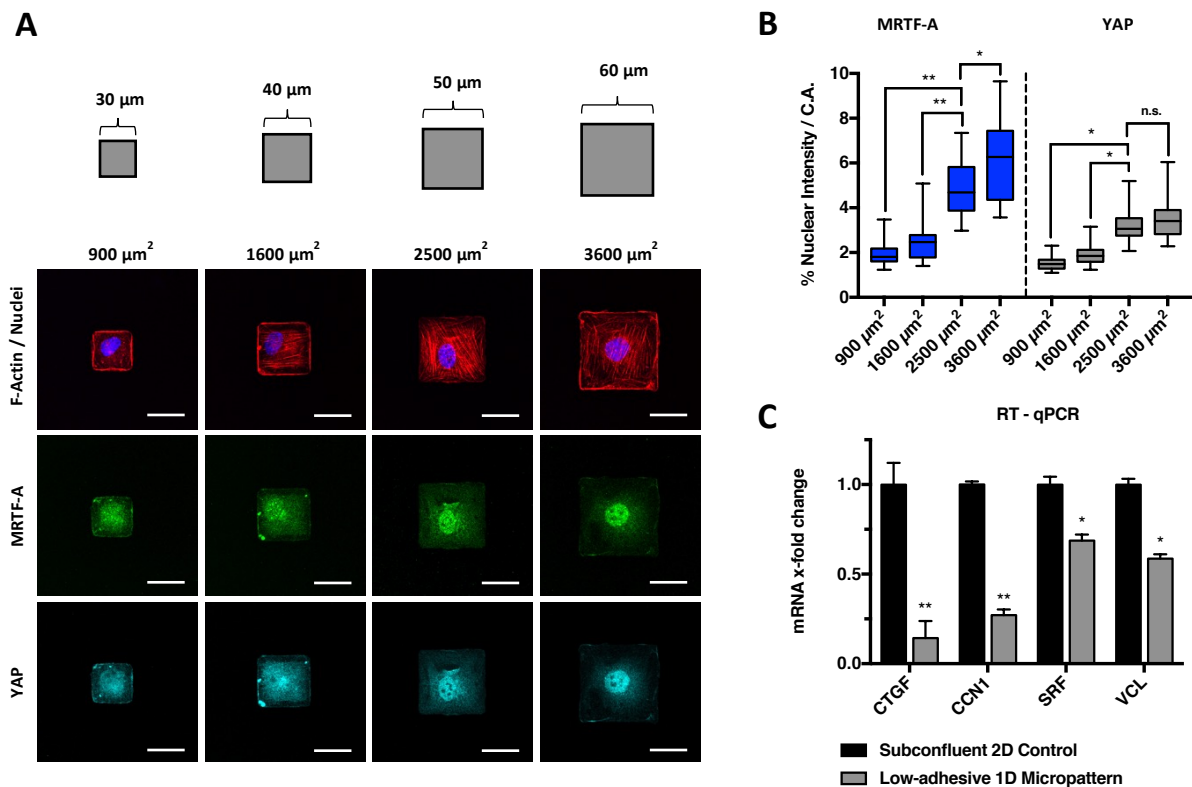


Figure 3-4 | Influence of adhesive surface area on MRTF-A and YAP subcellular localization in HUVEC. (A) HUVEC were seeded onto square micropatterns of varying surface areas ranging from 900 to 3600 μm^2 . After 20 h, cells were stained for F-actin, MRTF-A and YAP. Bars = 30 μm . **(B)** Nuclear levels of both transcription factors in terms of nuclear intensity divided by total cellular intensity were quantified in ≥ 30 cells derived from three independent experiments and normalized to the respective compartment area. Data is presented as box and whiskers (min to max) plot, statistical significance was determined by ordinary one-way ANOVA followed by Dunnett's multiple comparisons test. **(C)** Relative mRNA expression levels of prominent SRF and YAP / TAZ target genes were analyzed in HUVEC lysates collected from cells grown under normal 2D cell culture conditions and compared to cells grown on low-adhesive linear microtracks (3 μm line width). GAPDH was used as a housekeeper. Statistical significance was determined by student t-test, $p < 0.05$.

3 Results I: Regulation of MRTF-A and YAP in angiogenesis

To test whether an alteration of adhesive properties would result in an adapted expression of MRTF-A and YAP target genes, quantitative real-time PCR on four known SRF-MRTF-A and Hippo-YAP / TAZ targets was performed (Fig. 3-4C). In detail, we compared mRNA levels of sparsely cultured HUVEC with infinite spreading area to the expression levels of cells cultured on low-adhesive, narrow microtracks, which had been previously described in our lab ⁷⁶. Compared to the square patterns illustrated in Fig. 3-4A, which are sometimes occupied by multiple cells, the linear microtracks offer the advantage to collect lysates from a homogeneously low-adhesive cell population. In line with our findings for the nuclear levels of MRTF-A and YAP on differently sized squares, we found that mRNA levels were significantly reduced in cells grown on low-adhesive microtracks compared to cells in standard 2D cell culture (Fig. 3-4C).

Taken together, our results demonstrate that the adhesive properties of the microenvironment influence MRTF-A and YAP subcellular localization and transcriptional activity in endothelial cells. We further showed that there is a correlation between the provided adhesive area and nuclear levels of both transcription factors.

3.1.4 Influence of cell shape on nuclear levels of MRTF-A and YAP

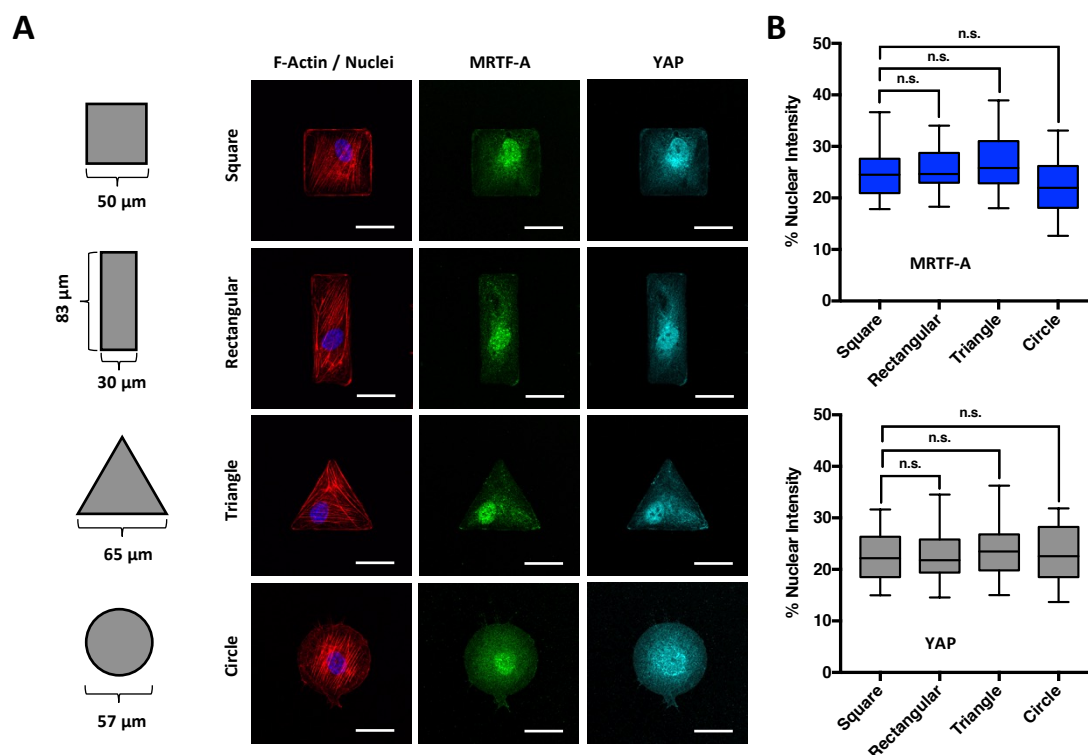


Figure 3-5 | Impact of cell shape variation on MRTF-A and YAP subcellular localization in HUVEC. (A) HUVEC were seeded onto 2500 μm² sized micropatterns of different geometries. After 20 h, cells were stained for F-actin, MRTF-A and YAP. Bars = 30 μm. (B) Nuclear levels of both transcription factors in terms of nuclear intensity divided by total cellular intensity were quantified in ≥ 30 cells in at least three independent experiments. Data is presented as box and whiskers (min to max) plot, statistical significance was determined by ordinary one-way ANOVA followed by Dunnett's multiple comparisons test.

3 Results I: Regulation of MRTF-A and YAP in angiogenesis

During sprouting angiogenesis, endothelial tip cells adapt a distinct morphology, which is characterized by the presence of filopodia and a stretched cellular shape. To examine the impact of different cell shapes on subcellular localization of MRTF-A and YAP, we used a set of four 2500 μm^2 sized microdomains with different geometrical shapes (Fig. 3-5A). We found that nuclear levels of MRTF-A and YAP on either of these microstructures varied in a small range of 20 – 30% (Fig. 3-5A). However, none of the applied shapes induced a significant difference in MRTF-A and YAP subcellular localization compared to the control square pattern. We therefore conclude that, unlike the presence of cell-cell contacts or the provided adhesive surface area, cell shape plays a minor role in regulating the activity of MRTF-A and YAP in endothelial cells.

3.2 MRTF-A and YAP underlie different regulatory kinetics in HUVEC

3.2.1 MRTF-A translocates during cell migration on dumbbell-shaped micropatterns

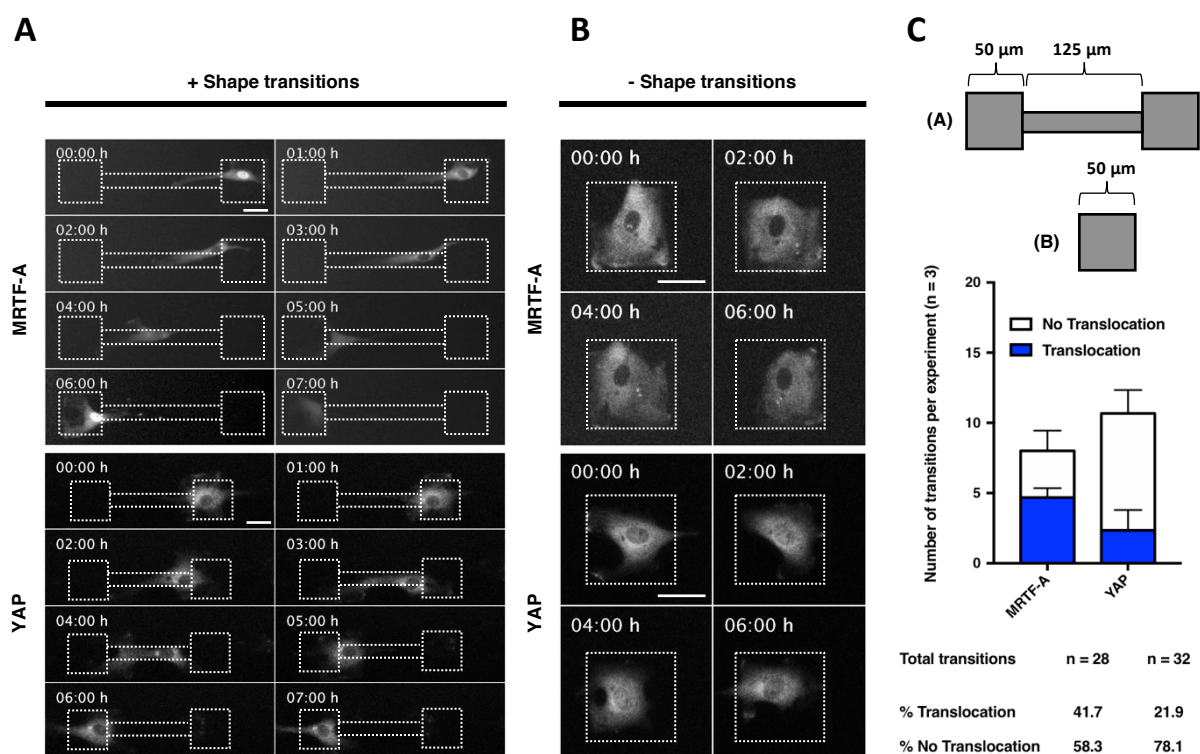


Figure 3-6 | Translocation dynamics of MRTF-A and YAP during migration on dumbbell-shaped micropatterns. Subconfluent HUVEC were transiently transfected with MRTF-A-GFP or hYAP1-GFP harboring expression vectors and after 24 h seeded either onto a micropattern composed of interconnected squares (**A**) or onto unconnected control patterns (**B**). Cell migration was subsequently analyzed by time-lapse imaging over the indicated time spans. Bars = 30 μm . (**C**) *Top*: Pattern geometries of the experiments depicted in (**A**) and (**B**). *Bottom*: Absolute and relative translocation events of MRTF-A and YAP. Relative numbers are normalized to the total number of shape transitions.

3 Results I: Regulation of MRTF-A and YAP in angiogenesis

The results described in section 3.1 suggest that MRTF-A and YAP react very similar to static microenvironmental conditions. However, this does not imply that the activity of these transcription factors is necessarily coupled at any time point in a more dynamic system. To analyze the activation kinetics of MRTF-A and YAP in response to a changing microenvironment, we used a dumbbell-shaped micropattern composed of interconnected squares (Fig. 3-6A). Time-lapse imaging of MRTF-A-GFP and hYAP1-GFP expressing HUVEC revealed that MRTF-A frequently translocated between the nuclear and the cytoplasmic compartment during cell migration between adjacent squares. More precisely, the transition phase between lines and squares served as a stimulus to nuclear redistribution of MRTF-A in our cells, while YAP remained mostly cytoplasmic in the same experiment (Fig. 3-6C). To exclude the possibility that the frequent shuttling of MRTF-A occurred as a random event, e.g. due to different expression levels of MRTF-A-GFP and hYAP1-GFP, we also imaged cells on unconnected control squares (Fig. 3-6B). Under these circumstances, we did not observe translocation of MRTF-A, proving that the described translocation on the dumbbell-shaped structures was indeed induced by the changes in pattern geometry. In summary, our results suggest that MRTF-A reacts more sensitive to dynamic changes of the cellular microenvironment than YAP.

3.2.2 Translocation kinetics of MRTF-A and YAP in response to fluid shear stress

Among the numerous mechanical challenges, which require an adaptation of cell morphology during angiogenesis, shear stress is probably the most important force encountered by the endothelium⁷⁹. To verify our assumption that MRTF-A reacts faster or more sensitive (ref. 3.2.1) to a given extracellular stimulus than YAP, we transfected endothelial cells with MRTF-A-GFP and hYAP1-GFP carrying constructs and analyzed the subcellular localization of both proteins under flow conditions (Fig. 3-7A). For this purpose, transfected cells were subjected to a constant shear stress of approximately 15 dyn / cm² and nuclear intensity traces were recorded over a time period of several hours. The results depicted in Fig. 3-7B demonstrate that while MRTF-A had completely translocated to the nucleus after 2 hours, nuclear redistribution of YAP was delayed until 5 hours after the onset of flow.

To confirm our results for endogenous MRTF-A and YAP, we performed immunostainings in fixed cells after 1 and 16 hours of flow cultivation (Fig. 3-7C). Similar to our results for the transfected cells, we found that MRTF-A translocated significantly faster than YAP in these experiments. Moreover, MRTF-A activity was readily reduced after 16 hours, whereas YAP was still localized in the nuclear compartment at this time point.

Finally, we addressed the question whether the above-described differential regulatory kinetics would result in time-dependent variations of MRTF-A and YAP target gene expression after an

3 Results I: Regulation of MRTF-A and YAP in angiogenesis

activating stimulus. In collaboration with the group of Prof. Wolfgang Enard (Department Biology II, LMU Munich, Germany), we generated transcriptome data (RNA-seq) of spreading endothelial cells at early (2 h) and late (4 h) time points and compared the number of upregulated (\log_2 -fold change > 2) MRTF-A and YAP target genes based on two recently published lists for the CARG-Box⁸⁰ and TEAD⁸¹ promoters (Fig. 3-7D). We found that, in support of our imaging data, the number of upregulated SRF target genes was strongly reduced after 4 hours, whereas YAP - and also shared YAP / MRTF-A target genes - showed a more consistent expression over time.

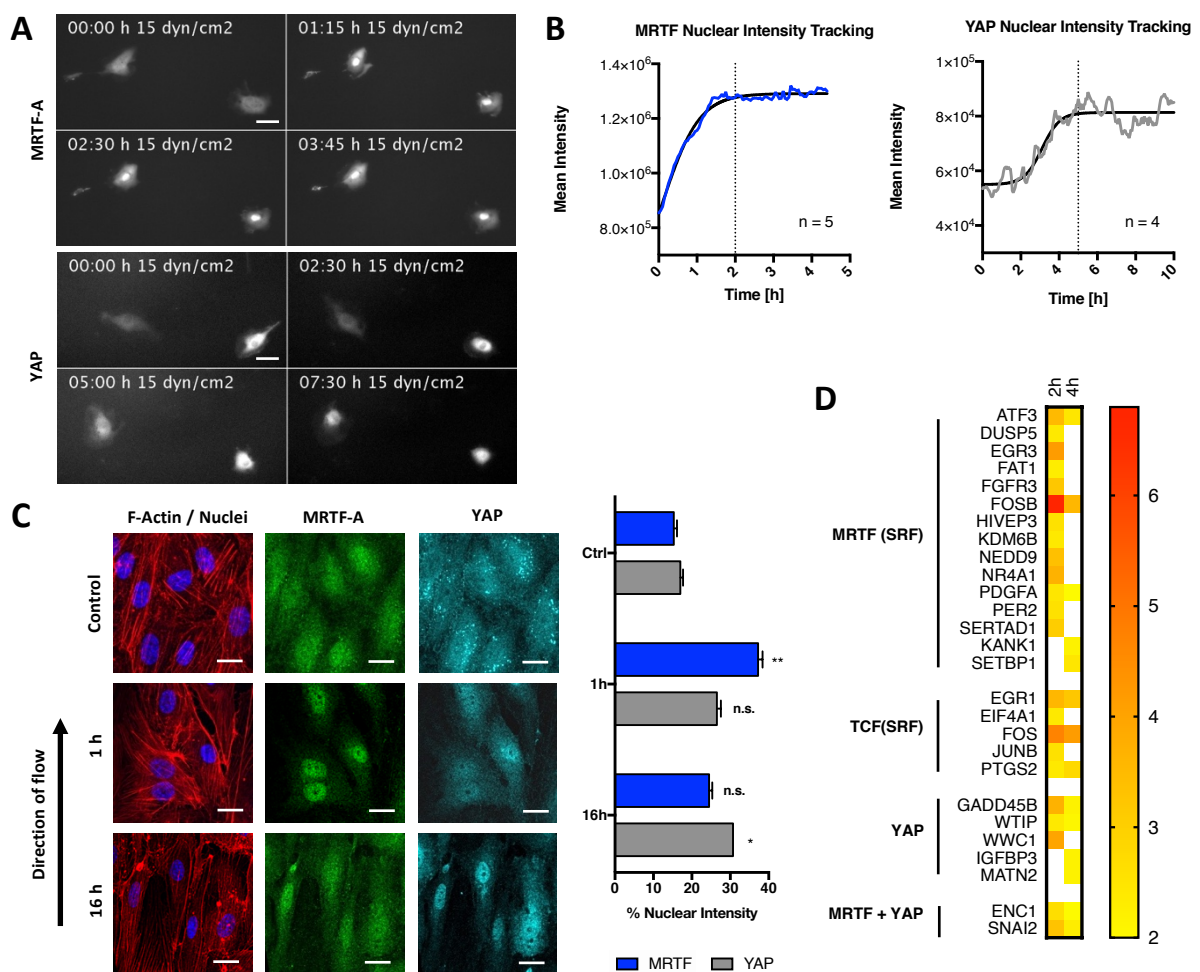


Figure 3-7 | (A) MRTF-A and YAP exhibit different activation kinetics in response to mechanical stress. MRTF-A-GFP or hYAP1-GFP expressing HUVEC were subjected to laminar shear stress (15 dyn / cm²) and time-lapse imaged in perfusion assay chambers over the indicated time spans. **(B)** Representative time traces of MRTF-A and YAP nuclear intensities after the onset of flow. **(C)** Representative IF stainings (left) and nuclear intensity quantification (right) of endogenous MRTF-A and YAP levels after 1 and 16 h of cultivation under the conditions described in (A). Bars = 30 μ m. **(D)** Transcriptome heatmap showing upregulated (\log_2 -fold change > 2) MRTF, TCF and YAP-driven target genes in spreading endothelial cells; analyzed data refers to confluent control cells.

3 Results I: Regulation of MRTF-A and YAP in angiogenesis

3.3 Regulation of MRTF-A and YAP in angiogenic model systems

3.3.1 Spatiotemporal differences in MRTF-A and YAP activity during tube formation

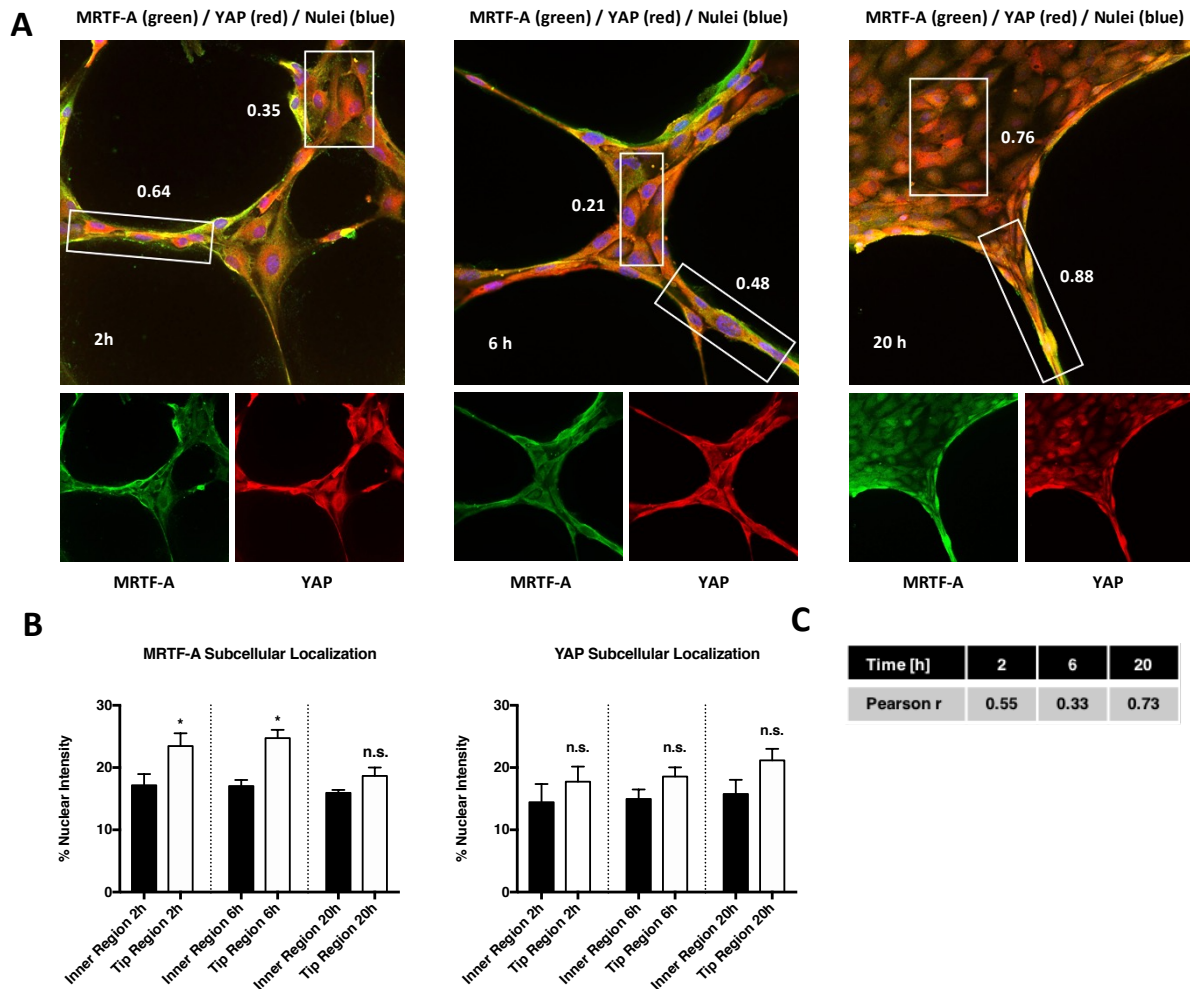


Figure 3-8 | Expression pattern and nuclear levels of MRTF-A and YAP during endothelial tube formation. (A) Endothelial cells (11×10^3) were seeded onto thin layers of Matrigel™ and incubated for indicated time spans. Tubular structures were stained for MRTF-A, YAP and DNA. (B) Subcellular localization of MRTF-A and YAP was determined via intensity quantification in Hoechst positive areas in relation to total signal intensity. Bars representing mean + SEM from three independent experiments, statistical significance was determined by unpaired student t-test, $p \leq 0.05$. (C) Pearson coefficients (r above threshold) were calculated to express the correlation between YAP and MRTF-A intensity distribution for central and sprouting regions at 2 h, 6 h and 20 h. Representative examples for each of the two regions are highlighted by white boxes in (A).

Having shown that MRTF-A and YAP share microenvironmental triggers, but underlie different kinetics in single endothelial cells, we went on to test whether the regulatory model depicted in Fig. 2-8 could be transferred to an angiogenic model system *in vitro*. Therefore, we performed tube formation assays on top of thin Matrigel™ layers and co-stained the resulting tubular structures for MRTF-A and YAP at three different time points (Fig. 3-8A). Next to the nuclear levels of both transcription factors, which were given by the signal intensity in Hoechst 33342 positive areas in relation to total signal intensity, Pearson correlation coefficients above

3 Results I: Regulation of MRTF-A and YAP in angiogenesis

threshold were calculated as a measure of correlation between MRTF-A and YAP at different positions within the network.

As it is demonstrated by the representative pictures in Fig. 3-8A, MRTF-A was higher expressed in mechanically strained tubular regions compared to inner areas of the network. In addition to the expression, also nuclear levels of MRTF-A were significantly higher in tubular regions, as it is shown by the quantification in Fig. 3-8B. For YAP, a similar, though not significant tendency was observed.

Apart from a location-dependent but otherwise congruent activity of MRTF-A and YAP at a given time point, we observed time-dependent variations in the correlation between both transcription factors. In detail, the correlation was highest in the mature network (20 h) with a Pearson coefficient of 0.73 compared to 0.55 and 0.33 at earlier time points (Fig. 3-8C). In line with our previous data (ref. sections 2.1 and 2.2.), this indicates that, although the principal response of MRTF-A and YAP to a given microenvironmental stimulus is similar, there are kinetic differences regarding their activation.

3.3.2 Retinal whole-mount stainings: expression patterns of MRTF-A and YAP *in vivo*

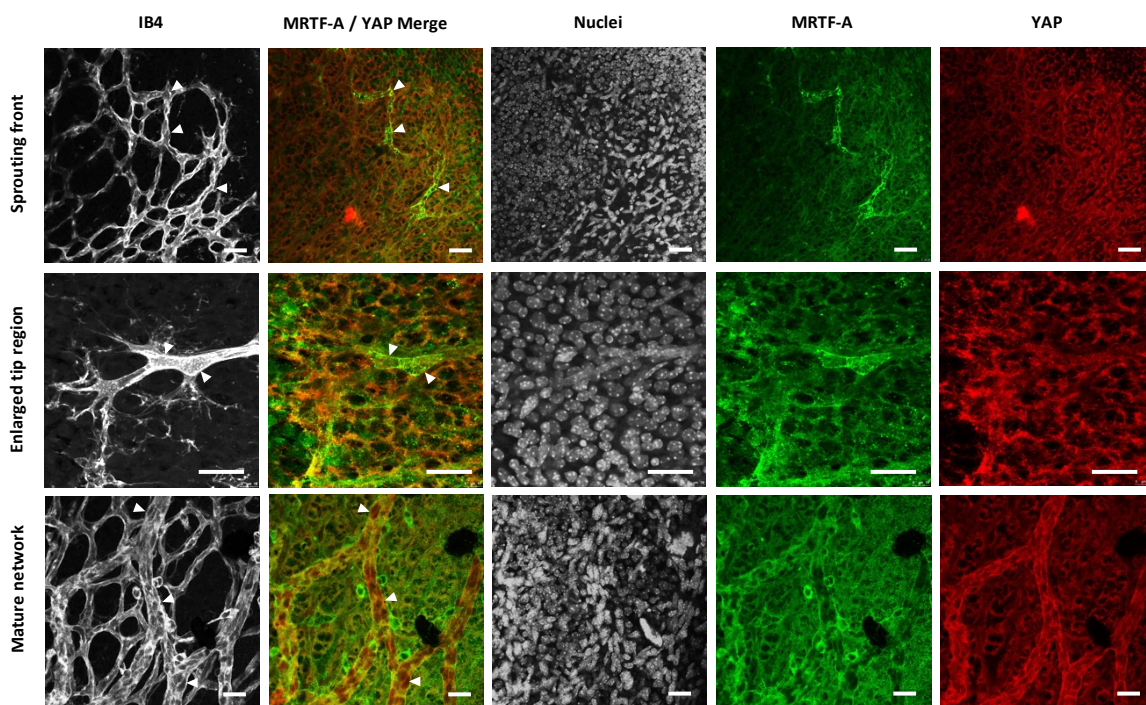


Figure 3-9 | Retinal whole-mount stainings of wild-type C57BL/6 mice at postnatal day 6 (P6). Retinal vasculature is visualized by IB4 labelling and samples are co-stained for MRTF-A and YAP. Representative images for the sprouting front and the inner network are shown, bars = 30 μ m.

3 Results I: Regulation of MRTF-A and YAP in angiogenesis

To examine the expression pattern of MRTF-A and YAP *in vivo*, we performed whole-mount stainings of C57BL/6 mouse retinas at postnatal day 6 (Fig. 3-9). We found that MRTF-A was highly expressed in sprouting regions of the developing retinal vasculature (upper panel). This is in line with a previous report of Franco et al.³⁴. Remarkably, the expression of MRTF-A was clearly reduced in already matured inner areas of the retina (bottom panel). Regarding the expression of YAP, we observed an adverse behavior, which becomes particularly evident when directly comparing both channels (see merged pictures in Fig. 3-9).

Taken together, the results presented in section 3.3 show that the activity of MRTF-A and YAP is regulated in a time- and location-dependent manner during tubular network formation *in vitro*. In line with this, we observed differential expression patterns of MRTF-A and YAP in the developing retinal vasculature *in vivo*.

4 Results II: Targeting of endothelial mechanosensing with actin binding compounds

4.1 Actin binding compounds regulate endothelial gene transcription

4.1.1 Transcriptional profiling of actin binding compounds

As a foundation to analyzing the effects of different actin binding compounds on transcriptional regulation in general and mechanosensitive signaling pathways in particular, we addressed the question whether moderate concentrations of these compounds would be able to significantly alter gene transcription in endothelial cells. For this purpose, a transcriptomic approach with four different actin binding compounds was performed in collaboration with the group of Prof. Wolfgang Enard (Department Biology II, LMU Munich, Germany). Fig. 4-1 summarizes the data obtained for the actin polymerizing compound Miuraenamamide A, which was kindly provided by the lab of Prof. Uli Kazmaier⁶⁶ (Institute for Organic Chemistry, Saarland University, Saarbrücken, Germany). As indicated by the topGO enrichment analysis shown in Fig. 4-1B, most of the genes that were significantly up- or downregulated after stimulation with Miuraenamamide A could be allocated to cytoskeleton-associated processes such as lamellipodium formation or actin filament organization. Notably, although the transcriptomic analysis yielded 594 genes that were regulated in response to Miuraenamamide A versus untreated control cells, there were only marginal differences between Miuraenamamide A and the commercially available actin polymerizing drug Jasplakinolide (Fig. 4-1D). We therefore decided to perform all further experiments with only Miuraenamamide A as an exemplary substance representing the class of actin polymerizing compounds.

Since the compound-induced polymerization of actin strongly affected gene regulation in our cells, we assumed that an increased depolymerization of actin might have similar effects. Therefore, we tested the influence of the commercially available actin depolymerizing compound Latrunculin B on gene transcription in HUVEC (Fig. 4-2). As shown by the Volcano plot of gene expression in Fig. 4-2B, 312 significantly regulated genes were detected in response to stimulation with 250 nM Latrunculin B. The subsequent topGO gene enrichment analysis showed that, in contrast to treatment with actin polymerizing compounds (Fig. 4-1), most of the regulated genes were assigned to cellular processes involved in angiogenesis and the response to hypoxia (Fig. 4-2C). In addition to Latrunculin B, we also tested the novel myxobacterial compound Chivosazole A, which was isolated from *Sorangium cellulosum* in the lab of Prof. Rolf Müller (Helmholtz Institute of Pharmaceutical Research Saarland, Saarbrücken, Germany)^{70,82}. In line with the previously tested actin polymerizers, we did not see a substantial difference when comparing the two depolymerizing compounds.

4 Results II: Targeting of endothelial mechanosensing with actin binding compounds

In sum, our data suggests that moderate concentrations of actin binding compounds are able to interfere with transcriptional regulation in endothelial cells. Moreover, although there were significant differences regarding the respective gene sets influenced by polymerizing versus depolymerizing compounds, class-internal differences were only marginal in our experiments.

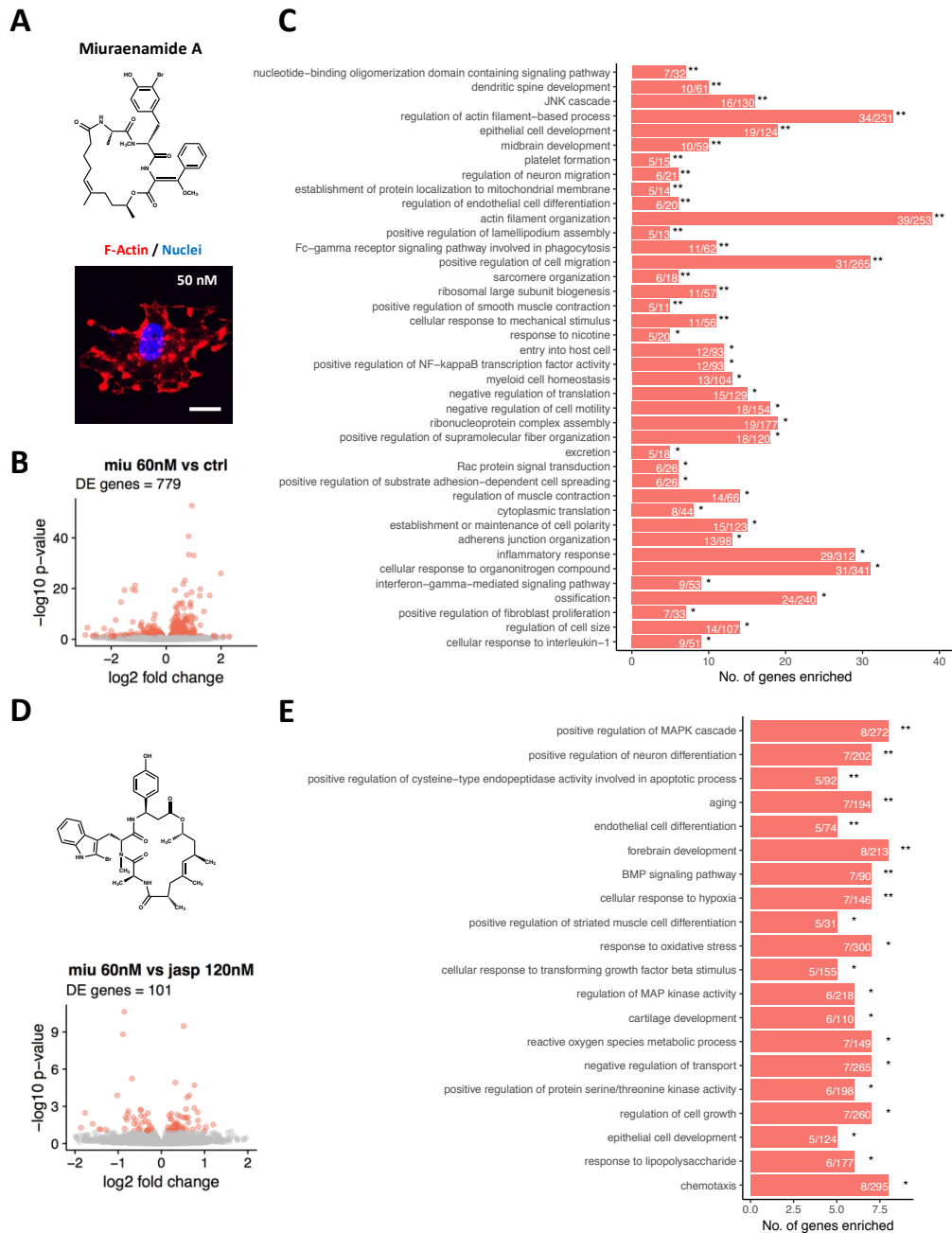


Figure 4-1 | Influence of actin polymerizing compound Miuraenamamide A on endothelial gene transcription. (A) *Top*: Molecular structure of Miuraenamamide A. *Bottom*: Representative F-actin staining in HUVEC after 4 h stimulation with 50 nM Miuraenamamide A. (B) Volcano plot of differential gene expression in cells stimulated with 60 nM Miuraenamamide A versus control. The colored points indicate significantly differentially expressed genes (FDR < 0.1). (C) Enriched and filtered topGO categories for stimulation with Miuraenamamide A versus control. (D) *Top*: Molecular structure of Jasplakinolide. *Bottom*: Volcano plot of differential gene expression in cells stimulated with 60 nM Miuraenamamide A versus 120 nM Jasplakinolide. (E) Enriched and filtered topGO categories for stimulation with 60 nM Miuraenamamide A versus 120 nM Jasplakinolide. Asterisks show the level of significance of Fisher's exact test for the enrichment of the particular term. p-values: * < 0.01; ** < 0.001; *** < 0.0001.

4 Results II: Targeting of endothelial mechanosensing with actin binding compounds

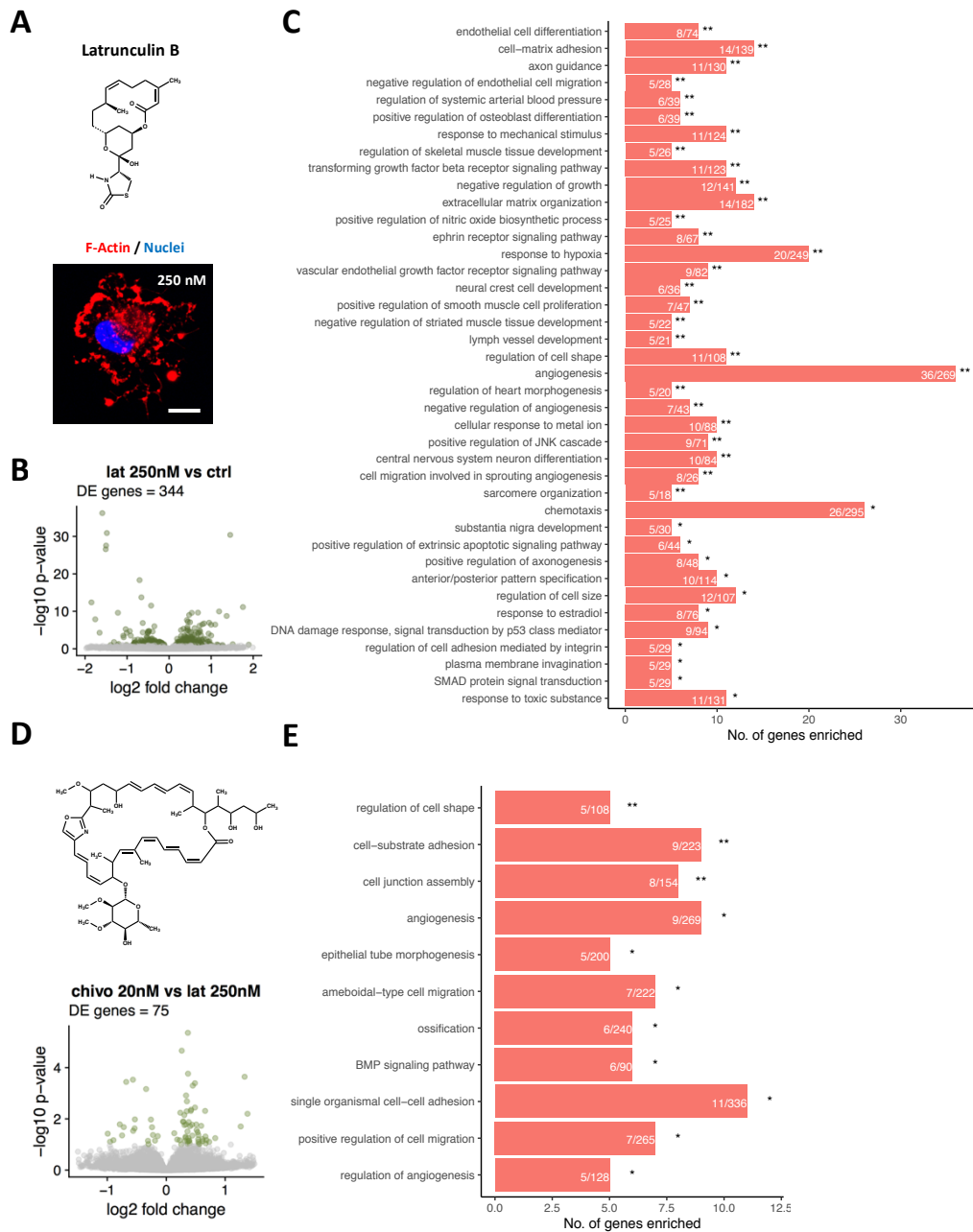


Figure 4-2 | Influence of actin depolymerizing compound Latrunculin B on endothelial gene transcription. (A) *Top*: Molecular structure of Latrunculin B. *Bottom*: Representative F-actin staining in HUVEC after 4 h stimulation with 250 nM Latrunculin B. (B) Volcano plot of differential gene expression in cells stimulated with 250 nM Latrunculin B versus control. The colored points indicate significantly differentially expressed genes (FDR < 0.1). (C) Enriched and filtered topGO categories for stimulation with Latrunculin B versus control. (D) *Top*: Molecular structure of Chivosazole A. *Bottom*: Volcano plot of differential gene expression in cells stimulated with 250 nM Latrunculin B versus 20 nM Chivosazole. (E) Enriched and filtered topGO categories for stimulation with 250 nM Latrunculin B versus 20 nM Chivosazole. Asterisks show the level of significance of Fisher's exact test for the enrichment of the particular term. p-values: * < 0.01; ** < 0.001; *** < 0.0001.

4 Results II: Targeting of endothelial mechanosensing with actin binding compounds

4.1.2 Influence on chromatin organization and epigenetic modification

Apart from the regulation of specific mechanosensitive transcription factors, actin is known to regulate gene expression via several other mechanisms and target structures such as polymerase function, chromatin organization or histone modification. Therefore, the effects of actin binding compounds on endothelial gene expression, as they are described in section 3.1.1, could be at least partially caused by an interference of these compounds with one or more of the aforementioned aspects.

To test whether actin binding compounds affect chromatin organization, we stimulated HUVEC with either Miuraenamamide A or Latrunculin B and visualized the respective chromatin structures using the DNA intercalating dye Hoechst 33342 (Fig. 4-3). The intensity scans and representative images shown in Fig. 4-3A1 illustrate that stimulation with either of the two compounds drastically affected chromatin architecture and nuclear shape. This was supported by an analysis of the cell percentage exhibiting an altered chromatin structure and the calculation of nuclear perimeter to area ratios in > 30 cells (Fig. 4-3A2).

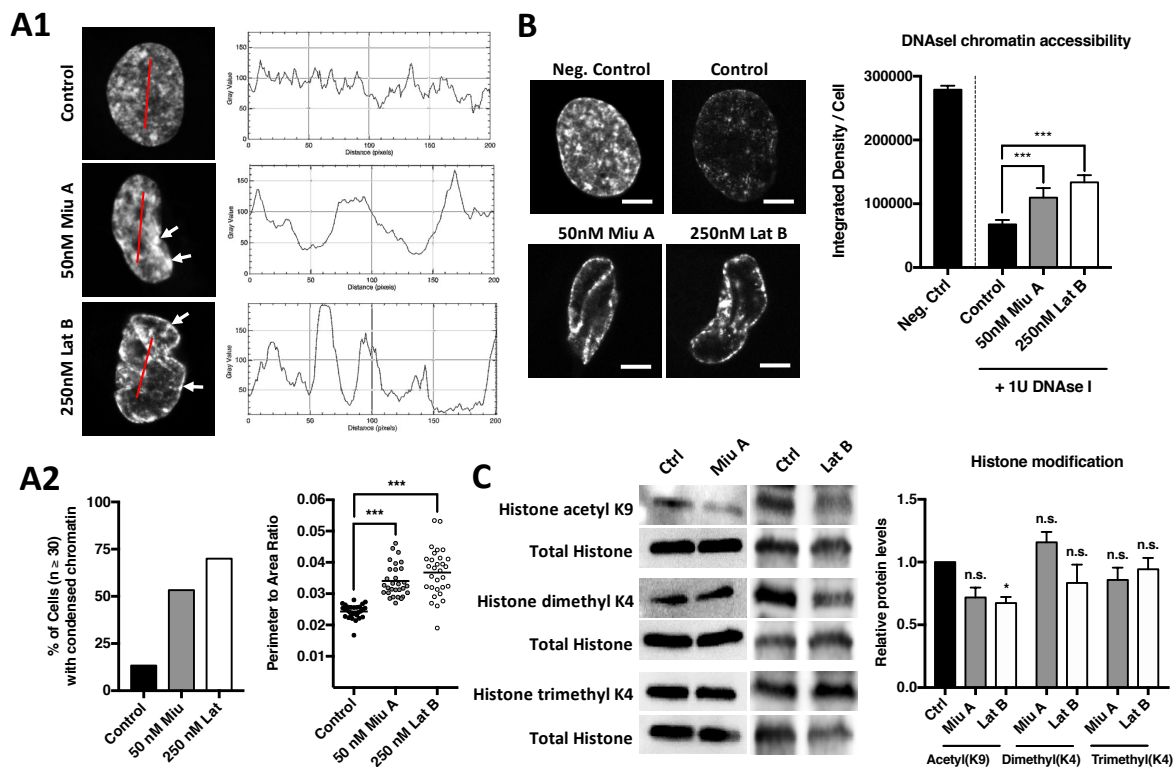


Figure 4-3 | Effects of Miuraenamamide A and Latrunculin B on nuclear structure, chromatin organization and histone modification. (A1) Hoechst staining of HUVEC nuclei after stimulation with either Miuraenamamide A or Latrunculin B. Positions of the intensity scans depicted on the right are indicated by red lines. **(A2)** Percentage of cells with a condensed chromatin phenotype (left) and nuclear perimeter to area ratio (right) after stimulation as in (A1). **(B)** Chromatin accessibility was determined by DNase I digestion and subsequent Hoechst 33342 staining of HUVEC nuclei. **(C)** Representative Western blot and quantified protein levels of methylated and acetylated histone forms after stimulation with either Miuraenamamide A or Latrunculin B. Statistical significance in all shown experiments was determined by ordinary one-way ANOVA followed by Dunnett's multiple comparisons test.

4 Results II: Targeting of endothelial mechanosensing with actin binding compounds

To assess the impact of Miuraenamides A and Latrunculin B on chromatin condensation in more detail, we performed a previously described DNase I digestion assay⁵⁸. As illustrated by the quantification of undigested and therefore inaccessible chromatin depicted in Fig. 4-3C, both Miuraenamides A and Latrunculin B significantly increased the fraction of condensed chromatin. We subsequently analyzed the effect of actin binding compounds on histone modification (Fig. 4-3C). Western blot analysis of acetylated and methylated histone forms after stimulation with either Miuraenamides A or Latrunculin B revealed that, apart from a minor decrease in histone acetylation, neither of the compounds significantly affected epigenetic histone modification.

4.1.3 Influence on polymerase function and rRNA synthesis

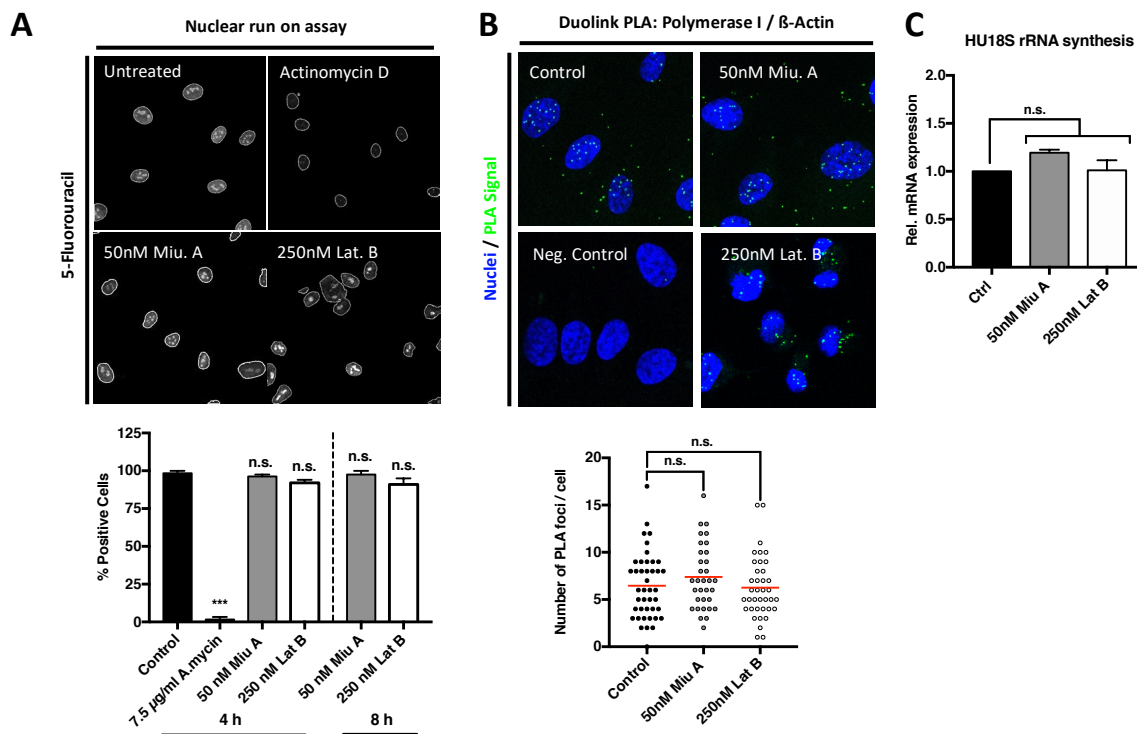


Figure 4-4 | Effects of Miuraenamides A and Latrunculin B on transcriptional capability and rRNA synthesis. (A) Representative images (top) and quantitative analysis (bottom) of nuclear run-on assays performed after pre-stimulation with Miuraenamides A or Latrunculin B. Actinomycin D = negative control. Cells were counted as positive upon the presence of visible nucleolar 5-FU foci. (B) Duolink proximity ligation assay showing the interaction between β -actin and DNA Polymerase I in Miuraenamides A and Latrunculin B-treated cells. (C) Relative 18S rRNA expression levels after stimulation with Miuraenamides A or Latrunculin B. Statistical significance in all experiments was determined by ordinary one-way ANOVA followed by Dunnett's multiple comparisons test.

As mentioned in the introduction, nuclear actin is essentially involved in transcriptional processes mediated by RNA polymerases I, II and III. To examine the influence of actin polymerizing and depolymerizing compounds on transcriptional capability, we performed nuclear run on assays (Fig. 4-4A). Nuclear run on assays are based on the incorporation of 5-

4 Results II: Targeting of endothelial mechanosensing with actin binding compounds

fluorouracil (5-FU) into nascent RNA transcripts⁴⁴. The resulting 5-FU containing transcripts can later be visualized and quantified as a measure of ongoing transcriptional activity. As shown in Fig. 4-4A, pre-stimulation with 7.5 µg/ml actinomycin D, a DNA intercalating drug, completely abrogated the incorporation of 5-FU in our cells. However, we did not observe a significant difference in the relative amount of nuclear 5-FU foci after 4 and 8 hours of stimulation with either Miuraenamamide A or Latrunculin B.

To verify our assumption that moderate doses of Miuraenamamide A and Latrunculin B are unable to disturb the interaction between DNA polymerases and nuclear β-actin, a Duolink proximity ligation assay (PLA) targeting DNA polymerase I and β-actin was performed. As shown by the representative images and the quantitative analysis in Fig. 4-4B, we could indeed detect an interaction between both proteins in the nuclear compartment. In line with our nuclear run on assay data, there was no significant change in the number of amplified PLA signals after stimulation with Miuraenamamide A or Latrunculin B. This was further supported by the quantitative real-time PCR analysis of 18S rRNA synthesis, which is transcribed by RNA polymerase I in the nucleoli (Fig. 4-4C).

In sum, our data states that RNA polymerase function and therefore cellular transcriptional capability is unaffected by the stimulation with actin binding compounds Miuraenamamide A or Latrunculin B.

4.2 Effects of actin binding compounds on nuclear actin

4.2.1 Visualization of nuclear actin with different actin probes

Due to its high cytoplasmatic abundancy and the related fluorescence intensities in this compartment, nuclear actin is hard to visualize in both living and fixed cells. To improve the detection intensity of polymerized nuclear actin, specialized protocols for phalloidin stainings and nuclear actin targeting probes have been developed in recent years^{42,43}.

In order to investigate the influence of Miuraenamamide A and Latrunculin B on the structure of nuclear actin, we used a phalloidin staining protocol that is based on glutaraldehyde fixation and the subsequent use of cytoskeleton stabilizing buffers (CSB, see section 6.2.3.2). As shown in Fig. 4-5A, polymerized nuclear actin was not present in the nuclei of untreated control NIH3T3 cells. Of note, we were able to visualize the transient formation of nuclear actin fibers in starved NIH3T3 cells after serum stimulation, as it had previously been reported by Baarlink et al.⁴⁶. Nevertheless, we could not detect any resembling structures after stimulation with actin binding compounds, regardless of whether the cells were treated long term or short term (Fig. 4-5A).

F-actin binding by phalloidin has been reported to be competitive with the actin polymerizing substance Jasplakinolide⁸³. Since this could also be the case for the structurally related

4 Results II: Targeting of endothelial mechanosensing with actin binding compounds

compound Miuraenamides A, we switched to a second visualization approach based on the expression of actin-binding antibody fragments fused to a nuclear localization sequence (nuclear actin chromobody, nAC, Fig. 3-5B). The major advantage of this probe is an improved signal to noise ratio compared to other actin binding substances that are distributed throughout the cytoplasm. Time-lapse imaging of nAC expressing cells - under the same stimulation conditions as described for the experiments with phalloidin - showed that Miuraenamides A and Latrunculin B led to increased signal intensities in the nucleolar compartment in a small fraction of cells (5 - 10%, left panel in Fig. 4-5B). However, since this could not be considered a general phenomenon, we concluded that neither of the two applied visualization techniques could prove a formation of polymerized or aggregated actin structures in response to stimulation with actin binding compounds in our cells.

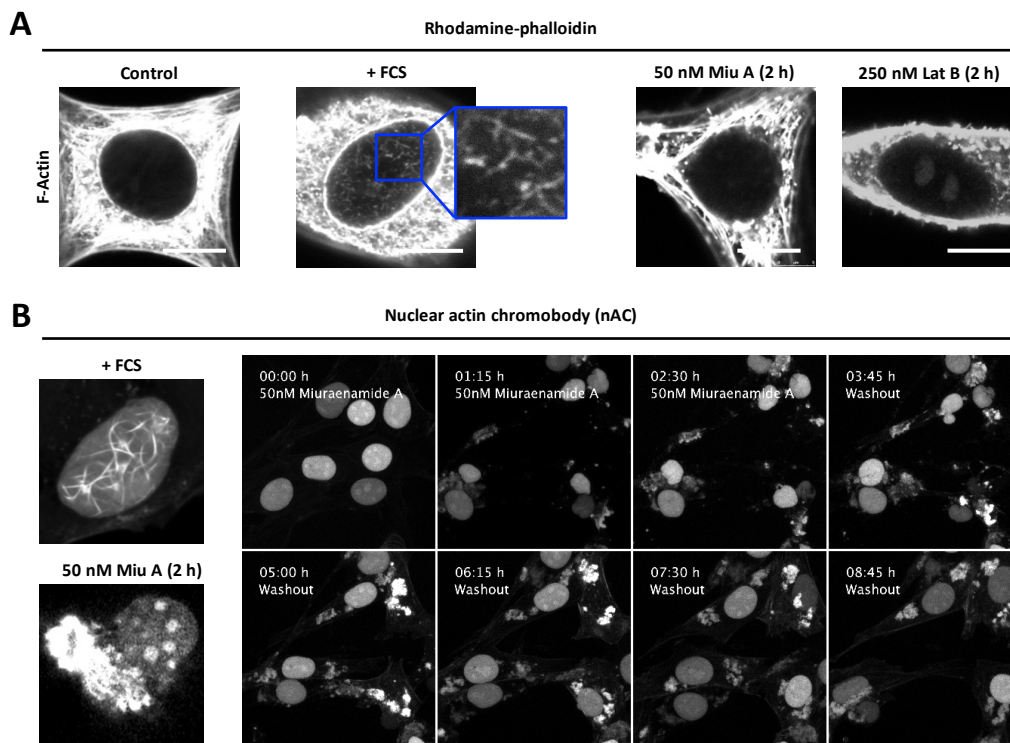


Figure 4-5 | Visualization of nuclear actin in NIH3T3 fibroblasts. (A) Phalloidin stainings of nuclear actin in NIH3T3 fibroblasts. FCS stimulation of starved cells was used as a positive control for induction of nuclear actin polymerization. **(B)** Representative images (left) and time lapse imaging series (right) of nAC-GFP expressing NIH3T3 fibroblasts after stimulation with FCS or 50 nM Miuraenamides A. All bars = 10 μ m.

4 Results II: Targeting of endothelial mechanosensing with actin binding compounds

4.2.2 Miuraenamamide A and Latrunculin B bidirectionally shift nuclear actin levels

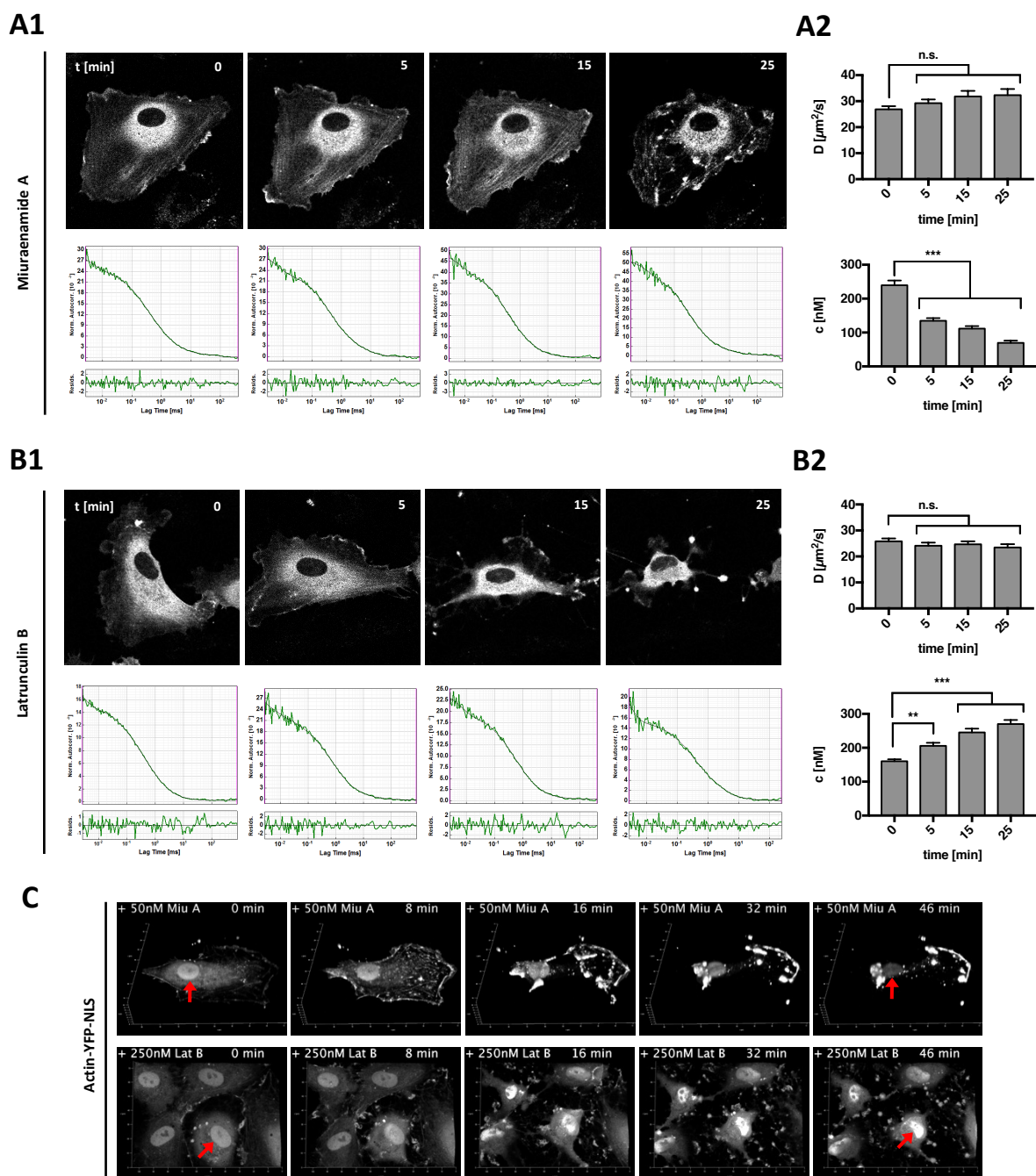


Figure 4-6 | Miuraenamamide A and Latrunculin B adversatively shift the concentration of nuclear actin. EGFP- β -actin expressing HUVEC were stimulated with Miuraenamamide A (**A1**) or Latrunculin B (**B1**) and the dynamics of nuclear actin were analyzed by single-points FCS measurements. The representative confocal images and autocorrelation curves depicted in panels A1 and B1 were acquired 0, 5, 15 and 25 minutes after stimulation. (**A2**) and (**B2**): Nuclear concentration and diffusion coefficients were determined in > 40 cells for each setting. Bars representing mean + SEM, statistical significance was determined by ordinary one-way ANOVA followed by Dunnett's multiple comparisons test. (**D**) Time lapse imaging series of actin-YFP-NLS expressing HUVEC after stimulation with Miuraenamamide A or Latrunculin B.

The results of section 4.2 thus far suggested that nanomolar concentrations of our two reference substances Miuraenamamide A and Latrunculin B have no significant impact on intranuclear actin. However, the lack of visible, large-scale filaments or even aggregates does

4 Results II: Targeting of endothelial mechanosensing with actin binding compounds

not exclude the possibility that shorter actin oligomers are formed upon stimulation with either of these compounds. Moreover, a disturbance of the cytoplasmatic actin pool might indirectly affect the number of actin monomers available for nuclear import.

To investigate the relevance of the above-mentioned aspects in endothelial cells, we performed fluorescence correlation spectroscopy (FCS) measurements with β -actin-GFP expressing HUVEC (Fig. 4-6A1 and 4-6B1). Time-resolved analysis of nuclear β -actin-GFP concentration and diffusion rate in response to stimulation with Miuraenamamide A revealed that, although there was no change in the diffusion coefficient and therefore aggregation state of intranuclear actin, the concentration significantly decreased over time (Fig. 4-6A2). Remarkably, the depolymerizing compound Latrunculin B caused an increase in the concentration of nuclear β -actin-GFP under similar conditions (Fig. 4-6B2).

Since a considerable fraction of nuclear actin could either be incorporated into larger protein complexes or form polymers, we also applied a two-component fitting model^{84,85} and obtained similar results for both diffusion coefficients (Fig. S1).

To confirm our assumption that actin binding compounds would rather affect the concentration of nuclear actin instead of its polymerization state, we transiently transfected endothelial cells with a fluorescence labeled β -actin-NLS construct, thereby increasing the steady state concentration of nuclear actin. Time lapse imaging of these cells after stimulation with either of the two compounds showed that, in line with our hypothesis, Miuraenamamide A and Latrunculin B led to a decrease of nuclear signal intensity or to an increase, respectively (Fig. 4-6C).

4.2.3 Influence of actin binding compounds on intranuclear polymerization state

The FCS data presented in Fig. 4-6 allowed us to gain insight into the response of nuclear actin to treatment with Miuraenamamide A or Latrunculin B. Unfortunately, due to the high concentration of cytoplasmatic actin, this compartment could not be measured with standard FCS techniques. In order to obtain comparative data for the polymerization state of actin in both the nuclear and the cytoplasmatic compartment, we switched to a novel approach termed raster image correlation spectroscopy (RICS⁸⁶⁻⁸⁸, Fig. 4-7A). These experiments were performed in collaboration with the group of Prof. Don C. Lamb (Department of Chemistry, Center for Integrated Protein Sciences, Munich, Germany). The major advantage of RICS is that a two-directional scanning process allows the reliable detection of a wide range of concentrations and diffusion coefficients, thereby enabling us to simultaneously detect aggregation in both compartments. Moreover, the larger observation area allows to exclude any disturbing structures like vesicles or larger fibers from the analysis (arbitrary region RICS⁸⁹), which is particularly important for cytoplasmatic measurements.

4 Results II: Targeting of endothelial mechanosensing with actin binding compounds

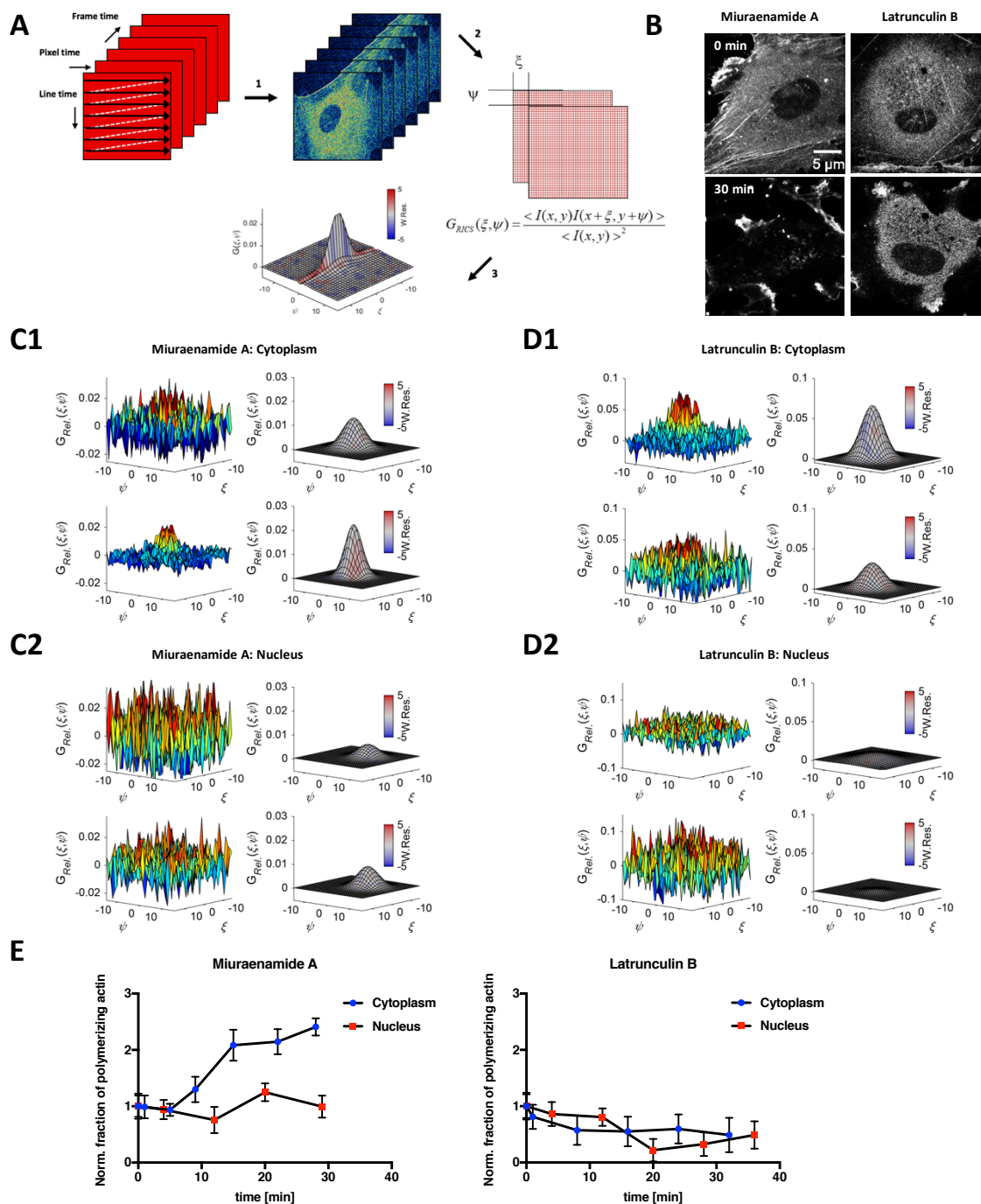


Figure 4-7 | RICS analysis of actin aggregation in response to actin binding compounds. (A) Schematic explanation of RICS data acquisition. (1) Images are acquired by a raster scan pattern providing diffusion information of particles moving on three different time scales. (2) The image series is correlated with spatial increments upon the horizontal and vertical axes, thus providing diffusion information on three different timescales. (3) By fitting the correlation values from (2), the information on particles and diffusion is extracted. **(B)** Representative images of EGFP- and mCherry- β -actin expressing HUVEC before (0 min) and 30 min after stimulation with 100 nM Miuraenamida A or 250 nM Latrunculin B. **(C + D)** Experimental ccrICS data obtained for the cytoplasmic **(C1 + D1)** and nuclear **(C2 + D2)** compartments upon stimulation with Miuraenamida A **(C1 + C2)** and Latrunculin B **(D1 + D2)**. Left: mean SCCFs in 3D, color coded for the correlation values: SCCF before (top) and 20 min after (bottom) compound addition. Right: two-component fits of the data before (top) and 20 min after (bottom) compound addition. Fits are color coded according to the value of the goodness-of-fit weighted residuals parameter ($W. Res.$), where gray illustrates a good fit and red–blue indicates regions where the residuals deviate by $> 5 \sigma$. **(E)** Time course of relative cross-correlation between EGFP- and mCherry- β -actin in the nuclear versus cytoplasmic compartment in response to Miuraenamida A (left) and Latrunculin B (right).

4 Results II: Targeting of endothelial mechanosensing with actin binding compounds

To increase the sensitivity of standard one-component RICS analysis, we analyzed cross-correlation of two fluorescently labelled β -actin derivatives, namely mCherry- and GFP-actin, over a time period of up to 45 minutes after stimulation with either Miuraenamides A or Latrunculin B (Fig. 4-7B). As demonstrated by the representative 2D Gaussian plots depicted in Fig. 4-7C, Miuraenamides A caused a drastic increase in relative cross-correlation throughout the cytoplasm, while the nuclear compartment remained unaffected in the same cells. The mean cross-correlation over time within the nuclear versus the cytoplasmic compartment is plotted in Fig. 4-7E. A similar tendency was observed for the autocorrelation of the EGFP and mCherry constructs alone (Fig. S2 + S3).

Notably, an excessive concentration of Miuraenamide (2 μ M) readily induced nuclear actin aggregates in actin-YFP-NLS expressing cells (Fig. 4-8), further supporting our hypothesis that moderate doses of actin polymerizing compounds are not able to reach the nucleus in a concentration that could induce aggregation.

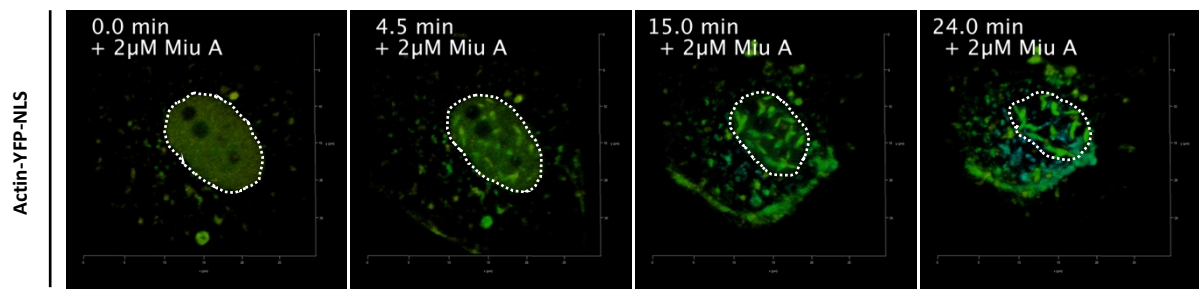


Figure 4-8 | High concentrations of Miuraenamides A induce nuclear actin aggregation in HUVEC. Time-lapse imaging series of YFP-NLS-actin expressing HUVEC after stimulation with 2 μ M Miuraenamides A. The nucleus is delineated with dashed white lines.

4 Results II: Targeting of endothelial mechanosensing with actin binding compounds

4.3 Effects of actin binding compounds on mechanosensitive pathways

4.3.1 Influence of Miuraenamides A on MRTF-A and YAP subcellular localization

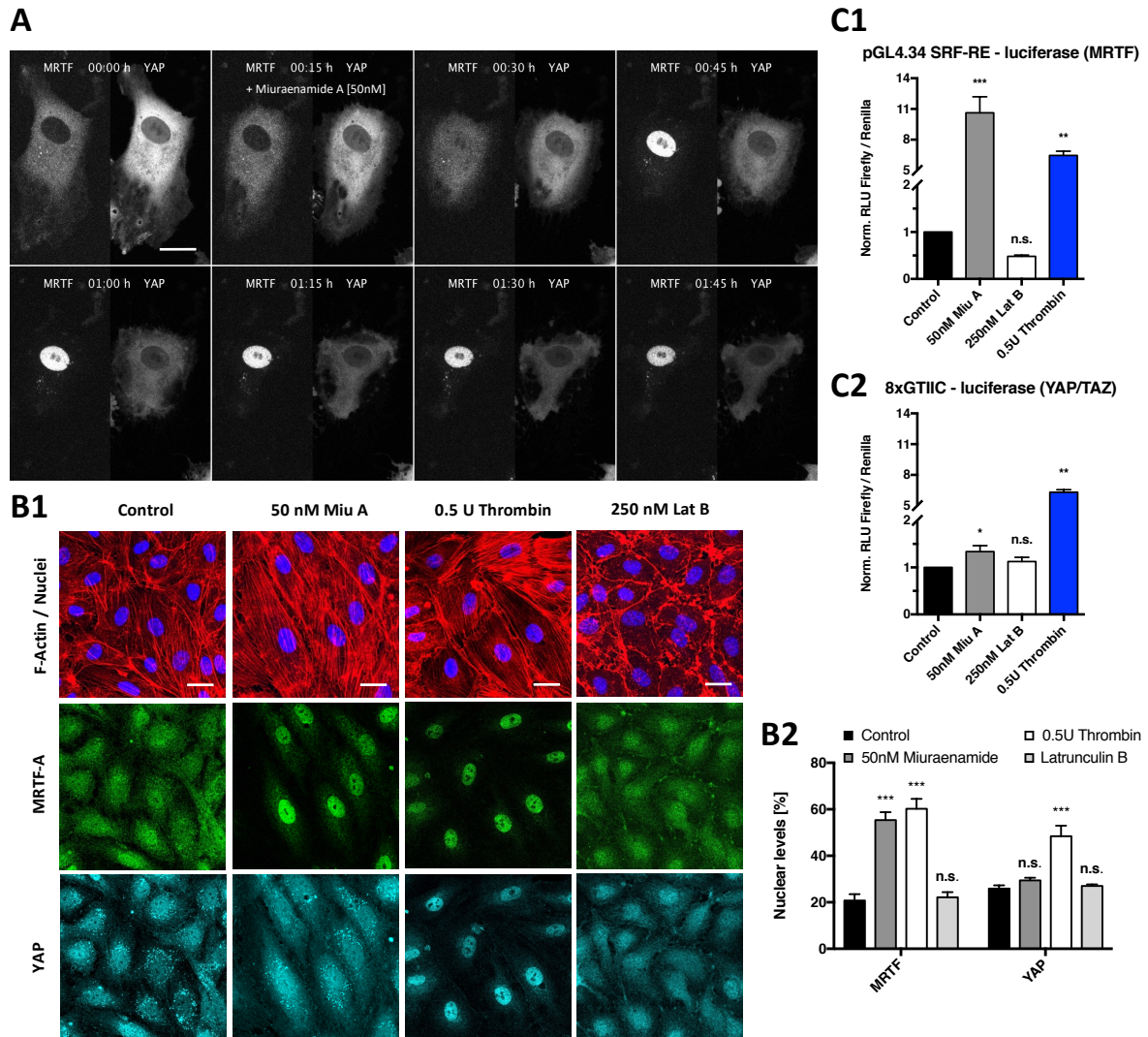


Figure 4-9 | Fig. 5 Miuraenamides A activates MRTF-A but not YAP. (A) Live cell imaging sequence of MRTF-A-GFP and hYAP1-mCherry co-expressing endothelial cell. The cell was imaged over a time span of 90 min after stimulation with 50 nM Miuraenamides A at $t = 15$ min. Bar = 30 μ m. **(B1)** Immunostaining of MRTF-A and YAP in confluent HUVEC after 5 h stimulation with either 50 nM Miuraenamides A, 250 nM Latrunculin B or 0.5 U thrombin. **(B2)** Quantification of nuclear MRTF-A and YAP levels for the experiment shown in (B1). Nuclear protein levels are expressed as nuclear signal intensity divided by total cellular intensity. **(C)** Dual luciferase reporter gene assays for SRF response element **(C1)** and YAP / TAZ promoter **(C2)**. Luciferase reporter activity is expressed as firefly RLU normalized to the constitutive renilla control construct.

Having characterized the effects of two representative actin binding compounds on general transcription-associated processes (4.1) as well as on nuclear actin structure and concentration (4.2), we went on to study how these substances influence the specific activity of the mechanosensitive transcription factors MRTF-A and YAP, which have both been extensively characterized regarding their physiological regulation in endothelial cells in the first part of this thesis (ref. section 3). In particular, we focused on the polymerizing compound

4 Results II: Targeting of endothelial mechanosensing with actin binding compounds

Miuraenamide A, since actin polymerization is commonly accepted as an activating stimulus for MRTF-A and YAP-dependent gene transcription (ref. sections 2.2.2, 2.2.3).

To simultaneously analyze the subcellular localization of MRTF-A and YAP in live cells, we co-transfected HUVEC with MRTF-A-GFP and hYAP1-mCherry carrying constructs (Fig. 4-9A). Upon stimulation with 50 nM Miuraenamide A, we observed a rapid and complete nuclear translocation of MRTF-A. In contrast, subcellular localization of YAP was not affected by Miuraenamide A, even at late time points. Since the translocation kinetics of both transcription factors could be influenced by overexpression and / or the GFP- and mCherry tags, we also analyzed the subcellular localization of endogenous MRTF-A and YAP via immunostaining of fixed cells (Fig. 4-9B). Similar to our observation in live cells, we found that Miuraenamide A triggered the nuclear translocation of MRTF-A, but not YAP in our cells. Moreover, we found that, while the Latrunculin B had no significant effect on the localization of either transcription factor, the protease-activated receptor (PAR) ligand thrombin, a strong activator of Rho GTPase-induced actin polymerization, activated both MRTF-A and YAP.

The different effects of Miuraenamide A, Latrunculin B and thrombin on MRTF-A and YAP activity could be further confirmed in dual luciferase reporter gene assays targeting the MRTF-A-binding serum response element (SRE) and the YAP-binding TEA domain (Fig. 4-9C).

In summary, our data shows that Miuraenamide A strongly activates the mechanosensitive transcription factor MRTF-A, while this compound has a minor effect on YAP. However, the actin polymerizing PAR ligand thrombin does not exhibit the same selectivity, indicating a more complex role of actin polymerization in the regulation of this protein.

4.3.2 Promotor activation and MRTF-A / YAP target gene expression

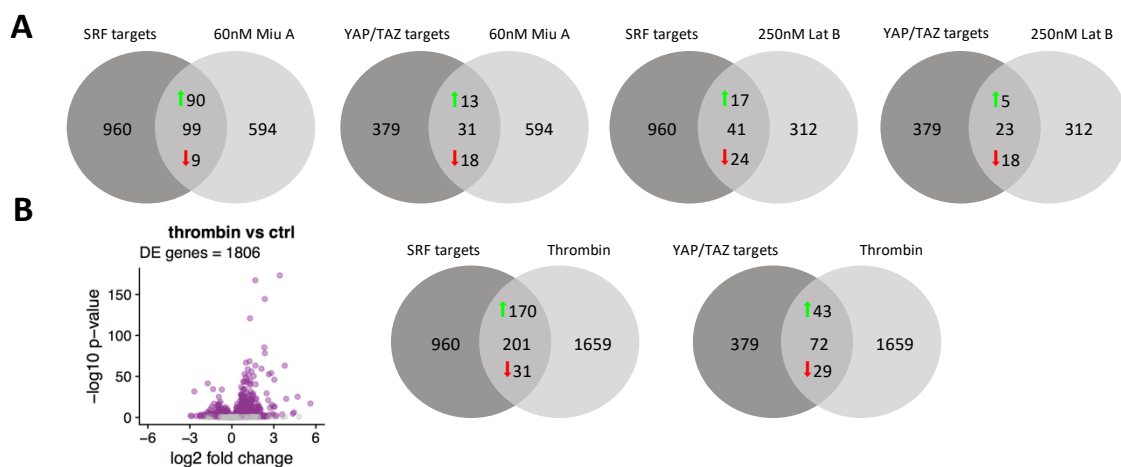


Figure 4-10 | Regulated SRF and YAP / TAZ target genes in response to stimulation with Miuraenamide A, Latrunculin B and thrombin. (A) Number of significantly up- and downregulated known SRF and YAP / TAZ target genes in response to stimulation with Miuraenamide A and Latrunculin B. **(B)** Volcano plot of gene expression and number of significantly up- and downregulated known SRF and YAP / TAZ target genes in response to stimulation with 0.5 U thrombin. The colored points indicate significantly differentially expressed genes (FDR < 0.1).

4 Results II: Targeting of endothelial mechanosensing with actin binding compounds

Our results at this stage pointed to the direction that Miuraenamide A activates the MRTF-A-SRF signaling axis, but on the other hand has only marginal influence on the transcriptional coactivator YAP. To verify this hypothesis on a transcriptional level, we went back to the transcriptomic approach introduced in section 4.1 and searched the data set for significantly up- and downregulated MRTF-A and YAP / TAZ target genes^{80,81}. We found that, in line with our data on subcellular localization and SRE promotor activity, Miuraenamide A upregulated 90 out of 99 detected MRTF-A target genes (Fig. 4-10A). On the other hand, only 13 out of 31 YAP / TAZ targets were positively regulated by this compound, thus supporting our assumption that Miuraenamide A is far more efficient in activating MRTF-A compared to YAP / TAZ. In line with our data from section 4.3.1, we moreover found that the majority of MRTF-A and YAP / TAZ target genes was downregulated by the depolymerizing compound Latrunculin B (Fig. 4-10A).

Apart from Miuraenamide A and Latrunculin B, we also generated transcriptome data for the Rho GTPase activator thrombin and found that, in good agreement with the data described in section 4.1, both MRTF-A (170 out of 201) and YAP / TAZ (43 out of 72) target genes were predominantly upregulated by this substance (Fig. 4-10B and Fig. S4). Therefore, our transcriptomic data underscores the finding that YAP is differently affected by actin polymerization induced by Miuraenamide A compared to the physiological PAR ligand thrombin.

4.3.3 Role of AMOTp130 in linking F-actin levels to YAP activity

The actin-dependent regulation of YAP has been a subject of ongoing debate over the last years⁹⁰⁻⁹². Although the protein family of angiomotins (AMOT), in particular its isoform AMOTp130, has been suggested to provide the regulatory link between actin polymerization state and subcellular localization of YAP, it is yet unclear whether the canonical Hippo kinase cascade is involved in this process.

In order to investigate the mechanism by which cytoskeletal changes are translated into an adapted YAP activity profile, we analyzed the protein levels of phosphorylated YAP (pYAP) after stimulation with Miuraenamide A, Latrunculin B and thrombin (Fig. 4-11A). We found that while Latrunculin B led to a slight but significant increase of pYAP levels, neither Miuraenamide A nor thrombin affected the phosphorylation state of YAP. Since thrombin-induced actin polymerization readily triggered YAP nuclear translocation and subsequent target gene expression (4.3.1 and 4.3.2), we concluded that the canonical Hippo pathway could not be the key mediator of this response. Therefore, we next assessed the role of AMOTp130 in actin-dependent activation of YAP. Overexpression of HA-tagged AMOTp130 in HUVEC revealed that the nuclear translocation of YAP upon stimulation with thrombin was

4 Results II: Targeting of endothelial mechanosensing with actin binding compounds

completely abrogated by AMOTp130 (compare arrows for transfected versus non-transfected cells in Fig. 4-11B). Importantly, stimulation with Miuraenamide A had no effect on YAP subcellular localization, regardless of AMOTp130 expression levels.

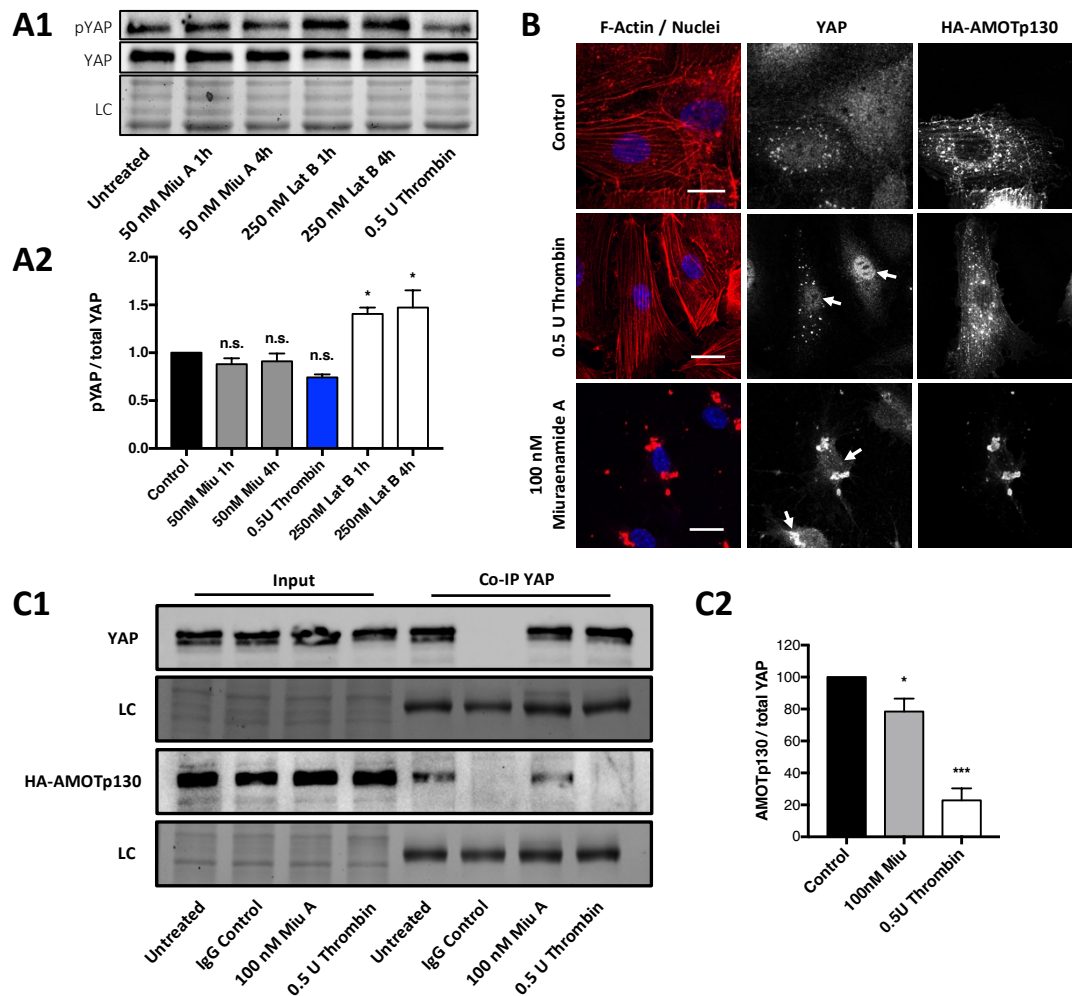


Figure 4-11 | Fig. 6 Miuraenamide A-induced actin polymerization fails to disrupt the interaction between AMOTp130 and YAP. (A) Western blot analysis (A1) and quantified protein levels (A2) of pYAP levels normalized to total YAP in cells treated with 50 nM Miuraenamide A, 250 nM Latrunculin B or 0.5 U thrombin. (B) HUVEC were transiently transfected with HA-AMOTp130 carrying constructs and after 2 h stimulation with either 0.5 U thrombin or 100 nM Miuraenamide co-stained for F-actin, YAP and the overexpressed variant of AMOTp130. Bars = 30 μ m. (C) HA-AMOTp130-expressing HUVEC were grown to confluency and stimulated as described in (B). After immunoprecipitation of endogenous YAP, bound AMOTp130 was detected via SDS-PAGE (C1, LC = loading control). (C2): Quantification of AMOTp130 levels normalized to total YAP, data derived from three independent experiments. Statistical significance in all experiments was determined using ordinary one-way ANOVA followed by Dunnett's multiple comparisons test.

To further investigate the role of AMOTp130 as a potential differentiator between Miuraenamide A- and thrombin-induced actin polymerization, Co-IP experiments targeting the interaction between YAP and AMOTp130 were performed (Fig. 4-11C). While we could indeed

4 Results II: Targeting of endothelial mechanosensing with actin binding compounds

detect an interaction between both proteins in untreated control cells, AMOTp130 was completely absent in the samples stimulated with thrombin. However, stimulation with Miuraenamide A only marginally weakened the interaction between YAP and AMOTp130 (Fig. 4-11C2).

In sum, our results confirm the role of AMOTp130 as a key mediator of actin-dependent YAP activation. Moreover, we found evidence that the regulatory crosstalk between AMOTp130, F-actin and YAP is the factor that determines the lacking YAP activation by Miuraenamide A.

Discussion

5 Discussion

5.1 MRTF and YAP: the unequal twins

5.1.1 MRTF and YAP share microenvironmental triggers

The sprouting of blood vessels from an existing vascular network involves the spatiotemporally coordinated degradation of the surrounding extracellular matrix followed by an invasion into it. This process requires a careful sensing and subsequent adaptation of endothelial cells to changing biophysical properties^{79,93}. Thus far, the majority of work on endothelial mechanosensing has focused on vascular remodeling processes and altered redox signaling in response to fluid shear stress^{79,94,95}. However, current knowledge on the physiological regulation and functional behavior of mechanosensitive signaling pathways in the context of angiogenesis is limited. To date, it is only known that both MRTF-SRF and Hippo-YAP / TAZ are mandatory for vascular development^{33,34,37,96}. In particular, the question of whether these two signaling pathways are completely redundant backup systems, or at least partially collaborating^{97,98}, remained open.

By varying the cell number on differently sized micro-adhesive squares, we observed that the loss of endothelial cell-cell contacts, a hallmark event in angiogenesis, serves as a trigger for nuclear translocation of both MRTF-A and YAP (Fig. 3-2). The role of cell-cell junctions in general, and of VE-Cadherins in particular, in regulating YAP subcellular localization has been described by Giampietro et al⁹⁹. We could confirm part of this work with our VE-cadherin blocking experiments and furthermore observed a functionally similar, though kinetically distinct response for MRTF-A (Fig. 3-3). Our present work thus expands the regulatory impact of VE-Cadherins on endothelial mechanosensing to the MRTF-SRF axis. Of note, the involvement of cadherin family proteins in the regulation of SRF is presumably not limited to VE-Cadherins. Busche et al. have reported similar findings for epithelial cell cadherins¹⁰⁰. Moreover, a recent study by Row et al. highlighted the role of Cadherin-11 as an upstream regulator of MRTF-A *in vivo*¹⁰¹.

Apart from their shared sensitivity towards cell-cell contacts, nuclear levels of both MRTF-A and YAP were influenced by the provided adhesive surface (Fig. 3-4). This was confirmed on a transcriptional level by the significantly reduced expression of MRTF-A and YAP target genes in a low-adhesive microenvironment (Fig. 3-4). In agreement with the findings reported here, Plessner et al. recently established a connection between integrin signaling, Rho GTPase activation and SRF-mediated transcription¹⁰². Consistently, Hermann et al. demonstrated that integrins synergize to trigger the expression of the invasion-promoting SRF target gene ISG15 (Interferon-stimulated gene 15)¹⁰³.

5 Discussion

Similar as for MRTF-A, we observed a clear correlation between adhesive square size and nuclear levels of the transcription factor YAP. The mechanism underlying this regulation is still incompletely understood. Zhao et al. previously showed that cell detachment initiates Lats1/2 kinase activity, and therefore YAP phosphorylation and cytoplasmic retention, in MCF10A cells¹⁰⁴. Mechanistically, a direct connection between integrins and Hippo signaling has been suggested¹⁰⁵. Due to the correlated behavior of both transcription factors on our square patterns, it is likely that integrins are a shared regulator of MRTF-A and YAP. Whether the activity of MRTF-A and YAP is ultimately regulated by the surface area or by the number of adhesive sites remains an open question. To address this issue, topographic micropatterns with a controlled number of adhesion sites could be used¹⁰⁶.

As a third parameter, we tested how a variation of cell shape would affect the subcellular localization of both transcription factors (Fig. 3-5). Although nuclear levels of MRTF-A and YAP were reduced in comparison to an unconfined control setting, we did not observe a shape-dependent regulation within the range of tested micropatterns. Interestingly, O'Connor et al. have reported a shape factor-dependent regulation of the SRF target TGF- β in epithelial cells under similar, though not completely identical experimental conditions¹⁰⁷. On the other hand, a global analysis of gene expression patterns performed by Stiles et al. concluded that spatial confinement *per se*, but not a particular cell shape, is the master regulator of an adapted transcriptional profile in human coronary artery endothelial cells¹⁰⁸. Since our observations in HUVEC point to a similar direction, there might be cell- or at least tissue-specific differences regarding the impact of cell shape on transcriptional regulation.

5.1.2 A question of time: how kinetics make the difference

The similar static response of MRTF-A and YAP to our different micropatterns does not allow to draw conclusions on potential kinetic variations in their regulation. We therefore analyzed translocation dynamics of both transcription factors during migration across a structurally challenging, dumbbell-shaped micropattern (Fig. 3-6). Our time-lapse imaging experiments on these interconnected squares revealed that MRTF-A reacts much more sensitive to this stimulus than YAP. Furthermore, the response of YAP to fluid shear stress was delayed compared to the rapid activation of MRTF-A (Fig. 3-7). In line with this, also inactivation of YAP, e.g. after the reformation of cell-cell contacts (Fig. 3-3), was markedly slower than in the case of MRTF-A.

The hypothesis on differential regulatory kinetics of MRTF-A and YAP in endothelial cells was supported by immunofluorescent co-stainings of both transcription factors at different stages of tubular network formation. In these experiments, MRTF-A expression levels were considerably reduced at nodal points of the inner network compared to the dynamic border

5 Discussion

regions already after two hours (Fig. 3-8). The reduction of total expression levels was accompanied by a significant drop in nuclear MRTF-A levels within confluent areas. However, we did not observe an equally rapid inactivation for YAP, which exhibited less pronounced differences in subcellular localization between outer and inner regions. The slow regulation of YAP was further reflected by a more consistent expression over time, resulting in a time-dependent variation of its correlation to MRTF-A expression (Fig. 3-8).

Our direct comparison of translocation dynamics, expression levels and subcellular localization of MRTF-A and YAP implicates that the kinetics and sensitivity of activation and inactivation are two of the most striking differentiators in the regulation of both transcription factors. In line with our present data for primary endothelial cells, Cui et al. have reported that MRTF-A is activated much faster than YAP when fibroblasts are subjected to cyclic stretching forces¹⁰⁹. In their experiments YAP activation was delayed by several hours when compared to the rapid nuclear translocation of MRTF-A¹⁰⁹. More recently, a study of the Posern group showed that a precise temporal control of MRTF-A is functionally required for the formation of mammary acini²⁴, thus highlighting the importance of MRTF-A regulation for spatiotemporally coordinated developmental processes.

Taken together, the results described in section 3.2 demonstrate that MRTF-A and YAP exhibit different kinetics in terms of their activation and inactivation. The regulatory aspects of both transcription factors, as described in sections 3.1 and 3.2., are summarized in the proposed regulatory scheme below (Fig. 5-1).

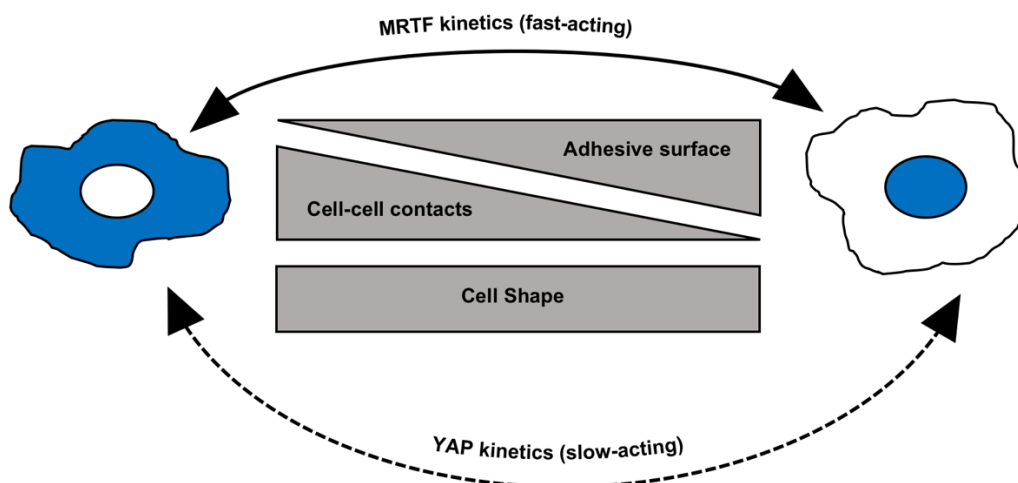


Figure 5-1 | Regulatory model of MRTF and YAP mechanosensing in endothelial cells

Based on the findings reported in the first part of this thesis, we suggest that - regardless of their shared activating stimuli - MRTF-A and YAP serve distinct functions in the regulation of angiogenesis. Due to its direct coupling to the polymerization state of actin (ref. section 2.2.2),

5 Discussion

MRTF-A could fulfill the role of a fast-responding mechanosensitive switch, which is rapidly activated at nascent sprouts and required for the highly dynamic process of tip cell invasion. In turn, the limited responsiveness of YAP to cytoskeletal remodeling points to the direction that this transcription factor could, once activated, serve to sustain a basal proliferative activity of endothelial cells during vessel development and maturation. On a functional level, this hypothesis is supported by the time-dependent expression of MRTF-A and YAP target genes in our transcriptomic approach (Fig. 3-7) and by the different expression patterns of both transcription factors in the developing murine retina (Fig. 3-9).

5.1.3 Master regulator or one out of many? The relationship between actin and YAP

A possible explanation for the divergent regulatory kinetics of MRTF-A and YAP can be found by looking at the differential role of actin in these two signaling cascades. In case of MRTF-A, its subcellular localization is directly coupled to the F- / G-actin equilibrium¹¹⁰. On the other hand, YAP is indirectly influenced by actin polymerization – presumably via angiomotins^{90,111}. Moreover, the canonical Hippo cascade is regulated by a variety of different stimuli³¹, which could at least partially annul each other or counteract the cytoskeletal influence. A physiological example for the complex influence of mechanical stimuli on YAP activity is given by its response to shear stress, which has been controversially discussed. Nakajima et al. reported that YAP is activated by fluid shear stress to promote vascular maintenance³⁸. In contrast, Xu et al. suggested that atheroprotective laminar flow would ultimately inhibit YAP in endothelial cells¹¹². Therefore, it might be possible that YAP is only activated in response to distinct mechanical cues. This has been suggested for disturbed flow conditions by Wang and colleagues¹¹³. Interestingly, YAP could be rapidly activated in our cells with thrombin (Fig. 4-9), pointing to the direction that its activation is not generally slow but rather dependent on the respective physiological context.

In any case, it will be important to answer the question whether there are upstream regulators of Hippo-YAP/TAZ that are completely independent from actin and other mechanical aspects. A possible pool of candidates is represented by the extensive group of G-protein coupled receptors, which can either activate or inactivate the Hippo pathway kinase Lats1/2^{30,31}.

5 Discussion

5.2 Actin polymerizers and mechanosensing: surprising selectivity

5.2.1 Miuraenamide A reveals the difference between MRTF and YAP

Apart from its distinct effect on nuclear actin levels, Miuraenamide A was identified as a potent activator of the mechanosensitive transcription factor MRTF-A (Fig. 4-9 and Fig. 4-10). This was to be expected, since monomeric actin serves as the direct and main regulator of MRTF-A^{16,17}. More remarkably, subcellular localization and thus activity of the actin-dependent transcription factor YAP remained unaffected by Miuraenamide A.

A regulatory connection between the actin cytoskeleton and YAP / TAZ has been extensively described^{31,91,92}. However, the underlying mechanism is not fully understood. Several research groups have demonstrated that the actin cytoskeleton is a major upstream regulator of the Hippo-YAP / TAZ pathway¹¹⁴. Still, it is not entirely clear whether a reduced activity of the canonical Hippo pathway kinases is mandatory or optional for actin-mediated activation of YAP^{111,115}. In this regard, our data points to the direction that actin polymerization per se does not necessarily interfere with YAP phosphorylation, regardless of whether the polymers are ultimately organized as a filamentous network or aggregate-like. In our experiments, a reduced interaction between AMOTp130 and YAP was sufficient to increase nuclear YAP levels independently from phosphorylation (Fig. 4-9 and Fig. 4-11). In line with previous work by Mana-Capelli et al., we therefore suggest that reduced Hippo pathway activity might act as an enhancer of actin-mediated YAP activation rather than being a prerequisite⁹⁰.

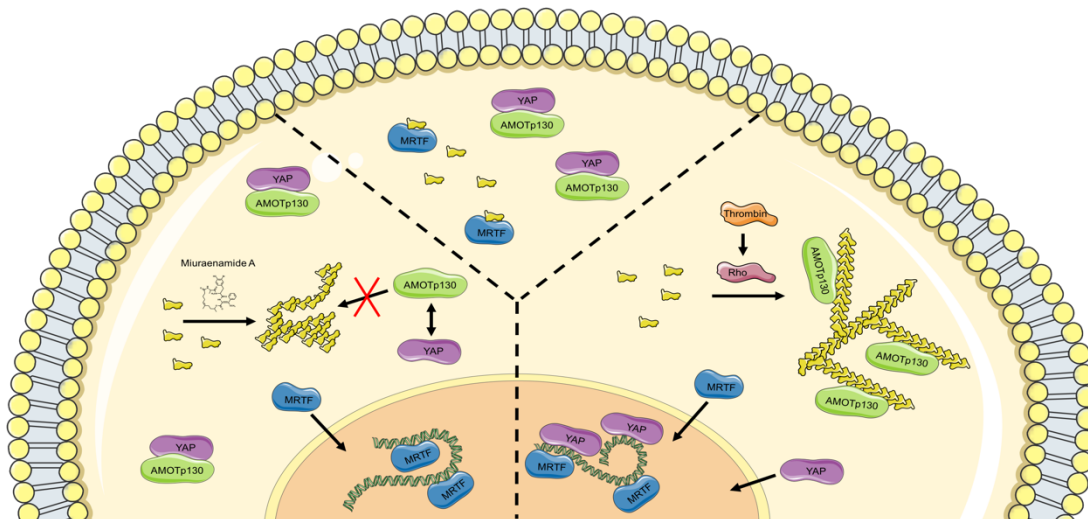


Figure 5-2 | Proposed regulatory model underlying the differential response of MRTF-A and YAP to Miuraenamide A-induced actin aggregation

5 Discussion

Based on our results, we developed the regulatory model shown in Fig. 8. In brief, our model states that the structure of polymerized actin decides over its ability to trigger nuclear translocation of YAP via cytoskeletal remodeling. In turn, our findings support the role of F-actin as a binding scaffold for the YAP inhibitory protein AMOTp130¹¹⁶.

MRTF-A and YAP are known for sharing a variety of target genes, such as CCN1 or CTGF⁹⁷. Moreover, a crosstalk between MRTF-A and YAP has recently been reported to be causative for the development of breast cancer metastasis⁹⁸. Similar findings by Speight et al. demonstrated a context-dependent switch in chemo- and mechanotransduction between MRTF-A and the YAP-related protein TAZ¹¹⁷. In this context, Miuraenamide A provides an interesting possibility for selective targeting of the MRTF-SRF signaling axis.

5.2.2 Actin binding compounds as cell biological tools: chances and pitfalls

On the one hand, our results showed that actin stabilizers, such as Miuraenamide A, are adequate tools to deplete endogenous G-actin. In addition, the results described here identified actin polymerizers and depolymerizers as pharmacological tools for the bidirectional modulation of nuclear actin levels (Fig. 4-7). In this context, it is important to mention that our FCS and RICS experiments prove that nuclear actin levels can be selectively altered without a change of intranuclear polymerization state.

On the other hand, the present work clearly demonstrates that actin binding compounds have experimental limitations that need to be considered. First, due to their aggregate-like structure, the resulting polymers cannot be functionally equated with physiological F-actin (Fig. 4-11). This is particularly important when it comes to the investigation of processes that involve the interaction of F-actin with specific binding partners. Previous work in our lab has demonstrated that actin aggregation by Chondramide B, a structural relative of Miuraenamide A, can simply trap binding partners in the resulting actin “clumps” without a specific interaction. Second, the transcriptome data introduced in Fig. 4-1 and Fig. 4-2 brought up a number of genes that are not directly connected to altered actin dynamics. Thus, it should be kept in mind that – similar to most other compounds - actin binders can have off target effects. In the case of actin polymerizing drugs, this issue is difficult to address, since most of these compounds share a common cyclic depsipeptide backbone (ref. section 2.4.1) and are thus likely to share common off target effects.

5 Discussion

5.3 Actin binding compounds predominantly act in the cytoplasm

5.3.1 Nuclear actin and transcription: a matter of concentration?

In the experiments described here, transcription was regulated by actin binding compounds at concentrations that affected the quantities of nuclear actin, but not its polymerization state (Fig. 4-5, Fig. 4-6). Our data thus implicates that, in order to manipulate transcriptional events, nuclear actin does not necessarily need to polymerize or depolymerize. Other examples that highlight the regulatory importance of nuclear actin levels rather than polymerization state, include but are not limited to the work of Spencer et al.⁵¹ and two studies of the Vartiainen lab^{44,118}. Second, our findings suggest that intranuclear actin polymerization does not significantly contribute to the mode of action of actin binding compounds. Nevertheless, this does not exclude the possibility that intranuclear actin polymerization is relevant in other physiological contexts such as DNA damage response, mitosis or spreading^{47,119-121}.

Nuclear and cytoplasmic actin pools are in a dynamic equilibrium, which is maintained via an active transport mechanism mediated by importin 9 and exportin 6^{44,45}. Since actin can only enter or exit the nucleus in monomeric form, we assume that an interference with the cytoplasmic polymerization state of actin can shift the steady state distribution of actin monomers between both compartments. As it is shown in the regulatory model presented in Fig. 5-3., we suggest that the change in nuclear actin concentration is a secondary result of an altered cytoplasmic G-actin availability and thus nuclear import rates.

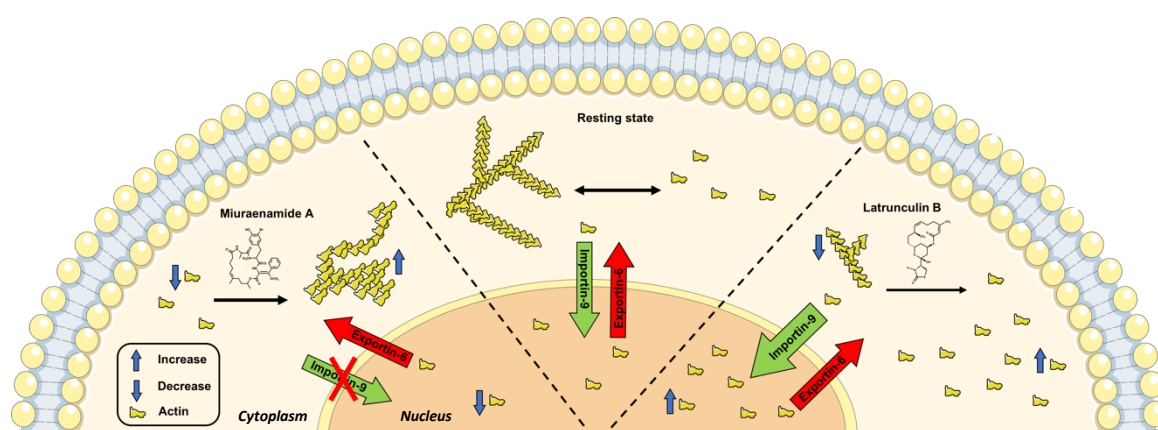


Figure 5-3 | Proposed model for the response of nuclear versus cytoplasmic actin to polymerizing and depolymerizing actin binding compounds.

5.3.2 Transcriptional effects of actin binding compounds: The cytoplasm sets the tone

We observed that extremely high concentrations of Miuraenamides A can induce nuclear actin aggregation in NLS-actin overexpressing cells (Fig. 4-8). However, the endogenous amount of readily accessible intranuclear actin monomers was insufficient to trigger polymerization

5 Discussion

with Miuraenamide A at any concentration. Since the cytoplasmatic concentration of actin is in the micromolar range ¹²², we assume that actin binding compounds are preferentially bound in the cytoplasm. In turn, these compounds are unable to reach the nucleus in sufficient quantities within the timescale required to influence transcriptional regulation via actin polymerization.

5.4 Outlook and future perspectives

5.4.1 Transcriptional targets beyond MRTF

MRTF-SRF signaling accounts for many, but by far not for all of the genes regulated in our transcriptomic analysis (Fig. 4-1, Fig. 4-2). In this context, the drastic changes in nuclear shape and chromatin structure induced by actin binding compounds provide an interesting track for further investigation (Fig. 4-3). It is well established that chromatin architecture is reorganized in response to cytoskeletal destabilization ^{10,12,123}. However, to our knowledge, very little is known about gene sets that are specifically regulated by changes in nuclear shape or a disruption of the LINC complex.

Elosegui-Artola et al. have recently described the nuclear entry of YAP in force-deformed cell nuclei ¹²⁴. Although both Miuraenamide A and Latrunculin B severely affected nuclear shape in our experiments (Fig. 4-3), we did not see any activation of YAP in either case (Fig. 4-9). An explanation for this could be that nuclear pore size is differently affected in nuclei which are deformed by force compared to cytoskeletal destabilization through actin binding compounds. To our knowledge, very little is known about gene sets that are specifically regulated by changes in nuclear shape ^{125,126}. Still, the nuclear deformation induced by actin binding compounds could be responsible for the regulation of distinct gene sets in our transcriptomic approach. Next to the use of actin binding compounds, a transient induction of nuclear deformation can be achieved with the dumbbell-shaped patterns introduced in Fig. 3-6. In combination with live cell mRNA probes, such as SmartFlareTM reagents, the dynamic transcription of force-dependent genes could be studied (Fig. 5-4).

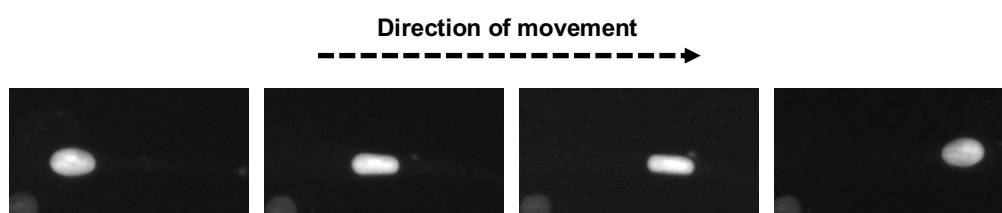


Figure 5-4 | Nuclear deformation during migration across dumbbell-shaped micropatterns. For visualization of cell nuclei, HUVEC were transiently transfected with nAC-GFP carrying plasmid constructs.

5 Discussion

5.4.2 Temporal control of microadhesive surfaces

Our results showed that the regulatory differences between MRTF-A and YAP are mainly based on kinetic aspects. Switchable micropatterns could provide an experimental route to further investigate this finding with adequate temporal resolution.

In general, temporally controllable micropatterns can be generated by purely chemical, combined photochemical or thermosensitive substrate approaches¹²⁷. A frequently used method involves the covalent coupling of protein-repellent PLL-PEG to azide groups¹²⁸. By in situ Huisgen reaction with cyclooctynes, these surfaces are rendered adhesive under biocompatible conditions¹²⁹.

Although the abovementioned strategy can be used to trigger dynamic processes like collective cell migration, it lacks the spatial resolution required to study cytoskeletal remodeling in single cells. To further elucidate the kinetics of MRTF-A and YAP nuclear translocation in single endothelial cells, photoswitchable surfaces could be used. For example, the provided adhesive surface area could be incrementally increased by local laser ablation of photocleavable PLL-PEG derivatives¹³⁰. In combination with live cell imaging of fluorescently labeled transcription factors, this would allow for a real-time analysis of MRTF-A and YAP subcellular localization in response to defined microenvironmental alterations.

5.4.3 Let there be light: a route for selective targeting of nuclear actin

Due to the abundance of cytoplasmic actin, the selective targeting of nuclear actin poses a significant experimental challenge. An interesting approach to overcome this obstacle is provided by the emerging field of optogenetics and photoswitchable reagents. In 2002, Nagel et al. reported that the expression of Channelrhodopsin-1, an ion channel found in green algae, produced light-gated conductance in *Xenopus laevis* oocytes¹³¹. In the following years, optogenetic techniques were further developed and successfully used in neurosciences¹³². In 2017, Baarlink et al. showed that nuclear actin depolymerization can be inhibited by the expression of an optogenetic cofilin-1 derivative¹¹⁹.

A closely related possibility for the selective targeting of intranuclear actin could be the development of photoswitchable actin binding compounds. In 2015, Borowiak et al. demonstrated that mitosis and cell death can be optically controlled by photostatins, a novel group of photoswitchable microtubule inhibitors¹³³. Given the availability of suitable molecular candidates, this concept could be transferred to target other cytoskeletal components, such as intermediate filaments or actin.

5 Discussion

5.5 Summary and Conclusion

In conclusion, the first part of this thesis provides a systematic comparative analysis of microenvironmental cues for the mechanosensitive regulation of blood vessel formation. Based on the application micropatterning techniques as a tool to mimic mechanobiological aspects of angiogenesis, we identify the loss of cell-cell contacts and changes in adhesive surface as major regulators of both MRTF-A and YAP nuclear translocation in endothelial cells. Apart from these similarities, we observe that MRTF-A exhibits significantly higher responsiveness than YAP on a short time scale. Our results are recapitulated in two angiogenic model systems, corroborating the hypothesis that both transcription factors are assigned different tasks within the spatiotemporal regulation of angiogenesis.

The second part of this study aims to investigate the transcriptional response to actin binding compounds in primary endothelial cells. We demonstrate that Miuraenamide A is a potent and selective activator of the MRTF-SRF signaling axis, since the aberrant structure of cytoplasmic aggregates formed by this compound prevents the activation of other mechanosensitive signaling pathways such as Hippo-YAP/TAZ. In turn, these findings emphasize that not every actin-dependent cellular process can be mimicked with actin binding compounds. Second, our data shows that, although actin binding compounds interfere with the quantities of nuclear actin, intranuclear polymerization state and transcriptional machineries in the nucleus remain largely unaffected. Thus, we conclude that actin binding compounds regulate transcription via the cytoplasm rather than the nucleus.

Materials & Methods

6 Material and Methods

6.1 Materials

6.1.1 Compounds

The myxobacterial compound Miuraenamides A was provided by the lab of Prof. Uli Kazmaier (Institute for Organic Chemistry, Saarland University, Saarbrücken, Germany) ⁶⁶. Chivosazole A was isolated from myxobacteria in the lab of Prof. Rolf Müller (Helmholtz Institute of Pharmaceutical Research Saarland, Saarbrücken, Germany). Both compounds were stored at -20 °C as 10 mM DMSO stock solutions and used at working concentrations between 50 - 100 nM containing < 0.1% DMSO.

Latrunculin B and Jasplakinolide were both purchased from Sigma (Taufkirchen, Germany) and handled according to the manufacturer's instructions.

6.1.2 Chemicals and reagents

The following table contains a list of all chemicals, reagents and kits used in this study. Antibodies (6.1.2.1), buffers and solutions (6.1.2.2) and plasmids (6.2.5) are listed separately.

Table 1 Chemicals and reagents

Reagent	Company
0.05% Bromophenol blue	Sigma-Aldrich, Taufkirchen, Germany
16% formalin, EM-grade	Polysciences Inc., PA, USA
5% Blotto solution	Thermo Scientific, MA, USA
AffiniPure F _{ab} fragments	Jackson Immunoresearch, PA, USA
Amersham ECL Reagent	GE Lifesciences, Chalfont St Giles, UK
Amphotericin B	PAN Biotech, Aidenbach, Germany
Ampicillin	Sigma-Aldrich, Taufkirchen, Germany
APS	Thermo Scientific, MA, USA
ATTO488 dye	ATTO-TEC GmbH, Siegen, Germany
Bovine serum albumin (BSA)	Sigma-Aldrich, Taufkirchen, Germany
Bradford Roti [®] Quant reagent	Bio-Rad, Munich, Germany
Collagen G	Biochrom AG, Berlin, Germany
Complete [®] protease inhibitor	Roche Diagnostics, Penzberg, Germany
Dimethylsulfoxide (DMSO)	Sigma-Aldrich, Taufkirchen, Germany
DNAseI-AlexaFluor 488	Thermo Scientific, MA, USA
DNAseI, RNAse-free	Thermo Scientific, MA, USA
Dulbecco's Modified Eagle Medium (DMEM)	PAA Laboratories, Pasching, Austria
Duolink [®] PLA kit and PLUS / MINUS probes	Sigma-Aldrich, Taufkirchen, Germany
Endothelial cell growth medium	Pellobiotech GmbH, Martinsried, Germany
Ethylendiaminetetraacetic acid (EDTA)	Sigma-Aldrich, Taufkirchen, Germany

6 Material and Methods

Reagent	Company
Ethylene glycol tetraacetic acid (EGTA)	Sigma-Aldrich, Taufkirchen, Germany
Exonuclease I	Thermo Scientific, MA, USA
Fetal calf serum (FCS)	Biochrom AG, Berlin, Germany
Fibronectin	Corning, NY, USA
FluorSave® reagent mounting medium	Merck, Darmstadt, Germany
Glutaraldehyde 50%	Fluka Biochem, Taufkirchen, Germany
Glycerol	Applchem, Darmstadt, Germany
High-Capacity cDNA Reverse Transcription Kit	Applied Biosystems, Waltham, USA
Hoechst 33342	Sigma-Aldrich, Taufkirchen, Germany
IB4-AlexaFluor 488	Thermo Scientific, MA, USA
IGEPAL CA-630	Sigma-Aldrich, Taufkirchen, Germany
Kanamycin	Sigma-Aldrich, Taufkirchen, Germany
KAPA HiFi HotStart polymerase	KAPA Biosystems, MA, USA
LB agar powder	Invitrogen, CA, USA
LB broth powder	Invitrogen, CA, USA
Matrigel™ REF 356231	Corning, NY, USA
Nextera XT Kit	Illumina, CA, USA
PageRuler™ Plus Prestained Protein Ladder	Fermentas, St. Leon-Rot, Germany
Penicillin / Streptomycin 100x	PAN Biotech, Aidenbach, Germany
Phenylmethylsulfonyl fluoride (PMSF)	Sigma-Aldrich, Taufkirchen, Germany
Plasmid Maxi Prep Kit	QIAGEN, Hilden, Germany
PLL(20 kDa)-g[3.5]-PEG(2 kDa)	Surface Solutions, Dübendorf, Switzerland
Polyacrylamide	Carl Roth, Karlsruhe, Germany
Potassium dihydrogen phosphate	Carl Roth, Karlsruhe, Germany
PowerUp™ SYBR® Green Master Mix	Applied Biosystems, MA, USA
Protein G agarose suspension	Roche, Basel, Switzerland
Pyronin Y	Sigma-Aldrich, Taufkirchen, Germany
Rhodamine/Phalloidin	Sigma-Aldrich, Taufkirchen, Germany
RNeasy® Mini Kit (250)	QIAGEN, Hilden, Germany
Rotiphorese™ Gel 30	Carl Roth, Karlsruhe, Germany
Sera-Mag carboxylated magnetic beads	Thermo Scientific, MA, USA
Sodium borohydride	Sigma-Aldrich, Taufkirchen, Germany
Sodium chloride	Carl Roth, Karlsruhe, Germany
Sodium deoxycholate	Carl Roth, Karlsruhe, Germany
Sodium dodecyl sulfate (SDS)	Carl Roth, Karlsruhe, Germany
Sodium fluoride (NaF)	Merck, Darmstadt, Germany
Sodium hydrogen phosphate	Carl Roth, Karlsruhe, Germany
Sodium orthovanadate (Na ₃ VO ₄)	ICN Biomedicals, OH, USA
Sodium pyrophosphate	Sigma-Aldrich, Taufkirchen, Germany
β-Glycerophosphate	Sigma-Aldrich, Taufkirchen, Germany
β-Mercaptoethanol	Sigma-Aldrich, Taufkirchen, Germany
Sylgard 184 Silicone Elastomer Kit	Corning, NY, USA
Targefect-HUVEC™	Targeting Systems, CA, USA
TEMED	Thermo Scientific, MA, USA
Tris Base	Sigma-Aldrich, Taufkirchen, Germany
Tris HCl	Sigma-Aldrich, Taufkirchen, Germany
Triton X-100	Sigma-Aldrich, Taufkirchen, Germany
Trypsin	PAN Biotech, Aidenbach, Germany
Tween 20	Sigma-Aldrich, Taufkirchen, Germany

6 Material and Methods

6.1.2.1 Antibodies

The following tables contain all antibodies used in this study. Primary and secondary antibodies are listed separately.

Table 2 Primary antibodies

Name	Species	Catalogue	Manufacturer	Dil. Fc. IF / WB
Angiomotin (D2O4H)	rabbit mAb IgG	#43130	CST	- / 1:1000
Anti-ACTB	mouse mAb IgG ₁	AMAB91241	Sigma	1:100 (Duolink)
Anti-BrdU Clone BU-33	mouse mAb IgG	B8434	Sigma	1:500 / -
HA-Tag (6E2)	mouse mAb IgG ₁	#2367	CST	1:150 / 1:1000
HistoneH3 (acetyl K9)	mouse mAb IgG ₁	ab12179	Abcam	- / 1:1000
HistoneH3 (dimethyl K4)	mouse mAb IgG ₁	25254	BPS	- / 1:1000
HistoneH3 (trimethyl K4)	mouse mAb IgG ₁	ab12209	Abcam	- / 1:1000
HistoneH3 total	rabbit polyclonal	ab1791	Abcam	- / 1:1000
MRTF-A	mouse mAb IgG _{2a}	sc-390324	SCBT	1:150 / -
POLR1A (Polymerase I)	rabbit mAb IgG ₁	HPA031513	Sigma	1:100 (Duolink)
VE-Cadherin D87F2	rabbit mAb IgG	#2500	CST	1:150 / -
VE-CadherinECD	mouse mAb IgG _{2a}	MABT134	Merck	1:100 (blocking)
YAP (B-8)	mouse mAb IgG _{2a}	sc-398182	SCBT	1:150 / 1:1000
YAP XP [®] D8H1X	rabbit mAb IgG	#14074	CST	1:150 / 1:1000

Table 3 Secondary antibodies, HRP- and IF-conjugates

Name	Species	Catalogue	Manufacturer	Dilution
AlexaFluor 488	goat anti-mouse	A-11001	Thermo Scientific	1:500
AlexaFluor 647	goat anti-rabbit	A-21245	Thermo Scientific	1:500
AlexaFluor 546	goat anti-mouse	A-11030	Thermo Scientific	1:500
HRP conjugate	goat anti-rabbit	#1706515	Bio-Rad	1:1000
HRP conjugate	goat anti-mouse	BZL07046	Biozol	1:1000

6.1.2.2 Buffers and solutions

Table 4 Buffers and solutions

Separation gel (pH 8.8)		Stacking gel (pH 6.8)	
Rotiphorese [™] Gel 30	25/33/40/50%	Rotiphorese [™] Gel 30	17%
Tris base	375 mM	Tris HCl	125 mM
SDS	0.1%	SDS	0.1%
TEMED	0.1%	TEMED	0.2%
APS	0.05%	APS	0.1%
H ₂ O		H ₂ O	

6 Material and Methods

Electrophoresis buffer		Tank buffer	
Tris base	4.9 mM	Tris base	48 mM
Glycine	38 mM	Glycine	39 mM
SDS	0.1%	Methanol	20%
H ₂ O		H ₂ O	
Standard lysis buffer		5x SDS sample buffer (pH 6.8)	
Tris HCl	50 mM	Tris HCl	3.125 M
NaCl	150 mM	Glycerol	50%
IGEPAL CA-630	1%	SDS	5%
Sodium deoxycholate	0.25%	DTT	2%
SDS	0.10%	Pyronin Y	0.025%
Na ₂ VO ₄	300 μM	H ₂ O	
NaF	1 mM	NP-40 lysis buffer	
β-Glycerophosphate	3 mM	NaCl	150 mM
Pyrophosphate	10 mM	IGEPAL CA-630	1%
H ₂ O		Tris HCl	50 mM
before use:		Sodium deoxycholate	0.25%
Complete [®] protease inh.	4 mM	EGTA	1 mM
PMSF	1 mM	H ₂ O	
H ₂ O ₂	600 μM	before use:	
		PMSF	1 mM
		Complete [®] protease inh.	1:10
PLA Washing buffer A (pH 7.4)		PLA Washing buffer B (pH 7.5)	
Tris base	10 mM	Tris base	35 mM
NaCl	150 mM	NaCl	100 mM
Tween 20	0.05%	Tris HCl	165 mM
H ₂ O		H ₂ O	
Cytoskeleton Stabilizing buffer		PBS (pH 7.4)	
Tris base	4.9 mM	NaCl	137 mM
Glycine	38 mM	KCl	2.7 mM
SDS	0.1%	Na ₂ HPO ₄	10 mM
H ₂ O		KH ₂ PO ₄	1.8 mM
		H ₂ O	
TBS-T (pH 7.6)			
Tris HCl	50 mM		
NaCl	150 mM		
Tween 20	0.1%		
H ₂ O			

6 Material and Methods

6.1.3 Technical equipment

Table 5 Technical devices and lab equipment

Device Name	Manufacturer
Axiovert 25/200 microscope	Zeiss, Jena, Germany
Bold Line incubation system	Okolab, Pozzuoli, Italy
ChemiDoc™ Touch imaging system	Bio-Rad GmbH, Dreieich, Germany
Digital UV Ozone Cleaner system	Novascan, IA, USA
HERACell 150i incubator	Thermo Scientific, MA, USA
HiSeq1500 sequencing device	Illumina, CA, USA
ibidi Gas Incubation system	ibidi, Martinsried, Germany
ibidi Heating system	ibidi, Martinsried, Germany
ibidi Pump system	ibidi, Martinsried, Germany
Megafuge 1.0 RS centrifuge	Thermo Scientific, MA, USA
Mikro 220R centrifuge	Hettich, Bäch, Switzerland
Mini PROTEAN 3 electrophoresis chambers	Bio-Rad GmbH, Dreieich, Germany
Mini Trans-Blot® system	Bio-Rad GmbH, Dreieich, Germany
Nanodrop® 1000 spectrophotometer	PEQLAB Biotechnologie GmbH
Nikon Eclipse Ti inverted microscope	Nikon, Düsseldorf, Germany
Orion II microplate luminometer	Titertek Berthold, Bad Wildbad, Germany
Peqlab heating block	VWR, Bruchsal, Germany
Power Pac 300 blotting device	Bio-Rad GmbH, Dreieich, Germany
QuantStudio™ 3 Real-Time PCR system	Applied Biosystems, MA, USA
SpectraFluor Plus™ plate reader	Tecan, Crailsheim, Germany
TCS SP8 SMD confocal microscope	Leica Microsystems, Wetzlar, Germany
Vi-Cell™ XR cell counter	Beckman Coulter, CA, USA
Vibrax VXR basic lab shaker	IKA, Staufen, Germany

6.1.4 Consumables

Table 6 Consumables

Product	Manufacturer
Cell culture dish, 60.1 cm ² and flasks, 75 cm ²	TPP, Trasadingen, Switzerland
Disposable pipettes: 5 ml, 10 ml, 25 ml	Greiner Bio, Frickenhausen, Germany
Falcon tubes: 15 ml, 50 ml	VWR, Bruchsal, Germany
MicroAmp® Fast Optical 96 Well plate, 0.1 mL	Applied Biosystems, MA, USA
MicroAmp® Optical Adhesive Film	Applied Biosystems, MA, USA
Microtiter plates: 6 well, 12 well, 96 well	Greiner Bio, Frickenhausen, Germany
Nitrocellulose membrane (0.2 µM) Hybond-ECL™	Amersham Bioscience, Freiburg, Germany
PCR tubes	Eppendorf, Hamburg, Germany
Pipette tips: 10 µl, 100 µl, 1000 µl	Sarstedt, Nümbrecht, Germany
Polyvinylidene difluoride (PVDF) membrane	Amersham Bioscience, Freiburg, Germany
Safe-Lock Tubes: 0.5 ml, 1.5 ml, 2.0 ml	Eppendorf, Hamburg, Germany
µ-Slide 18 well ibitreat	ibidi, Martinsried, Germany
µ-Slide 8 well (glass, ibitreat, uncoated)	ibidi, Martinsried, Germany
µ-Slide Angiogenesis	ibidi, Martinsried, Germany
µ-Slides I 0.4 Luer	ibidi, Martinsried, Germany

6 Material and Methods

6.2 Methods

6.2.1 Cell culture

6.2.1.1 Cell lines and culture media

All cells were cultivated at 37 °C and high humidity under 5% CO₂ atmosphere. Cell culture media were supplemented with 1% penicillin / streptomycin and amphotericin B.

Human umbilical vein endothelial cells (HUVEC) were purchased from Promocell. Cells were cultivated with endothelial cell growth medium from PELO Biotech supplemented with ECGM Kit enhanced and 10% FCS. All experiments were performed in passage #6.

NIH3T3 cells were purchased from Sigma-Aldrich and cultivated with DMEM supplemented with 10% FCS. To ensure equal adhesive conditions across different assay formats, fibronectin coated surfaces were used in all experiments.

6.2.1.2 Cell counting and passaging

For detachment of adherent cells, the growth medium was removed and cells were shortly rinsed with prewarmed PBS. After 5 min incubation with trypsin / EDTA at 37 °C, tryptic digestion was stopped by the addition of standard growth medium. Cells were centrifuged at 1.000 rpm for 5 min and the pellet was resuspended in full growth medium.

Cells were counted using a ViCell™ XR cell counter. Upon reaching confluence, cells were either split 1:2 into 75 cm² cell culture flasks or seeded at subconfluent densities for further experiments.

6.2.2 Microcontact printing

For the generation of microadhesive surface patterns, silicon template wafers carrying the desired microfeatures were generated in the lab of Prof. Joachim Rädler (Chair for Soft Condensed Matter, LMU, Munich). Polydimethylsiloxane (PDMS) stamps were crafted by pouring a 10:1 mixture of the monomer and its crosslinker on top of these wafers. After removal of air bubbles under vacuum atmosphere, the samples were left overnight for polymerization at 50 °C. The resulting PDMS stamps were cut out with a scalpel and hydrophilized for 20 min using a commercially available UV ozone cleaner. Stamps were coated with 50 µg/ml fibronectin for 2 h and excess protein solution was removed by rinsing with sterile H₂O. The protein pattern was then transferred onto the surface of uncoated µ-Slides 8 well via microcontact printing (µCP, 1 h). Surrounding areas were blocked for cell adhesion by 15 min incubation with a sterile aqueous solution of 1 mg/ml PLL(20kDa)-g[3.5]-PEG(2kDa). Excess

6 Material and Methods

PLL(20kDa)-g[3.5]-PEG(2kDa) solution was removed by short rinsing with PBS. 200 μ l cell suspension (5000 cells / well) were added to each well and after cell attachment, the medium was changed to remove residual unattached cells.

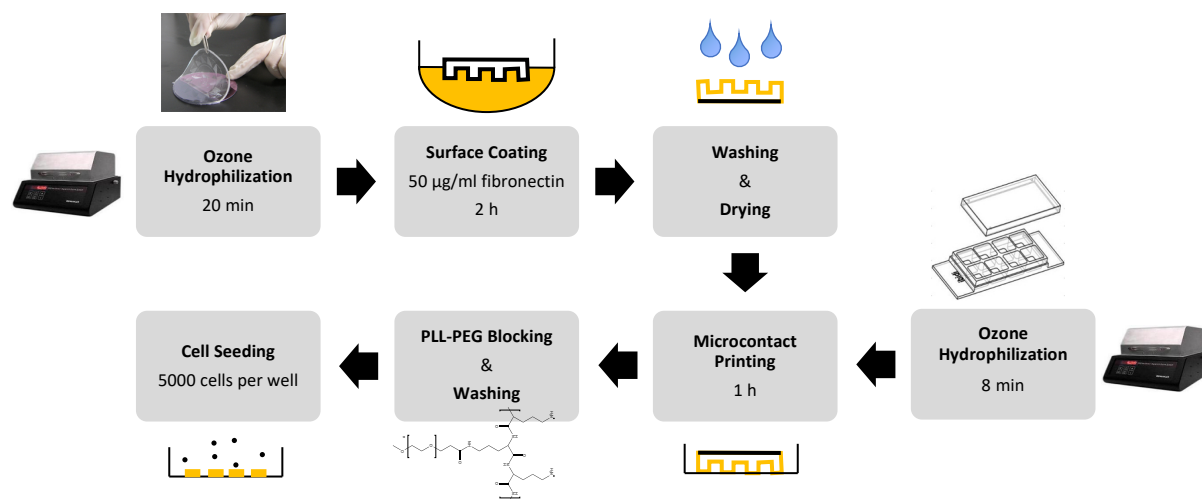


Figure 6-1 | Microcontact printing workflow

6.2.3 Confocal Imaging

Confocal images were acquired using a Leica TCS SP8 SMD microscope equipped with hybrid detectors (Leica HyD) and the following HC PL APO objectives: 40x / 1.30 OIL, 63x / 1.40 OIL, 63x / 1.20 W CORR. Pinhole size was adjusted to 1.0 airy units and scanning was performed between 400-600 Hz. An average of four frames was acquired for every channel in sequential scanning mode. The following laser lines and excitation sources were used: 405 nm (Diode), 561 nm (DPSS), 488 nm and 647 nm (both Argon).

6.2.3.1 Immunofluorescence stainings

For immunofluorescence stainings, cells were shortly rinsed with PBS + Ca^{2+} / Mg^{2+} followed by 10 min fixation with 4% EM grade formaldehyde. After 5 min washing with PBS, samples were permeabilized for 10 min with 0.5% TX-100 in PBS. Unspecific binding was blocked by 30 min incubation with 5% goat serum in PBS at RT. Cells were then incubated overnight with primary antibodies diluted in PBS + 0.2% BSA (4 °C). After 3 x 10 min washing with PBS, samples were incubated with secondary antibodies, rhodamine phalloidin (1:300) and Hoechst 33342 (0.5 μ g/ml) for 1 hour at RT, washed again 3 x 10 min with PBS and sealed with one drop of FluorSave reagent mounting medium and cover slips. All stainings were performed in ibiTreat 8 well μ -slides coated with fibronectin.

6 Material and Methods

6.2.3.2 Visualization of nuclear actin

Nuclear actin stainings were performed with cytoskeleton stabilizing buffers (CSB) and 2% glutaraldehyde fixation as previously described ¹³⁴. In brief, an initial 1 min prefixation with 0.5% Triton X-100 + 0.25% glutaraldehyde in CSB was followed by 15 min fixation with 2% glutaraldehyde in CSB. Autofluorescence was quenched using freshly prepared 1 mg/ml NaBH₄ solution in CSB and after repeated washing steps, samples were incubated with rhodamine phalloidin (1:300) and Hoechst 33342 (0.5 µg/ml) for 1 h at RT. After one additional washing step with PBS, samples were mounted with one drop of FluorSave reagent and sealed with custom cover slips.

6.2.3.3 Nuclear run on assays

For quantification of 5-fluorouracil (5-FU) incorporation during RNA synthesis (nuclear run on assay), cells were pretreated with either Miuraenamamide A, Latrunculin B or Actinomycin D (negative control) at indicated concentrations. After incubation with a 5 mM 5-FU solution for the last 90 min of stimulation, samples were immunostained as described in section 6.2.3.1. Nuclear 5-FU foci were quantified using the ImageJ particle analyzer tool according to the available online instructions.

6.2.3.4 Single cell F- / G-actin ratios

For determination of F- / G-actin ratios, cells were co-stained with rhodamine phalloidin (1:300 dilution, detection of F-actin) and DNaseI-AF488 (1:600 dilution), which binds G-actin monomers with high affinity ⁷⁷. F- / G-actin levels were quantified as the quotient of total rhodamine phalloidin / DNaseI-AF488 signal intensity ⁷⁸. The staining was performed using the buffers and reagents described in section 6.2.3.1.

6.2.3.5 DNase I chromatin digestion

To quantify the fraction of condensed chromatin after stimulation with actin binding compounds, cells were fixed with cold methanol for 10 min. Subsequently, accessible chromatin regions were digested for 2 h at 37 °C using 1 unit of DNase I per well. Undigested DNA was visualized with Hoechst 33342 (0.5 µg/ml) and cellular heterochromatin content was quantified as total signal intensity of each image divided by the respective cell number. Untreated samples with and without DNase I digestion were used for normalization and as negative controls.

6 Material and Methods

6.2.4 Angiogenesis assays

6.2.4.1 Tube formation assay

Tube formation assays were performed in μ -Slides Angiogenesis from ibidi. 11×10^3 HUVEC were seeded onto thin layers of polymerized MatrigelTM (REF 356231) and the samples were incubated for appropriate time spans at 37 °C, 5% CO₂ and high humidity.

For immunofluorescence stainings of tube formation samples, cells were initially washed with PBS + Ca²⁺ / Mg²⁺ and subsequently fixed with 4% EM grade formaldehyde in PBS for 40 min. Samples were permeabilized for 20 minutes with 0.5% TX-100 in and unspecific binding was blocked by overnight incubation (4 °C) with 5% goat serum in PBS supplemented with 30 μ g/ml anti-mouse AffiniPure F_{ab} fragments. After 20 min washing with PBS + 0.2% BSA, samples were incubated overnight (4 °C) with primary antibodies diluted in PBS + 0.2% BSA. Subsequently, cells were washed 3 x 20 min with PBS + 0.2% BSA and secondary antibodies, Hoechst 33342 (0.5 μ g/ml) and rhodamine phalloidin (1:300) were added. After overnight incubation at 4 °C, samples were again washed 3 x 20 min and one drop of FluorSave mounting medium was added 1 h before imaging.

6.2.4.2 Retinal whole-mount stainings

Wild-type C57BL/6 pups (n = 4) were sacrificed at postnatal day 6 (P6). The preparation and staining of murine retinas was performed as previously described by Pitulescu et al ¹³⁵. In brief, eyeballs were removed and fixed for 2 h in 4% EM grade formaldehyde in PBS. After retinal preparation, retinas were blocked and permeabilized for 2 h at RT with 1% BSA, 0.3% TX-100 in PBS. Retinal vasculature was labelled using an IsolectinB4-AlexaFluor 488 conjugate. Overnight incubation with primary antibodies targeting MRTF-A and YAP was followed by several washing steps and addition of secondary antibodies. Nuclei were visualized with Hoechst 33342 (0.5 μ g/ml) and after two more washing steps, retinas were mounted in uncoated μ -slides 8 well using FluorSave mounting medium. All animal procedures were approved and controlled by the local Ethics Committee and carried out according to the guidelines of the German law of protection of animal life.

6.2.5 Plasmids and transfections

Primary endothelial cells were transiently transfected using the commercially available Targefect-HUVECTM transfection system at serum-free conditions according to the manufacturer's instructions. One day prior to transfection, 125.000 cells / ml were seeded in CollagenG coated 6 well plates or in 8 well μ -slides. A total amount of 1.2 μ g plasmid DNA

6 Material and Methods

was used per well and cells were subjected to the transfection mixture for 2 h. Live cell imaging and all other experiments were performed between 24 - 48 h after transfection.

Table 7 Plasmid constructs

Name	Insert	Backbone	Bac. Res.	Company
8xGTIIC-luciferase	TEAD reporter	pGL3b	Ampicillin	Addgene #34615
HA-AMOT p130	AMOTp130	pcDNA3-HA	Ampicillin	Prof. Zhao Lab
mCherry-C3-hYAP1	hYAP1	mod. pEGFP-C3	Kanamycin	Prof. Vollmar Lab
mCherry- β -actin	ACTB	n.a.	Kanamycin	Addgene #54966
MRTF-A-GFP	MRTF-A	n.a.	Kanamycin	Prof. Grosse Lab
nAC-NLS-TagGFP	VHH-Actin	n.a.	Kanamycin	Prof. Grosse Lab
pCAG-mGFP- β -actin	ACTB	pCAG	Kanamycin	Addgene #21948
pCMV-Lifeact-TagRFP	Lifeact	pCMV	Ampicillin	ibidi GmbH
pEGFP-C3-hYAP1	hYAP1	pEGFP-C3	Kanamycin	Addgene #17843
pGL4.34[luc2P/SRF-RE]	SRE reporter	pGL4	Ampicillin	Promega Inc.
pGL4.74[hRluc/TK]	hRluc	pGL4	Ampicillin	Promega Inc.
YFP-NLS- β -actin	ACTB	pEYFP-C1	Kanamycin	Addgene #60613

6.2.6 Live cell imaging

Live cell imaging was performed at 37 °C under 5% CO₂ atmosphere and 80% humidity using a Bold Line incubation system from Okolab. Cells were imaged 24 h after transfection.

6.2.6.1 Cell migration

Cell migration on dumbbell-shaped micropatterns was imaged on a Nikon Eclipse Ti Inverted Microscope equipped with a 4 x / 0.13 PlanFluor objective and a Cool LED pE-100 excitation light source. Cells were imaged at 37 °C under 5% CO₂ atmosphere and 80% humidity using a Heating and Gas Incubation System from ibidi.

6.2.6.2 Perfusion Assay

Unidirectional flow cell culture experiments were performed with an ibidi Pump system. 4×10^5 HUVEC were seeded into fibronectin-coated μ -Slides I 0.4 Luer two days before the experiment and transiently transfected with GFP-labelled MRTF-A or YAP 24 h before imaging. Shear stress was kept constant at 15 dyn / cm², resulting in a final flow rate of approximately 15 ml / min.

6 Material and Methods

6.2.7 Reporter gene assay

Luciferase reporter gene assays were performed using an Orion II microplate luminometer equipped with Simplicity analysis software. Samples were stimulated 24 - 48 h after transfection and analyzed in duplicates. Firefly reporter RLU were normalized to a constitutive renilla control (firefly / renilla transfection ratio of 10:1) using the Dual Luciferase reporter gene assay kit from Promega Inc. Background luminescence was subtracted by measuring mock transfected control samples.

6.2.8 Duolink proximity ligation assay

Duolink proximity ligation assays (PLA) were performed using the Duolink[®] PLA kit and suitable PLUS / MINUS probes from Sigma-Aldrich. Storage and handling of all reagents was carried out according to the manufacturer's instructions. As a blocking reagent and antibody diluent, 2% BSA in PBS was used. PLA Washing buffers A and B were prepared as described in 0 and stored at 4 °C. PLA speckles were manually counted using ImageJ.

6.2.9 Western blot

6.2.9.1 Sample preparation

For cell lysis, cells were shortly rinsed with cold PBS and an appropriate amount of standard lysis buffer was added to each well. Samples were frozen at -80 °C for minimum 30 min and subsequently transferred to Eppendorf tubes. To remove residual cell debris, samples were centrifuged at 14.000 rpm, 4 °C for 10 min. The total protein amount of each sample was determined using Bradford assay and the resulting concentrations were adjusted with 1x SDS sample buffer. Samples were then boiled for 3 min at 95 °C and stored at -20 °C until further usage.

6.2.9.2 SDS-PAGE

Proteins were separated in terms of molecular weight using discontinuous SDS polyacrylamide gel electrophoresis as described by Laemmli ¹³⁶. In brief, equal sample amounts were loaded onto discontinuous separation gels with an acrylamide concentration ranging between 10 – 15% according to the respective molecular weight of the protein of interest. Protein samples were initially stacked at a current of 100 V for 21 min before the actual separation was performed at 200 V for 45 min. The total protein amount of each lane was quantified using

6 Material and Methods

stain-free technology¹³⁷ and the molecular weight of the resulting bands was assessed by comparison with a PageRuler™ Plus Prestained Protein Ladder.

6.2.9.3 Protein transfer and detection

After separation, proteins were transferred onto nitrocellulose or polyvinylidene difluoride (PVDF) membranes by electro tank blotting¹³⁸. Membranes were pre-equilibrated in tank buffer for 30 min and protein transfer was carried out at 100 V, 4 °C for 90 min.

For protein detection, membranes were first blocked for unspecific binding in 5% blotto solution for 2 h. Subsequently, primary antibodies were added and membranes were incubated overnight at 4 °C. After four washing steps with TBS-T, membranes were incubated with appropriate HRP-conjugated secondary antibodies for 2 h at RT. Unbound secondary antibodies were removed by washing 3 x 5 min with TBS-T and 5 min with H₂O. Chemiluminescence was detected using Amersham ECL reagents and a ChemiDoc Touch imaging system from Bio-Rad.

6.2.10 Immunoprecipitation (Co-IP)

Co-IP experiments were performed using a standard NP-40 lysis buffer described in 0. All incubation steps were carried out under gentle agitation. After washing with cold PBS and subsequent addition of lysis buffer, cell lysates were scraped off the plate and transferred into Eppendorf tubes. Samples were centrifuged for 10 min at 9000 rpm to remove residual cell debris. The protein concentration of the supernatant was determined using Bradford assay and adjusted to equal values with NP-40 lysis buffer. A minimum of 500 µg was used for immunoprecipitation. Samples were incubated with 3 µg precipitation antibody for 2 h at RT followed by the addition of 40 µl protein G agarose suspension. After 2 h incubation at RT, beads were washed 3 x with 500 µl cold PBS, resuspended in 50 µl 2x sample buffer and boiled for 5 minutes at 95 °C. All samples were spun down using a table centrifuge and the supernatants were kept for Western blot analysis.

6.2.11 Quantitative real-time PCR and primers

Quantitative real-time PCR experiments were performed on an Applied Biosystems® QuantStudio™ 3 real-time PCR system. Relative changes in mRNA expression were assessed by the previously described $\Delta\Delta CT$ method¹³⁹. Samples were measured in triplicates and GAPDH was used as a housekeeper in all experiments. SYBR™ Green Master Mix was used for the detection of amplified cDNA.

6 Material and Methods

6.2.11.1 Sample preparation

mRNA was isolated from cell lysates using the RNeasy® Mini Kit from Qiagen according to the manufacturer's instructions. For each of the resulting samples, mRNA concentration was determined on a Nanodrop® 1000 spectrophotometer. mRNA samples were stored at -80 °C. To generate cDNA samples from isolated mRNA, the High-Capacity cDNA Reverse Transcription Kit from Applied Biosystems was used according to the manufacturer's instructions. cDNA samples were stored at 4 °C.

6.2.11.2 Primers

The following primers were purchased from Metabion (Planegg, Germany):

Table 8 qPCR primers

Target	Forward Sequence	Reverse Sequence
CTGF	5'-TGGAGTTCAAGTGCCCTGAC-3'	5'-CTCCCACTGCTCCTAAAGCC-3'
CCN1	5'-ACCCTTCTCCACTTGACCAG-3'	5'-CTTGGCGCAGACCTTACAG-3'
GAPDH	5'-ACGGGAAGCTTGTCATCAAT-3'	5'-CATCGCCCCACTTGATTTT-3'
hu18SrRNA	5'-CGACGACCCATTCGAACGTCT-3'	5'-CTCTCCGGAATCGAACCTGA-3'
SRF	5'-GTTTCAGCAGTTCAGCTCCA-3'	5'-TGTAGCTCGGTGAGGTTGCT-3'
Vinculin	5'-GAGAGATATGCCACCAGCATT-3'	5'-GCACTGAGTAAGGGTCTGACTG-3'

6.2.12 Transcriptomic analysis

6.2.12.1 Sample generation

Sample generation was performed by Christoph Ziegenhain (group of Prof. Wolfgang Enard). mRNA was cleaned up from cell lysates with Sera-Mag carboxylated magnetic beads and reverse transcribed using a slightly modified SCRiB-seq protocol ¹⁴⁰. During reverse transcription, sample-specific barcodes and unique molecular identifiers were incorporated into first strand cDNA. Next, samples were pooled and excess primers digested by Exonuclease I.

cDNA was preamplified using KAPA HiFi HotStart polymerase from KAPA Biosystems. Sequencing libraries were constructed from cDNA using the Illumina Nextera XT Kit. Resulting libraries were quantified and sequenced at 10 nM on an Illumina HiSeq1500 sequencing device. To obtain gene-wise expression values, raw sequencing data was processed using the zUMIs pipeline ¹⁴¹ using the Human genome build hg19 and Ensembl gene models (GRCh37.75).

6 Material and Methods

6.2.12.2 Data processing and analysis

Results Part I (performed by Ludwig Geistlinger)

Differential expression analysis of the obtained RNA-seq read counts was carried out using edgeR, which applies generalized linear models (GLMs) based on the negative-binomial distribution while incorporating normalization factors for different library sizes¹⁴². Exploratory data analysis was carried out using the EnrichmentBrowser package¹⁴³.

Results Part II (performed by Zane Kliesmete)

Transcriptomic analysis was performed using the free statistical software R (v. 3.4.2). DESeq2 package (v.1.16.1) was used for normalization and differential expression (DE) analysis. DESeq2 models transcriptional count data using negative binomial distribution. Additional filtering was done using HTSFilter (v.1.16.0) to remove constant, lowly expressed genes. The final gene set consisted of 15 232 genes.

DE testing was based on Wald test. Multiple testing was accounted for by applying a global false discovery rate (FDR) correction to all comparisons. All genes with FDR < 0.1 were considered significant.

Enrichment analysis for Gene Ontology terms was performed using topGO package (v.2.28.0), specifying the ontology of Biological Processes (BP). Fisher's exact test was applied to measure the significance of enrichment.

6.2.13 FCS

The setup for FCS measurements consisted of a Leica TCS SP8 SMD microscope combined with a Picoquant LSM Upgrade Kit including the following devices: Sepia Multichannel Picosecond Diode Laser (PDL 808), Dual Channel Single Photon Avalanche Diodes (SPAD) detection unit, Dual SPAD power supply (DSN 102), 4 Channel Router (PHR 800) and a PicoHarp 300 TCSPC Module and Picosecond Event Timer (PH300).

For all FCS measurements, a 63x Zeiss water immersion lens and ibidi 8 well μ -slides with glass bottoms were used. The effective volume (V_{eff}) and structure parameter (κ) were precisely measured at the start of each experiment using a pure 1nM ATTO488 dye from ATTO-TEC GmbH. Three different points were measured in every cell nucleus for 45 s per point. This process was repeated for 4 different time points (0, 5, 15, 25 min) with the respective compound being added after the zero-time point measurement.

6 Material and Methods

FCS curves were analyzed using the Picoquant SymPhoTime V 5.2.4.0 software. In detail, the FCS curves were fitted for 1 species using the triplet state (extended) model. Additionally, control FCS measurements without compounds were performed over the same time points to account for any bleaching effect on the GFP-actin in the cell over time.

$$G_{3D}(\tau) = \left[1 + \sum_{j=1}^m \left[-T_j + T_j e^{\left(\frac{-\tau}{\tau_{r,j}} \right)} \right] \right] \sum_{i=1}^n \rho_i \left[1 + \left(\frac{\tau}{\tau_i} \right)^{\alpha_i} \right]^{-1} \left[1 + \frac{1}{\kappa^2} \left(\frac{\tau}{\tau_i} \right)^{\alpha_i} \right]^{-1/2} + G_{INF}$$

$$V_{Eff3D} = \pi^{3/2} w_0^2 z_0^2 ; D_{i3D} = \frac{w_0^2}{4 \tau_i} \quad \langle C \rangle = \frac{\langle N \rangle}{V_{Eff} N_A} ; \sum_{i=1}^n \rho_i = \frac{1}{\langle N \rangle \left(1 - \sum_{j=1}^m T_j \right)}$$

Figure 6-2 | FCS equations

6.2.14 RICS

RICS measurements were performed on a home-built PIE-FI microscope and calibrations were performed on single-measurement basis, as described elsewhere¹⁴⁴. The following laser lines were used for excitation: 475 nm for GFP-actin and 561 nm for mCherry-actin. The laser power was measured using a slide power meter to be ~ 1.1 μW at the sample level. The measurements were performed using a 100x oil NA 1.49 objective. Image calculations from the raw photon data and subsequent analysis were performed with our Microtime Image Analysis (MIA) software. MIA is a stand-alone program (MATLAB; The MathWorks GmbH) for global, serial, and automated analysis of CLSM images (using continuous-wave excitation or PIE) that can perform RICS and ccRICS, as well as other image correlation methods. To localize the GFP- and mCherry-labeled actin, a wide-field imaging system was used. For prolonged imaging conditions at 37 °C, a home-built autofocus system was used to avoid the possible focal drift in z direction. The wide-field and autofocus systems are further described in¹⁴⁴.

RICS and ccRICS were performed consecutively on the cytoplasm and on the nucleus. The data was obtained recording 150 frames per z position (12 × 12 μm or 300 × 300 pixels) at a frame time of τ_f = 1 s, interframe time τ_{if} = ~ 0.5 s, line time τ_l = 3.33 ms, pixel dwell time τ_p = 11.11 μs, and pixel size δr = 40 nm. The RICS and ccRICS processing was performed as explained elsewhere¹⁴⁴.

The RICS experiments were corrected for cellular movement by applying a moving average correction prior to correlation of the image. For analyzing the different cellular regions, we designated an arbitrary ROI where the unwanted pixels (e.g. due to heterogeneities in the nucleus or from pixels outside of the cell) were removed. The correlation functions were then

6 Material and Methods

determined using the ARICS algorithm. A two-component model assuming a 3D Gaussian focus shape was used for fitting the SACFs (eq. 2).

$$G(\xi, \psi) = \frac{\gamma}{N_{mob}} \cdot \left(1 + \frac{4D \cdot |\xi\tau_p + \psi\tau_l|}{\omega_r^2}\right)^{-1} \cdot \left(1 + \frac{4D \cdot |\xi\tau_p + \psi\tau_l|}{\omega_z^2}\right)^{-\frac{1}{2}} \cdot \exp\left(-\frac{\delta r^2(\xi^2 + \psi^2)}{\omega_r^2 + 4D \cdot |\xi\tau_p + \psi\tau_l|}\right) + \frac{\gamma}{N_{imm}} \cdot \exp\left(-\frac{\delta r^2(\xi^2 + \psi^2)}{\omega_r^2 + 4D \cdot |\xi\tau_p + \psi\tau_l|}\right) \quad (2)$$

where ξ and ψ denote the spatial lag in pixels along the fast and the slow scanning axis, respectively. The scanning parameters: τ_p , τ_l , and δr , represent the pixel dwell time, the line time (i.e. the time difference between the start of two consecutive lines), and the pixel size, respectively. ω_r and ω_z are the lateral and axial focus sizes, respectively, defined as the distance from the focus center to the point where the signal intensity has decreased to $1/e^2$ of the maximum. The shape factor γ is $2^{-3/2}$ for a 3D Gaussian. The vertical lines denote that the absolute value should be taken over the absolute time lag. The correlation at zero lag time was omitted from analysis due to the contribution of uncorrelated shot noise.

The fitting was used to extract the quantitative number of mobile and immobile fraction of molecules. The “immobile” fraction refers to particles that did not move significant on the time necessary to image them (~ 30 ms), but are dynamic on the timescale of frames, otherwise they would have been removed by the moving average correction. A single, static-component was used for fitting the SCCFs (eq. 3) and used to extract the quantitative number of “immobile” molecules.

$$G(\xi, \psi) = \frac{\gamma}{N_{imm}} \cdot \exp\left(-\frac{\delta r^2((\xi + s_x)^2 + (\psi + s_y)^2)}{\omega_r^2 + 4D \cdot |\xi\tau_p + \psi\tau_l|}\right) \quad (3)$$

where s_x and s_y are the spatial offsets in x and y directions between the two images, respectively.

The normalized fraction of polymerizing actin was obtained by the division of the SCCF amplitude by the SACF amplitude of the EGFP-labeled actin.

6 Material and Methods

6.2.15 Statistical analysis

All images and time lapse sequences were analyzed and processed using ImageJ version 1.5. Pearson correlation coefficients were calculated using the Coloc2 plugin for ImageJ according to the available online instructions.

Statistical analysis (mean, standard deviation, standard error of the mean, unpaired student t-test, Sidak corrected one-way ANOVA test, Dunnett's multiple comparisons test) was performed with GraphPad Prism Version 7.0a for Mac OS X.

Unless stated otherwise, all data are derived from three independent experiments.

References

7 References

- 1 Vaupel, P., Mutschler, E. & Schaible, H. G. *Anatomie, Physiologie, Pathophysiologie des Menschen*. (Wissenschaftliche, 2015).
- 2 Potente, M., Gerhardt, H. & Carmeliet, P. Basic and therapeutic aspects of angiogenesis. *Cell* **146**, 873-887, doi:10.1016/j.cell.2011.08.039 (2011).
- 3 Blanco, R. & Gerhardt, H. VEGF and Notch in tip and stalk cell selection. *Cold Spring Harb Perspect Med* **3**, a006569, doi:10.1101/cshperspect.a006569 (2013).
- 4 Hanahan, D. & Weinberg, R. A. Hallmarks of cancer: the next generation. *Cell* **144**, 646-674, doi:10.1016/j.cell.2011.02.013 (2011).
- 5 Zhao, Y. & Adjei, A. A. Targeting Angiogenesis in Cancer Therapy: Moving Beyond Vascular Endothelial Growth Factor. *Oncologist* **20**, 660-673, doi:10.1634/theoncologist.2014-0465 (2015).
- 6 Bielenberg, D. R. & Zetter, B. R. The Contribution of Angiogenesis to the Process of Metastasis. *Cancer J* **21**, 267-273, doi:10.1097/PPO.000000000000138 (2015).
- 7 Mammoto, A., Mammoto, T. & Ingber, D. E. Mechanosensitive mechanisms in transcriptional regulation. *Journal of cell science* **125**, 3061-3073, doi:10.1242/jcs.093005 (2012).
- 8 Vogel, V. & Sheetz, M. Local force and geometry sensing regulate cell functions. *Nature reviews. Molecular cell biology* **7**, 265-275, doi:10.1038/nrm1890 (2006).
- 9 Sukharev, S. & Anishkin, A. Mechanosensitive channels: what can we learn from 'simple' model systems? *Trends Neurosci* **27**, 345-351, doi:10.1016/j.tins.2004.04.006 (2004).
- 10 Versaevel, M. *et al.* Super-resolution microscopy reveals LINC complex recruitment at nuclear indentation sites. *Scientific reports* **4**, 7362, doi:10.1038/srep07362 (2014).
- 11 Tapley, E. C. & Starr, D. A. Connecting the nucleus to the cytoskeleton by SUN-KASH bridges across the nuclear envelope. *Curr Opin Cell Biol* **25**, 57-62, doi:10.1016/j.ceb.2012.10.014 (2013).
- 12 Isermann, P. & Lammerding, J. Nuclear mechanics and mechanotransduction in health and disease. *Curr Biol* **23**, R1113-1121, doi:10.1016/j.cub.2013.11.009 (2013).
- 13 Mendez, M. G. & Janmey, P. A. Transcription factor regulation by mechanical stress. *The international journal of biochemistry & cell biology* **44**, 728-732, doi:10.1016/j.biocel.2012.02.003 (2012).
- 14 Treisman, R. Identification of a protein-binding site that mediates transcriptional response of the c-fos gene to serum factors. *Cell* **46**, 567-574 (1986).
- 15 Sotiropoulos, A., Gineitis, D., Copeland, J. & Treisman, R. Signal-regulated activation of serum response factor is mediated by changes in actin dynamics. *Cell* **98**, 159-169 (1999).
- 16 Miralles, F., Posern, G., Zaromytidou, A. I. & Treisman, R. Actin dynamics control SRF activity by regulation of its coactivator MAL. *Cell* **113**, 329-342 (2003).
- 17 Vartiainen, M. K., Guettler, S., Larjani, B. & Treisman, R. Nuclear actin regulates dynamic subcellular localization and activity of the SRF cofactor MAL. *Science* **316**, 1749-1752, doi:10.1126/science.1141084 (2007).
- 18 Grosse, R. & Vartiainen, M. K. To be or not to be assembled: progressing into nuclear actin filaments. *Nature reviews. Molecular cell biology* **14**, 693-697, doi:10.1038/nrm3681 (2013).
- 19 Sun, Q. *et al.* Defining the mammalian CArGome. *Genome research* **16**, 197-207, doi:10.1101/gr.4108706 (2006).
- 20 Miano, J. M., Long, X. & Fujiwara, K. Serum response factor: master regulator of the actin cytoskeleton and contractile apparatus. *Am J Physiol Cell Physiol* **292**, C70-81, doi:10.1152/ajpcell.00386.2006 (2007).
- 21 Gualdrini, F. *et al.* SRF Co-factors Control the Balance between Cell Proliferation and Contractility. *Mol Cell* **64**, 1048-1061, doi:10.1016/j.molcel.2016.10.016 (2016).

7 References

- 22 Mokalled, M. H. *et al.* Myocardin-related transcription factors are required for cardiac development and function. *Dev Biol*, doi:10.1016/j.ydbio.2015.09.006 (2015).
- 23 Connelly, J. T. *et al.* Actin and serum response factor transduce physical cues from the microenvironment to regulate epidermal stem cell fate decisions. *Nature cell biology* **12**, 711-718, doi:10.1038/ncb2074 (2010).
- 24 Seifert, A. & Posern, G. Tightly controlled MRTF-A activity regulates epithelial differentiation during formation of mammary acini. *Breast Cancer Res* **19**, 68, doi:10.1186/s13058-017-0860-3 (2017).
- 25 Harvey, K. F., Pflieger, C. M. & Hariharan, I. K. The Drosophila Mst ortholog, hippo, restricts growth and cell proliferation and promotes apoptosis. *Cell* **114**, 457-467 (2003).
- 26 Tapon, N. *et al.* salvador Promotes both cell cycle exit and apoptosis in Drosophila and is mutated in human cancer cell lines. *Cell* **110**, 467-478 (2002).
- 27 Justice, R. W., Zilian, O., Woods, D. F., Noll, M. & Bryant, P. J. The Drosophila tumor suppressor gene warts encodes a homolog of human myotonic dystrophy kinase and is required for the control of cell shape and proliferation. *Genes & development* **9**, 534-546 (1995).
- 28 Zhao, B. *et al.* TEAD mediates YAP-dependent gene induction and growth control. *Genes & development* **22**, 1962-1971, doi:10.1101/gad.1664408 (2008).
- 29 Zhao, B. *et al.* Inactivation of YAP oncoprotein by the Hippo pathway is involved in cell contact inhibition and tissue growth control. *Genes & development* **21**, 2747-2761, doi:10.1101/gad.1602907 (2007).
- 30 Yu, F. X. *et al.* Regulation of the Hippo-YAP pathway by G-protein-coupled receptor signaling. *Cell* **150**, 780-791, doi:10.1016/j.cell.2012.06.037 (2012).
- 31 Yu, F. X. & Guan, K. L. The Hippo pathway: regulators and regulations. *Genes & development* **27**, 355-371, doi:10.1101/gad.210773.112 (2013).
- 32 Franco, C. A. *et al.* Serum response factor is required for sprouting angiogenesis and vascular integrity. *Developmental cell* **15**, 448-461, doi:10.1016/j.devcel.2008.07.019 (2008).
- 33 Franco, C. A. & Li, Z. SRF in angiogenesis: branching the vascular system. *Cell adhesion & migration* **3**, 264-267 (2009).
- 34 Franco, C. A. *et al.* SRF selectively controls tip cell invasive behavior in angiogenesis. *Development* **140**, 2321-2333, doi:10.1242/dev.091074 (2013).
- 35 Weini, C. *et al.* Endothelial depletion of murine SRF/MRTF provokes intracerebral hemorrhagic stroke. *Proc Natl Acad Sci U S A* **112**, 9914-9919, doi:10.1073/pnas.1509047112 (2015).
- 36 Weini, C. *et al.* Endothelial SRF/MRTF ablation causes vascular disease phenotypes in murine retinae. *The Journal of clinical investigation* **123**, 2193-2206, doi:10.1172/JCI64201 (2013).
- 37 Wang, X. *et al.* YAP/TAZ Orchestrate VEGF Signaling during Developmental Angiogenesis. *Developmental cell* **42**, 462-478 e467, doi:10.1016/j.devcel.2017.08.002 (2017).
- 38 Nakajima, H. *et al.* Flow-Dependent Endothelial YAP Regulation Contributes to Vessel Maintenance. *Developmental cell* **40**, 523-536 e526, doi:10.1016/j.devcel.2017.02.019 (2017).
- 39 Choi, H. J. *et al.* Yes-associated protein regulates endothelial cell contact-mediated expression of angiopoietin-2. *Nature communications* **6**, 6943, doi:10.1038/ncomms7943 (2015).
- 40 Foster, C. T., Gualdrini, F. & Treisman, R. Mutual dependence of the MRTF-SRF and YAP-TEAD pathways in cancer-associated fibroblasts is indirect and mediated by cytoskeletal dynamics. *Genes & development* **31**, 2361-2375, doi:10.1101/gad.304501.117 (2017).
- 41 Bettinger, B. T., Gilbert, D. M. & Amberg, D. C. Actin up in the nucleus. *Nature reviews. Molecular cell biology* **5**, 410-415, doi:10.1038/nrm1370 (2004).
- 42 Melak, M., Plessner, M. & Grosse, R. Actin visualization at a glance. *Journal of cell science*, doi:10.1242/jcs.189068 (2017).

7 References

- 43 Belin, B. J., Cimini, B. A., Blackburn, E. H. & Mullins, R. D. Visualization of actin filaments and monomers in somatic cell nuclei. *Molecular biology of the cell* **24**, 982-994, doi:10.1091/mbc.E12-09-0685 (2013).
- 44 Dopie, J., Skarp, K. P., Rajakyla, E. K., Tanhuanpaa, K. & Vartiainen, M. K. Active maintenance of nuclear actin by importin 9 supports transcription. *Proc Natl Acad Sci U S A* **109**, E544-552, doi:10.1073/pnas.1118880109 (2012).
- 45 Stuken, T., Hartmann, E. & Gorlich, D. Exportin 6: a novel nuclear export receptor that is specific for profilin.actin complexes. *EMBO J* **22**, 5928-5940, doi:10.1093/emboj/cdg565 (2003).
- 46 Baarlink, C., Wang, H. & Grosse, R. Nuclear actin network assembly by formins regulates the SRF coactivator MAL. *Science* **340**, 864-867, doi:10.1126/science.1235038 (2013).
- 47 Belin, B. J., Lee, T. & Mullins, R. D. DNA damage induces nuclear actin filament assembly by Formin-2 and Spire-(1/2) that promotes efficient DNA repair. *Elife* **4**, doi:10.7554/eLife.07735 (2015).
- 48 Andrin, C. *et al.* A requirement for polymerized actin in DNA double-strand break repair. *Nucleus* **3**, 384-395, doi:10.4161/nucl.21055 (2012).
- 49 Bohnsack, M. T., Stuken, T., Kuhn, C., Cordes, V. C. & Gorlich, D. A selective block of nuclear actin export stabilizes the giant nuclei of *Xenopus* oocytes. *Nature cell biology* **8**, 257-263, doi:10.1038/ncb1357 (2006).
- 50 Virtanen, J. A. & Vartiainen, M. K. Diverse functions for different forms of nuclear actin. *Curr Opin Cell Biol* **46**, 33-38, doi:10.1016/j.ceb.2016.12.004 (2017).
- 51 Spencer, V. A. *et al.* Depletion of nuclear actin is a key mediator of quiescence in epithelial cells. *Journal of cell science* **124**, 123-132, doi:10.1242/jcs.073197 (2011).
- 52 Egly, J. M., Miyamoto, N. G., Moncollin, V. & Chambon, P. Is actin a transcription initiation factor for RNA polymerase B? *EMBO J* **3**, 2363-2371 (1984).
- 53 Scheer, U., Hinssen, H., Franke, W. W. & Jockusch, B. M. Microinjection of actin-binding proteins and actin antibodies demonstrates involvement of nuclear actin in transcription of lampbrush chromosomes. *Cell* **39**, 111-122 (1984).
- 54 Szerlong, H. *et al.* The HSA domain binds nuclear actin-related proteins to regulate chromatin-remodeling ATPases. *Nat Struct Mol Biol* **15**, 469-476, doi:10.1038/nsmb.1403 (2008).
- 55 Kapoor, P., Chen, M., Winkler, D. D., Luger, K. & Shen, X. Evidence for monomeric actin function in INO80 chromatin remodeling. *Nat Struct Mol Biol* **20**, 426-432, doi:10.1038/nsmb.2529 (2013).
- 56 Kapoor, P. & Shen, X. Mechanisms of nuclear actin in chromatin-remodeling complexes. *Trends in cell biology* **24**, 238-246, doi:10.1016/j.tcb.2013.10.007 (2014).
- 57 Galarneau, L. *et al.* Multiple links between the NuA4 histone acetyltransferase complex and epigenetic control of transcription. *Mol Cell* **5**, 927-937 (2000).
- 58 Serebryanny, L. A., Cruz, C. M. & de Lanerolle, P. A Role for Nuclear Actin in HDAC 1 and 2 Regulation. *Scientific reports* **6**, 28460, doi:10.1038/srep28460 (2016).
- 59 Hofmann, W. A. *et al.* Actin is part of pre-initiation complexes and is necessary for transcription by RNA polymerase II. *Nature cell biology* **6**, 1094-1101, doi:10.1038/ncb1182 (2004).
- 60 Hu, P., Wu, S. & Hernandez, N. A role for beta-actin in RNA polymerase III transcription. *Genes & development* **18**, 3010-3015, doi:10.1101/gad.1250804 (2004).
- 61 Philimonenko, V. V. *et al.* Nuclear actin and myosin I are required for RNA polymerase I transcription. *Nature cell biology* **6**, 1165-1172, doi:10.1038/ncb1190 (2004).
- 62 Miyamoto, K. & Gurdon, J. B. Transcriptional regulation and nuclear reprogramming: roles of nuclear actin and actin-binding proteins. *Cellular and molecular life sciences : CMLS* **70**, 3289-3302, doi:10.1007/s00018-012-1235-7 (2013).
- 63 Percipalle, P. & Visa, N. Molecular functions of nuclear actin in transcription. *J Cell Biol* **172**, 967-971, doi:10.1083/jcb.200512083 (2006).
- 64 Allingham, J. S., Klenchin, V. A. & Rayment, I. Actin-targeting natural products: structures, properties and mechanisms of action. *Cellular and molecular life sciences : CMLS* **63**, 2119-2134, doi:10.1007/s00018-006-6157-9 (2006).

7 References

- 65 Low, I. & Wieland, T. The interaction of phalloidin. Some of its derivatives, and of other cyclic peptides with muscle actin as studied by viscosimetry. *FEBS letters* **44**, 340-343 (1974).
- 66 Karmann, L., Schultz, K., Herrmann, J., Muller, R. & Kazmaier, U. Total syntheses and biological evaluation of miuraenamides. *Angew Chem Int Ed Engl* **54**, 4502-4507, doi:10.1002/anie.201411212 (2015).
- 67 Iizuka, T. *et al.* Miuraenamides A and B, novel antimicrobial cyclic depsipeptides from a new slightly halophilic myxobacterium: taxonomy, production, and biological properties. *J Antibiot (Tokyo)* **59**, 385-391, doi:10.1038/ja.2006.55 (2006).
- 68 Spector, I., Shochet, N. R., Kashman, Y. & Groweiss, A. Latrunculins: novel marine toxins that disrupt microfilament organization in cultured cells. *Science* **219**, 493-495 (1983).
- 69 Bubb, M. R., Spector, I., Bershady, A. D. & Korn, E. D. Swinholide A is a microfilament disrupting marine toxin that stabilizes actin dimers and severs actin filaments. *The Journal of biological chemistry* **270**, 3463-3466 (1995).
- 70 Diestel, R. *et al.* Chivosazoles A and F, cytostatic macrolides from myxobacteria, interfere with actin. *Chembiochem* **10**, 2900-2903, doi:10.1002/cbic.200900562 (2009).
- 71 Ingber, D. E., Wang, N. & Stamenovic, D. Tensegrity, cellular biophysics, and the mechanics of living systems. *Rep Prog Phys* **77**, 046603, doi:10.1088/0034-4885/77/4/046603 (2014).
- 72 Thery, M. Micropatterning as a tool to decipher cell morphogenesis and functions. *Journal of cell science* **123**, 4201-4213, doi:10.1242/jcs.075150 (2010).
- 73 Anderson, D. E. & Hinds, M. T. Endothelial cell micropatterning: methods, effects, and applications. *Ann Biomed Eng* **39**, 2329-2345, doi:10.1007/s10439-011-0352-z (2011).
- 74 Chen, L. J. & Kaji, H. Modeling angiogenesis with micro- and nanotechnology. *Lab Chip* **17**, 4186-4219, doi:10.1039/c7lc00774d (2017).
- 75 Vartanian, K. B., Berny, M. A., McCarty, O. J., Hanson, S. R. & Hinds, M. T. Cytoskeletal structure regulates endothelial cell immunogenicity independent of fluid shear stress. *Am J Physiol Cell Physiol* **298**, C333-341, doi:10.1152/ajpcell.00340.2009 (2010).
- 76 Schuster, S. L. *et al.* Contractility as a global regulator of cellular morphology, velocity, and directionality in low-adhesive fibrillary micro-environments. *Biomaterials* **102**, 137-147, doi:10.1016/j.biomaterials.2016.06.021 (2016).
- 77 Cramer, L. P., Briggs, L. J. & Dawe, H. R. Use of fluorescently labelled deoxyribonuclease I to spatially measure G-actin levels in migrating and non-migrating cells. *Cell motility and the cytoskeleton* **51**, 27-38, doi:10.1002/cm.10013 (2002).
- 78 Nobusue, H. *et al.* Regulation of MKL1 via actin cytoskeleton dynamics drives adipocyte differentiation. *Nature communications* **5**, 3368, doi:10.1038/ncomms4368 (2014).
- 79 Chatterjee, S., Fujiwara, K., Perez, N. G., Ushio-Fukai, M. & Fisher, A. B. Mechanosignaling in the vasculature: emerging concepts in sensing, transduction and physiological responses. *Am J Physiol Heart Circ Physiol* **308**, H1451-1462, doi:10.1152/ajpheart.00105.2015 (2015).
- 80 Esnault, C. *et al.* Rho-actin signaling to the MRTF coactivators dominates the immediate transcriptional response to serum in fibroblasts. *Genes & development* **28**, 943-958, doi:10.1101/gad.239327.114 (2014).
- 81 Zanconato, F. *et al.* Genome-wide association between YAP/TAZ/TEAD and AP-1 at enhancers drives oncogenic growth. *Nature cell biology* **17**, 1218-1227, doi:10.1038/ncb3216 (2015).
- 82 Janssen, D., Albert, D., Jansen, R., Muller, R. & Kalesse, M. Chivosazole A--elucidation of the absolute and relative configuration. *Angew Chem Int Ed Engl* **46**, 4898-4901, doi:10.1002/anie.200605198 (2007).
- 83 Holzinger, A. Jasplakinolide: an actin-specific reagent that promotes actin polymerization. *Methods Mol Biol* **586**, 71-87, doi:10.1007/978-1-60761-376-3_4 (2009).

7 References

- 84 Wachsmuth, M., Waldeck, W. & Langowski, J. Anomalous diffusion of fluorescent probes inside living cell nuclei investigated by spatially-resolved fluorescence correlation spectroscopy. *J Mol Biol* **298**, 677-689, doi:10.1006/jmbi.2000.3692 (2000).
- 85 McDonald, D., Carrero, G., Andrin, C., de Vries, G. & Hendzel, M. J. Nucleoplasmic beta-actin exists in a dynamic equilibrium between low-mobility polymeric species and rapidly diffusing populations. *J Cell Biol* **172**, 541-552, doi:10.1083/jcb.200507101 (2006).
- 86 Hendrix, J. & Lamb, D. C. Implementation and application of pulsed interleaved excitation for dual-color FCS and RICS. *Methods Mol Biol* **1076**, 653-682, doi:10.1007/978-1-62703-649-8_30 (2014).
- 87 Brown, C. M. *et al.* Raster image correlation spectroscopy (RICS) for measuring fast protein dynamics and concentrations with a commercial laser scanning confocal microscope. *J Microsc* **229**, 78-91, doi:10.1111/j.1365-2818.2007.01871.x (2008).
- 88 Digman, M. A. & Gratton, E. Analysis of diffusion and binding in cells using the RICS approach. *Microsc Res Tech* **72**, 323-332, doi:10.1002/jemt.20655 (2009).
- 89 Hendrix, J., Dekens, T., Schrimpf, W. & Lamb, D. C. Arbitrary-Region Raster Image Correlation Spectroscopy. *Biophys J* **111**, 1785-1796, doi:10.1016/j.bpj.2016.09.012 (2016).
- 90 Mana-Capelli, S., Paramasivam, M., Dutta, S. & McCollum, D. Angiomotins link F-actin architecture to Hippo pathway signaling. *Molecular biology of the cell* **25**, 1676-1685, doi:10.1091/mbc.E13-11-0701 (2014).
- 91 Matsui, Y. & Lai, Z. C. Mutual regulation between Hippo signaling and actin cytoskeleton. *Protein & cell* **4**, 904-910, doi:10.1007/s13238-013-3084-z (2013).
- 92 Reddy, P., Deguchi, M., Cheng, Y. & Hsueh, A. J. Actin cytoskeleton regulates Hippo signaling. *PLoS one* **8**, e73763, doi:10.1371/journal.pone.0073763 (2013).
- 93 Santos-Oliveira, P. *et al.* The Force at the Tip - Modelling Tension and Proliferation in Sprouting Angiogenesis. *PLoS Comput Biol* **11**, e1004436, doi:10.1371/journal.pcbi.1004436 (2015).
- 94 Ando, J. & Yamamoto, K. Vascular mechanobiology: endothelial cell responses to fluid shear stress. *Circ J* **73**, 1983-1992 (2009).
- 95 Tzima, E. *et al.* A mechanosensory complex that mediates the endothelial cell response to fluid shear stress. *Nature* **437**, 426-431, doi:10.1038/nature03952 (2005).
- 96 Kim, J. *et al.* YAP/TAZ regulates sprouting angiogenesis and vascular barrier maturation. *The Journal of clinical investigation* **127**, 3441-3461, doi:10.1172/JCI93825 (2017).
- 97 Yu, O. M., Miyamoto, S. & Brown, J. H. Myocardin-Related Transcription Factor A and Yes-Associated Protein Exert Dual Control in G Protein-Coupled Receptor- and RhoA-Mediated Transcriptional Regulation and Cell Proliferation. *Mol Cell Biol* **36**, 39-49, doi:10.1128/MCB.00772-15 (2015).
- 98 Kim, T. *et al.* MRTF potentiates TEAD-YAP transcriptional activity causing metastasis. *EMBO J*, doi:10.15252/embj.201695137 (2016).
- 99 Giampietro, C. *et al.* The actin-binding protein EPS8 binds VE-cadherin and modulates YAP localization and signaling. *J Cell Biol* **211**, 1177-1192, doi:10.1083/jcb.201501089 (2015).
- 100 Busche, S., Descot, A., Julien, S., Genth, H. & Posern, G. Epithelial cell-cell contacts regulate SRF-mediated transcription via Rac-actin-MAL signalling. *Journal of cell science* **121**, 1025-1035, doi:10.1242/jcs.014456 (2008).
- 101 Row, S., Liu, Y., Alimperti, S., Agarwal, S. K. & Andreadis, S. T. Cadherin-11 is a novel regulator of extracellular matrix synthesis and tissue mechanics. *Journal of cell science* **129**, 2950-2961, doi:10.1242/jcs.183772 (2016).
- 102 Plessner, M., Melak, M., Chinchilla, P., Baarlink, C. & Grosse, R. Nuclear F-actin formation and reorganization upon cell spreading. *The Journal of biological chemistry*, doi:10.1074/jbc.M114.627166 (2015).
- 103 Hermann, M. R. *et al.* Integrins synergize to induce expression of the MRTF-A/SRF target gene ISG15 for promoting cancer cell invasion. *Journal of cell science*, doi:10.1242/jcs.177592 (2016).

7 References

- 104 Zhao, B. *et al.* Cell detachment activates the Hippo pathway via cytoskeleton reorganization to induce anoikis. *Genes & development* **26**, 54-68, doi:10.1101/gad.173435.111 (2012).
- 105 Dupont, S. Role of YAP/TAZ in cell-matrix adhesion-mediated signalling and mechanotransduction. *Exp Cell Res*, doi:10.1016/j.yexcr.2015.10.034 (2015).
- 106 Ventre, M., Natale, C. F., Rianna, C. & Netti, P. A. Topographic cell instructive patterns to control cell adhesion, polarization and migration. *J R Soc Interface* **11**, 20140687, doi:10.1098/rsif.2014.0687 (2014).
- 107 O'Connor, J. W. & Gomez, E. W. Cell adhesion and shape regulate TGF-beta1-induced epithelial-myofibroblast transition via MRTF-A signaling. *PLoS one* **8**, e83188, doi:10.1371/journal.pone.0083188 (2013).
- 108 Stiles, J. M. *et al.* Morphological restriction of human coronary artery endothelial cells substantially impacts global gene expression patterns. *The FEBS journal* **280**, 4474-4494, doi:10.1111/febs.12410 (2013).
- 109 Cui, Y. *et al.* Cyclic stretching of soft substrates induces spreading and growth. *Nature communications* **6**, 6333, doi:10.1038/ncomms7333 (2015).
- 110 Posern, G., Sotiropoulos, A. & Treisman, R. Mutant actins demonstrate a role for unpolymerized actin in control of transcription by serum response factor. *Molecular biology of the cell* **13**, 4167-4178, doi:10.1091/mbc.02-05-0068 (2002).
- 111 Chan, S. W. *et al.* Hippo pathway-independent restriction of TAZ and YAP by angiomin. *The Journal of biological chemistry* **286**, 7018-7026, doi:10.1074/jbc.C110.212621 (2011).
- 112 Xu, S., Koroleva, M., Yin, M. & Jin, Z. G. Atheroprotective laminar flow inhibits Hippo pathway effector YAP in endothelial cells. *Transl Res* **176**, 18-28 e12, doi:10.1016/j.trsl.2016.05.003 (2016).
- 113 Wang, K. C. *et al.* Flow-dependent YAP/TAZ activities regulate endothelial phenotypes and atherosclerosis. *Proc Natl Acad Sci U S A* **113**, 11525-11530, doi:10.1073/pnas.1613121113 (2016).
- 114 Gaspar, P. & Tapon, N. Sensing the local environment: actin architecture and Hippo signalling. *Curr Opin Cell Biol* **31**, 74-83, doi:10.1016/j.ceb.2014.09.003 (2014).
- 115 Dai, X. *et al.* Phosphorylation of angiomin by Lats1/2 kinases inhibits F-actin binding, cell migration, and angiogenesis. *The Journal of biological chemistry* **288**, 34041-34051, doi:10.1074/jbc.M113.518019 (2013).
- 116 Zhao, B. *et al.* Angiomin is a novel Hippo pathway component that inhibits YAP oncoprotein. *Genes & development* **25**, 51-63, doi:10.1101/gad.2000111 (2011).
- 117 Speight, P., Kofler, M., Szaszi, K. & Kapus, A. Context-dependent switch in chemo/mechanotransduction via multilevel crosstalk among cytoskeleton-regulated MRTF and TAZ and TGFbeta-regulated Smad3. *Nature communications* **7**, 11642, doi:10.1038/ncomms11642 (2016).
- 118 Sharili, A. S., Kenny, F. N., Vartiainen, M. K. & Connelly, J. T. Nuclear actin modulates cell motility via transcriptional regulation of adhesive and cytoskeletal genes. *Scientific reports* **6**, 33893, doi:10.1038/srep33893 (2016).
- 119 Baarlink, C. *et al.* A transient pool of nuclear F-actin at mitotic exit controls chromatin organization. *Nature cell biology*, doi:10.1038/ncb3641 (2017).
- 120 Plessner, M. & Grosse, R. Extracellular signaling cues for nuclear actin polymerization. *European journal of cell biology*, doi:10.1016/j.ejcb.2015.05.009 (2015).
- 121 Hendzel, M. J. The F-act's of nuclear actin. *Curr Opin Cell Biol* **28**, 84-89, doi:10.1016/j.ceb.2014.04.003 (2014).
- 122 Pollard, T. D. Actin and Actin-Binding Proteins. *Cold Spring Harb Perspect Biol* **8**, doi:10.1101/cshperspect.a018226 (2016).
- 123 Dahl, K. N., Ribeiro, A. J. & Lammerding, J. Nuclear shape, mechanics, and mechanotransduction. *Circulation research* **102**, 1307-1318, doi:10.1161/CIRCRESAHA.108.173989 (2008).
- 124 Elosegui-Artola, A. *et al.* Force Triggers YAP Nuclear Entry by Regulating Transport across Nuclear Pores. *Cell*, doi:10.1016/j.cell.2017.10.008 (2017).

7 References

- 125 Dechat, T. *et al.* Nuclear lamins: major factors in the structural organization and function of the nucleus and chromatin. *Genes & development* **22**, 832-853, doi:10.1101/gad.1652708 (2008).
- 126 Thomas, C. H., Collier, J. H., Sfeir, C. S. & Healy, K. E. Engineering gene expression and protein synthesis by modulation of nuclear shape. *Proc Natl Acad Sci U S A* **99**, 1972-1977, doi:10.1073/pnas.032668799 (2002).
- 127 Piel, M. & Thery, M. Methods in Cell Biology. Micropatterning in cell biology part B. Preface. *Methods Cell Biol* **120**, xv-xvi, doi:10.1016/B978-0-12-417136-7.09989-4 (2014).
- 128 van Dongen, S. F., Maiuri, P., Marie, E., Tribet, C. & Piel, M. Triggering cell adhesion, migration or shape change with a dynamic surface coating. *Adv Mater* **25**, 1687-1691, doi:10.1002/adma.201204474 (2013).
- 129 van Dongen, S. F. M. *et al.* Reactive protein-repellent surfaces for the straightforward attachment of small molecules up to whole cells. *Chemical Science* **3**, 3000-3006, doi:10.1039/C2SC20652H (2012).
- 130 Nakanishi, J. *et al.* Spatiotemporal control of migration of single cells on a photoactivatable cell microarray. *J Am Chem Soc* **129**, 6694-6695, doi:10.1021/ja070294p (2007).
- 131 Nagel, G. *et al.* Channelrhodopsin-1: a light-gated proton channel in green algae. *Science* **296**, 2395-2398, doi:10.1126/science.1072068 (2002).
- 132 Deisseroth, K. Optogenetics: 10 years of microbial opsins in neuroscience. *Nat Neurosci* **18**, 1213-1225, doi:10.1038/nn.4091 (2015).
- 133 Borowiak, M. *et al.* Photoswitchable Inhibitors of Microtubule Dynamics Optically Control Mitosis and Cell Death. *Cell* **162**, 403-411, doi:10.1016/j.cell.2015.06.049 (2015).
- 134 Small, J., Rottner, K., Hahne, P. & Anderson, K. I. Visualising the actin cytoskeleton. *Microsc Res Tech* **47**, 3-17, doi:10.1002/(SICI)1097-0029(19991001)47:1<3::AID-JEMT2>3.0.CO;2-2 (1999).
- 135 Pitulescu, M. E., Schmidt, I., Benedito, R. & Adams, R. H. Inducible gene targeting in the neonatal vasculature and analysis of retinal angiogenesis in mice. *Nat Protoc* **5**, 1518-1534, doi:10.1038/nprot.2010.113 (2010).
- 136 Laemmli, U. K. Cleavage of structural proteins during the assembly of the head of bacteriophage T4. *Nature* **227**, 680-685 (1970).
- 137 Gurtler, A. *et al.* Stain-Free technology as a normalization tool in Western blot analysis. *Anal Biochem* **433**, 105-111, doi:10.1016/j.ab.2012.10.010 (2013).
- 138 Kurien, B. T. & Scofield, R. H. Introduction to protein blotting. *Methods Mol Biol* **536**, 9-22, doi:10.1007/978-1-59745-542-8_3 (2009).
- 139 Fleige, S. *et al.* Comparison of relative mRNA quantification models and the impact of RNA integrity in quantitative real-time RT-PCR. *Biotechnol Lett* **28**, 1601-1613, doi:10.1007/s10529-006-9127-2 (2006).
- 140 Soumillon, M., Cacchiarelli, D., Semrau, S., van Oudenaarden, A. & Mikkelsen, T. S. Characterization of directed differentiation by high-throughput single-cell RNA-Seq. *bioRxiv*, doi:10.1101/003236 (2014).
- 141 Parekh, S., Ziegenhain, C., Vieth, B., Enard, W. & Hellmann, I. zUMIs: A fast and flexible pipeline to process RNA sequencing data with UMIs. *bioRxiv*, doi:10.1101/153940 (2017).
- 142 Robinson, M. D., McCarthy, D. J. & Smyth, G. K. edgeR: a Bioconductor package for differential expression analysis of digital gene expression data. *Bioinformatics* **26**, 139-140, doi:10.1093/bioinformatics/btp616 (2010).
- 143 Geistlinger, L., Csaba, G. & Zimmer, R. Bioconductor's EnrichmentBrowser: seamless navigation through combined results of set- & network-based enrichment analysis. *BMC Bioinformatics* **17**, 45, doi:10.1186/s12859-016-0884-1 (2016).
- 144 Hendrix, J. *et al.* Live-cell observation of cytosolic HIV-1 assembly onset reveals RNA-interacting Gag oligomers. *J Cell Biol* **210**, 629-646, doi:10.1083/jcb.201504006 (2015).

Appendix

8 Appendix

8.1 Supplementary Figures

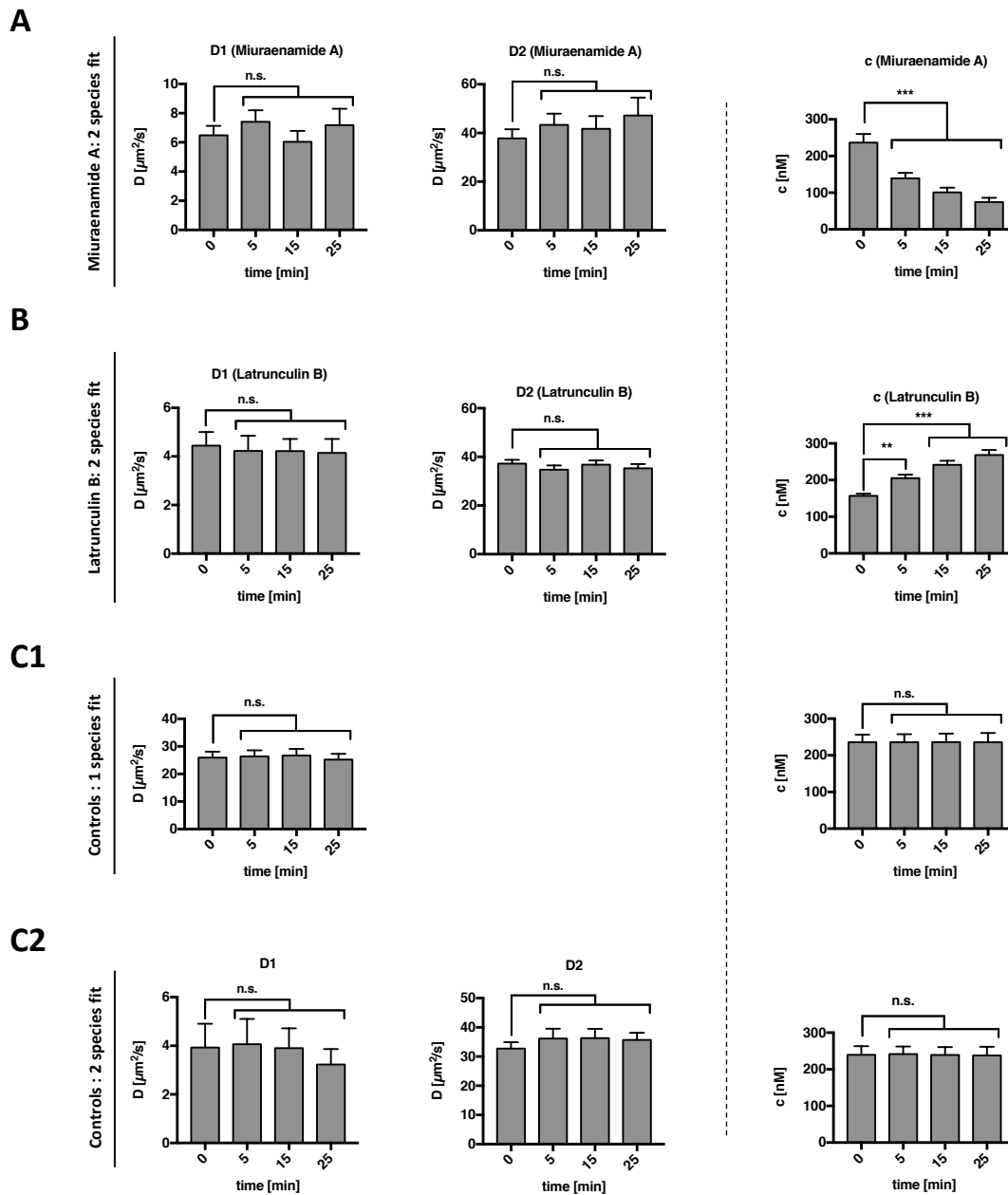
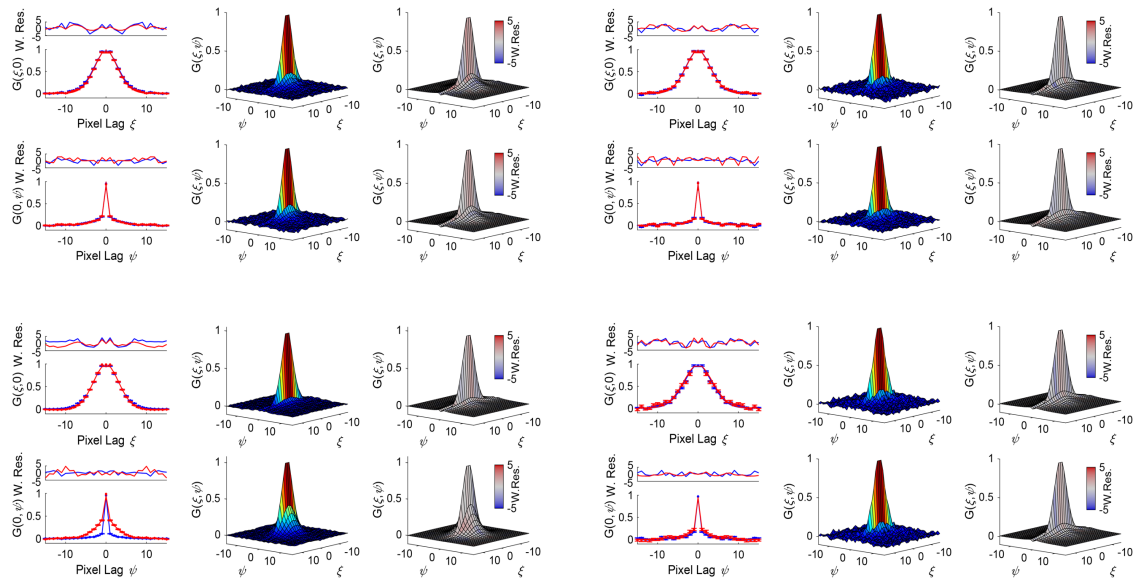


Figure S1 | FCS controls and 2 species fitting. (A) 2 species fit for EGFP- β -actin diffusion coefficients and nuclear concentration after stimulation with Miuraenamamide A. **(B)** 2 species fit for EGFP- β -actin diffusion coefficients and nuclear concentration after stimulation with Latrunculin B. **(C1)** 1 species fit for EGFP- β -actin diffusion coefficient and nuclear concentration in untreated control cells. **(C2)** 2 species fit for EGFP- β -actin diffusion coefficients and nuclear concentration in untreated control cells. ≥ 40 cells were analyzed in for each of the three settings. Bars representing mean + SEM, statistical significance was determined by ordinary one-way ANOVA followed by Dunnett's multiple comparisons test.

A



B

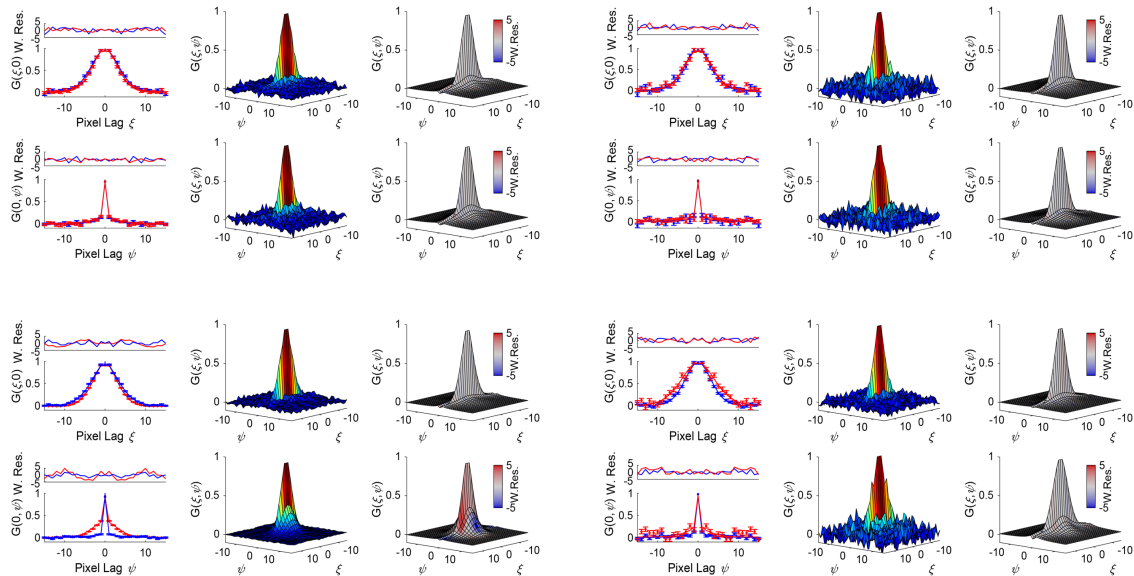


Figure S2 | RICS analysis of nuclear versus cytoplasmic actin polymerization in response to Miuraenamide A and Latrunculin B. (A) RICS data for the cytoplasmic (*left*) and nuclear (*right*) compartment upon the addition of 250 nM Latrunculin B. On the upper and lower left, the correlations along pixel lags $(\xi, 0)$ and $(0, \psi)$ are shown, respectively. Blue and red curves represent the correlations before and 20 minutes after the addition of Latrunculin B. In the middle, the mean SACFs are depicted in 3D, color coded with the correlation values (the SACF before (*top*) and 20 minutes after the addition of Latrunculin B (*bottom*)). On the upper and lower right, the two-component fits of the data are shown before and 20 minutes after the addition of Latrunculin B. Fits are color coded according to the value of the goodness-of-fit weighted residuals parameter (W. Res.), where gray illustrates a good fit and red–blue indicates regions where the residuals deviate by $> 5\sigma$. The same explanation applies for the nuclear data depicted in the right panels. (B) RICS data obtained for the cytoplasmic (*left*) and nuclear (*right*) compartments upon addition of 100 nM Miuraenamide. Further explanation applies as in (A).

8 Appendix

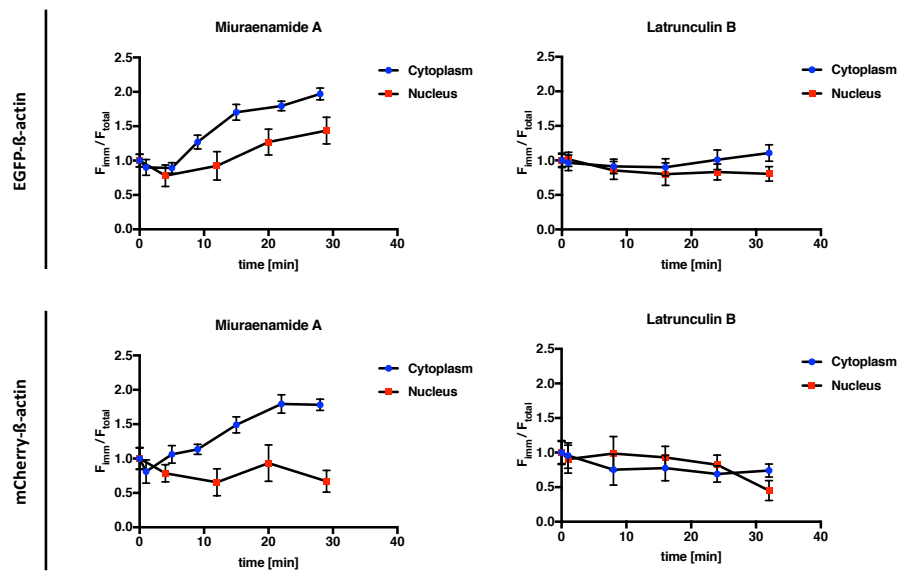


Figure S3 | Time course of F_{imm} / F_{total} for EGFP- and mCherry- β -actin in the nuclear versus cytoplasmic compartment in response to 100 nM Miuraenamide A or 250 nM Latrunculin B.

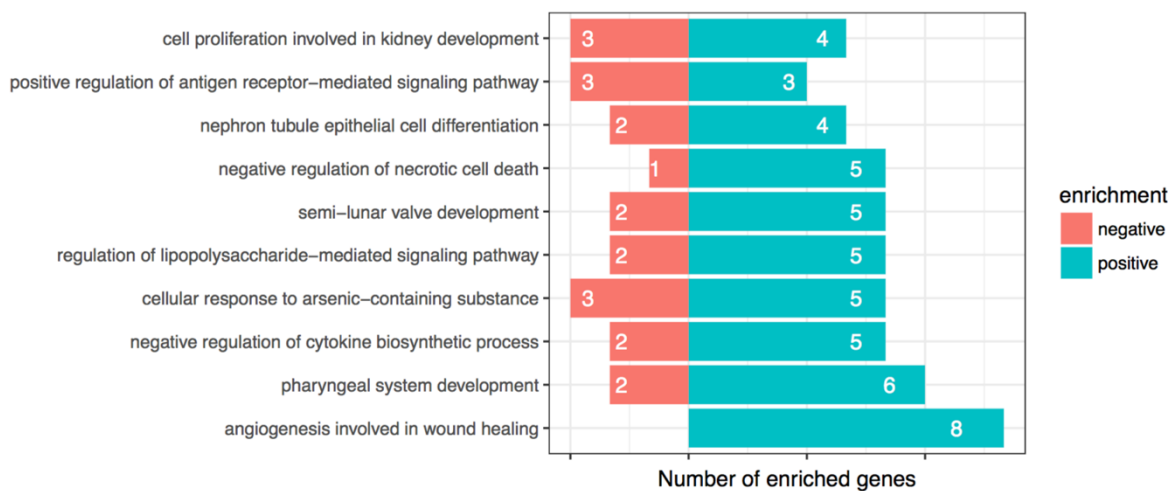


Figure S4 | topGO analysis of gene expression for 0.5 U thrombin versus control. Cells were stimulated for 4 h. The numbers in each bar indicate the number of enriched genes over the number of annotated genes in this term. Asterisks show the level of significance of Fisher's exact test for the enrichment of the particular term. * p-value < 0.01; ** p-value < 0.001; *** p-value < 0.0001.

8.2 List of Figures and Tables

8.2.1 Figures

Figure 2-1 Principle mechanisms of mechanosensitive signal transduction	4
Figure 2-2 The serum response factor pathway.....	5
Figure 2-3 Upstream regulators of mammalian YAP/TAZ	6
Figure 2-4 Chemical structures of different natural actin binding compounds.....	9
Figure 2-5 Overview of different micropatterning techniques.	10
Figure 3-1 Microcontact printing as a tool to study mechanosensitive signaling cues in endothelial cells...	13
Figure 3-2 Role of endothelial cell-cell contacts in regulating MRTF-A and YAP subcellular localization.....	14
Figure 3-3 VE-cadherins mediate the inhibitory effect of cell-cell contact formation on MRTF-A and YAP. .	15
Figure 3-4 Influence of adhesive surface area on MRTF-A and YAP subcellular localization in HUVEC.....	16
Figure 3-5 Impact of cell shape variation on MRTF-A and YAP subcellular localization in HUVEC.....	17
Figure 3-6 Translocation of MRTF-A and YAP during migration on dumbbell-shaped micropatterns.....	18
Figure 3-7 (A) MRTF-A and YAP exhibit different activation kinetics in response to mechanical stress.....	20
Figure 3-8 Expression pattern and nuclear levels of MRTF-A and YAP during endothelial tube formation ..	21
Figure 3-9 Retinal whole-mount stainings of wild-type C57BL/6 mice at postnatal day 6 (P6).....	22
Figure 4-1 Influence of actin polymerizing compound Miuraenamamide A on endothelial gene transcription.	25
Figure 4-2 Influence of actin depolymerizing compound Latrunculin B on endothelial gene transcription.	26
Figure 4-3 Effects of Miuraenamamide A and Latrunculin B on nuclear structure, chromatin organization and histone modification.	27
Figure 4-4 Effects of Miuraenamamide A and Latrunculin B on transcriptional capability and rRNA synthesis.	28
Figure 4-5 Visualization of nuclear actin in NIH3T3 fibroblasts.....	30
Figure 4-6 Miuraenamamide A and Latrunculin B adversatively shift the concentration of nuclear actin.	31
Figure 4-7 RICS analysis of actin aggregation in response to actin binding compounds.....	33
Figure 4-8 High concentrations of Miuraenamamide A induce nuclear actin aggregation in HUVEC.....	34
Figure 4-9 Fig. 5 Miuraenamamide A activates MRTF-A but not YAP.....	35
Figure 4-10 Regulated SRF and YAP / TAZ target genes in response to stimulation with Miuraenamamide A, Latrunculin B and thrombin.....	36
Figure 4-11 Fig. 6 Miuraenamamide A-induced actin polymerization fails to disrupt the interaction between AMOTp130 and YAP.	38
Figure 5-1 Regulatory model of MRTF and YAP mechanosensing in endothelial cells.....	43
Figure 5-2 Proposed regulatory model underlying the differential response of MRTF-A and YAP to Miuraenamamide A-induced actin aggregation.....	45
Figure 5-3 Proposed model for the response of nuclear versus cytoplasmic actin to polymerizing and depolymerizing actin binding compounds.	47
Figure 5-4 Nuclear deformation during migration across dumbbell-shaped micropatterns.....	48
Figure 6-1 Microcontact printing workflow	58
Figure 6-2 FCS equations	66

8 Appendix

8.2.2 Tables

Table 1 Chemicals and reagents.....	52
Table 2 Primary antibodies	54
Table 3 Secondary antibodies, HRP- and IF-conjugates	54
Table 4 Buffers and solutions.....	54
Table 5 Technical devices and lab equipment	56
Table 6 Consumables	56
Table 7 Plasmid constructs.....	61
Table 8 qPCR primers.....	64
Table 9 List of abbreviations	82

8.3 Abbreviations

Table 9 List of abbreviations

Abbreviation	Full name
°C	degree celsius
2D	two-dimensional
3D	three-dimensional
AMOT	angiomin
ANOVA	analysis of variance
BSA	bovine serum albumin
cDNA	complementary DNA
cm	centimeter
CSB	cytoskeleton stabilizing buffer
DNA	deoxyribonucleic acid
ECD	extracellular domain
EGFP	enhanced green fluorescent protein
EM	electron microscopy
FCS (1)	fetal calf serum
FCS (2)	fluorescence correlation spectroscopy
FDR	false discovery rate
GFP	green fluorescent protein
GLM	generalized linear model
h	hour
HA	hemagglutinin
Hertz	Hz
HRP	horseradish peroxidase
HyD	hybrid detector
IB4	isolectin B4
IF	immunofluorescence
kDA	kilodalton
LINC	linker of the nucleoskeleton and the cytoskeleton
luc	luciferase
MAL	megakaryotic acute leukemia

8 Appendix

Abbreviation	Full name
mg	milligram
min	minute
ml	milliliter
mM	millimolar
mRNA	messenger RNA
MRTF	myocardin related transcription factor
nAC	nuclear actin chromobody
NES	nuclear export signal
ng	nanogram
NLS	nuclear localization signal
nm	nanometer
nM	nanomolar
PBS	phosphate buffered saline
PDMS	polydimethylsiloxane
PEG	polyethylene glycol
PLL	poly-L-lysine
PVDF	Polyvinylidene difluoride
RFP	red fluorescent protein
RICS	raster image correlation spectroscopy
RLU	relative light units
RNA	ribonucleic acid
rpm	rotations per minute
rRNA	ribosomal RNA
RT	room temperature
s	second
SD	standard deviation
SEM	standard error of the mean
SMD	single molecule detection
SRE	serum response element
SRF	serum response factor
TAZ	transcriptional coactivator with PDZ binding motif
TCF	ternary complex factor
TEAD	<i>TEF-1</i> , <i>TEC1</i> , <i>ABAA domain</i>
V	Volt
YAP	yes-associated protein
YFP	yellow fluorescent protein
μ CP	microcontact printing
μ g	microgram
μ l	microliter
μ m	micrometer
μ M	micromolar

8.4 List of Publications

First authorship:

- I. **Florian A. Gegenfurtner**, Berenice Jahn, Helga Wagner, Christoph Ziegenhain, Wolfgang Enard, Ludwig Geistlinger, Joachim O. Rädler, Angelika M. Vollmar and Stefan Zahler
Micropatterning as a tool to identify regulatory triggers and kinetics of actin-mediated mechanosensing in angiogenesis
Accepted for publication – **Journal of Cell Science**
- II. **Florian A. Gegenfurtner**, Themistoklis Zisis, Nader Al Danaf, Waldemar Schrimpf, Zane Kliesmete, Christoph Ziegenhain, Wolfgang Enard, Uli Kazmaier, Don C. Lamb, Angelika M. Vollmar and Stefan Zahler
Transcriptional effects of actin binding compounds: the cytoplasm sets the tone
Under Review – **BMC Biology**

Co-authorship:

- III. Simon L. Schuster, Felix J. Segerer, **Florian A. Gegenfurtner**, Kerstin Kick, Christoph Schreiber, Max Albert, Angelika M. Vollmar, Joachim O. Rädler and Stefan Zahler
Contractility as a global regulator of cellular morphology, velocity, and directionality in low-adhesive fibrillary micro-environments.
Biomaterials, 2016, 102:137-47
- IV. Bojan Ljepoja, Christoph Schreiber, **Florian A. Gegenfurtner**, Stefan Zahler, Joachim O. Rädler, Ernst Wagner and Andreas Roidl
miR-200c affects cell migration and morphology via the inhibition of filamin expression
Manuscript in preparation

8.5 Scientific presentations

8.5.1 Oral presentations

Microenvironmental triggers and regulatory kinetics of mechanosensitive transcription factors MRTF and YAP in endothelial cells

Florian A. Gegenfurtner, Joachim O. Rädler, Angelika M. Vollmar and Stefan Zahler

International PhD Students/Postdoc Meeting of the German Pharmaceutical Society - DPhG 2017, Frankfurt am Main, Germany

8.5.2 Poster presentations

Actin-related mechanosensing in endothelial cells – micropatterns as a tool to dissect the angiogenic process

Florian A. Gegenfurtner, Joachim O. Rädler, Angelika M. Vollmar and Stefan Zahler

EMBO | EMBL Symposium: Actin in Action: from Molecules to Cellular Functions 2016, Heidelberg, Germany

Effects of the actin binding compound Miuraenamides A on mechanosensitive gene expression in endothelial cells

Florian A. Gegenfurtner, Rolf Müller, Uli Kazmaier, Angelika M. Vollmar and Stefan Zahler

Annual Meeting of the German Pharmaceutical Society - DPhG 2016, Munich, Germany

Microenvironmental triggers and regulatory kinetics of mechanosensitive transcription factors MRTF and YAP in endothelial cells

Florian A. Gegenfurtner, Charlott Leu, Joachim O. Rädler, Angelika M. Vollmar and Stefan Zahler

SFB1032 Workshop 2017: From Nanoagents to Living Matter 2017, Tutzing, Germany

8.6 Associated master and bachelor theses

Franz Geisslinger, bachelor thesis (May 2017):

Influence of substrate stiffness on endothelial mechanosensing

Berenice Jahn, master thesis (August 2016):

Functional characterization of Yes-associated protein YAP regarding its actin-dependent regulation in endothelial cells

Katharina Schloss, bachelor thesis (May 2015):

Modulation of the MRTF-SRF signaling axis by interference with the actin cytoskeleton in endothelial cells

8.7 Acknowledgements

Mein herzlichster Dank gilt Frau Prof. Dr. Angelika Vollmar und Herrn Prof. Dr. Stefan Zahler für die Möglichkeit, meine Dissertation am Lehrstuhl für Pharmazeutische Biologie anzufertigen. Die Begleitung meines wissenschaftlichen Werdegangs und auch meiner persönlichen Weiterentwicklung habe ich stets als gelungene Mischung aus fachlich kompetenter Betreuung und dem Vertrauen zur selbstständigen Verwirklichung von Ideen empfunden. Insbesondere hat mir der wissenschaftliche und persönliche Austausch in unseren monatlichen Achievement-Meetings große Freude bereitet und meine Motivation in zähen Phasen am Leben erhalten.

Der Prüfungskommission bestehend aus Herrn Prof. Dr. Stefan Zahler, Frau Prof. Dr. Angelika M. Vollmar, Herrn Prof. Dr. Ernst Wagner, Herrn Prof. Dr. Franz Paintner, Herrn PD Dr. Stylianos Michalakis und Herrn Prof. Dr. Franz Bracher möchte ich für die Bereitschaft zur Bewertung meiner Arbeit und dem damit verbundenen Zeitaufwand herzlich danken. Ein besonderer Dank gilt zudem Herrn Prof. Dr. Joachim Rädler für die Konzeption und organisatorische Leitung des Sonderforschungsbereichs 1032 Nanoagents.

Herrn Prof. Dr. Robert Grosse möchte ich für die große Gastfreundschaft während meines Forschungsaufenthalts an der Philipps-Universität Marburg danken. Die aufschlussreichen wissenschaftlichen Einblicke und die Bereitstellung von Plasmiden und Antikörpern haben wesentlich zum Erfolg der vorliegenden Dissertation beigetragen.

Dr. Simon Schuster und Dr. Kerstin Kick danke ich für die engagierte Betreuung meiner Masterarbeit und die herzliche Einführung in den Arbeitskreis Vollmar. Die gemeinsame Zeit im Labor, auf SFB Tagungen und während der Betreuung diverser Studentenpraktika habe ich sehr genossen.

Meiner Masterstudentin Berenice Jahn und meinen beiden Bachelorstudenten Katharina Schloss und Franz Geisslinger danke ich für die motivierte Projektteilnahme, den fachlichen Austausch und die im Rahmen meiner Dissertation geleistete Laborarbeit.

Ein großer Dank gilt dem gesamten Arbeitskreis Vollmar. Auch und vor allem wegen euch hat es mir die vergangenen Jahre viel Freude bereitet, in Grosshadern zu wohnen und zu forschen. In diesem Zuge möchte ich besonders Jana Peliskova und Kerstin Loske für die herausragende technische Unterstützung meiner Arbeit danken. Den zahlreichen ehemaligen und aktuellen Doktoranden, insbesondere Max, Henriette und meinen Labornachbarn aus

8 Appendix

B4.074, danke ich für die über das Labor hinausreichende Freundschaft und all die gemeinsamen Unternehmungen.

Meinen Eltern und meiner Schwester Steffi danke ich für die große Unterstützung in allen Lebenslagen und für die Ermöglichung meiner Ausbildung. Danke, dass ich trotz kleinerer Irrwege immer das Vertrauen und die Freiheit bekommen habe, meinen Weg zu gehen.

Zu guter Letzt danke ich meiner Frau Katrin. Danke, dass Du mich stets verstehst und in allen Situationen unterstützt. Das gemeinsame Verfolgen unserer Ziele haben die vergangenen Jahre zu einer unvergesslichen Zeit werden lassen.